Micromorphology of Last Glacial Maximum Grounding line sediments around the Antarctic Peninsula

By

Holly Arnold BSc

Department of Earth Sciences

Submitted
In partial fulfillment of the requirements
for the degree

Master of Science

Brock University, Faculty of Mathematics and Science
St. Catharines, Ontario

Abstract

Sediments recovered from seven Last Glacial Maximum grounding lines sites, around the Antarctic Peninsula, were analyzed using micromorphology. This is the first evidence that grounding line sediments from around the Antarctic Peninsula have complex deformational histories and subglacial origins. It was determined that grounding zone wedge contain multiple units, or diamicton layers, with homogenized boundaries. The multiple diamicton units/layers are due to the accretionary formation of a grounding line wedge. All the sediments were deposited via deformation, and continual reincorporation, homogenization of lower diamicton layers by upper diamicton layers produced what macroscopically appeared to be a single massive diamicton unit. The morainal ridge that was sampled, alternatively, is composed of a single unit, or diamicton layer, that was subglacial in origin and believed to have been pushed out to form a ridge that was subsequently deformed via glacial push.

Acknowledgements

First and foremost I would like to thank Hester Jiskoot for introducing me to this field of study. You sparked an interest in a field that I had never previously considered, and inspired me to continue down the path I'm on. If it weren't for your support, and the opportunities you gave me, I wouldn't be where I am today.

I would like to thank David Huntley, who showed me that even digging pits for samples surrounded by millions of bugs can be fun. It was your enthusiasm that kept me going, and made me come back.

Ólafur Ingólfsson, you showed me the Arctic and helped me reconcile my notion of diamictons. You related these massive landforms I'd seen in Canada produced by ancient ice sheets to those produced by modern day glaciers. You cemented the idea that I had the ability to question everything, a notion that I was only just beginning to grasp. In such a short amount of time I learned more from you than I could have imagined, thank you.

Thank you to the scientists at Rice University who collected the samples used in this study, and the lab technicians at Brock who processed them.

John Menzies, I couldn't have done it with out you. Thank you for the opportunity to learn from you, and your continued support through this process. You have irrevocably changed my views, and taught me so much about this field. Words can't describe how grateful I am.

Table of Contents

List of Tables

List of Figures

List of Abbreviations

WAIS	West Antarctic Ice Sheet
EAIS	East Antarctic Ice Sheet
LGM	Last Glacial Maximum
APIS	Antarctic Peninsula Ice Sheet
TAM	Trans Antarctic Mountains
EOC	End of Core

Chapter 1 – Introduction

1.0 Introduction

The use of micromorphology as a means to interpret, more accurately, the subglacial conditions and processes occurring in the glacial environment is becoming more common (van der Meer, 1993, 1997; Carr, 1999, 2000, 2001; Hiemstra, 1999, 2001; Khatwa & Tulazyk, 2001; Ó Cofaigh *et al.*, 2005a; Menzies *et al.*, 2006, 2010; Larson *et al.*, 2007). The ability to analyze the internal structures formed during the sediment's depositional history is the greatest strength of this method. As micromorphology requires only a small amount of material for analysis its use in the description of cores, where sediments recovery is limited, becomes invaluable (Carr, 1999).

During the Pleistocene the Antarctic Peninsula Ice Sheet, in most regions, advanced to the outer continental shelf; a detailed history of advance and retreat is recorded in the sedimentary deposits, glacial erosional surfaces, and geomorphic features. Since sampling of these deposits on the continental shelf of the Antarctic Peninsula is only possible through cores, the use of the micromorphology to study them is ideal. During the Austral summer of 2002, geophysical and geological data were collected during the NBP02-01 cruise. The majority of the data collected was used by Fretwell (2005) and Heroy (2006) to determine the glacial history in the region. Their investigation was focused on landform identification and retreat history, with analysis of diamictons retrieved via coring as a means to determine whether or not they were subglacial deposits. Seven cores from their study were selected and 18 micromorphological samples were collected from the diamictons they identified to determine their depositional history. The grounding line zone was the area of interest in this study as it is a dynamic environment with a complex depositional history, making micromorphology a perfect tool to uncover it.

Chapter 2 - Background: Antarctic Peninsula glacial history, grounding lines, and micromorphology

2.0 – Introduction

The sediments in the cores selected for this study were deposited near fluctuating grounding lines of the Late Pleistocene West Antarctic Ice Sheet around the Antarctic Peninsula and were subjected to variable ice flow and depositional conditions. By analyzing the microscopic signatures, the sediments give clues as to the subglacial temperature and rheology at the grounding line of the ice sheet. The grounding line environment is the area of interest in this study, as oscillations in this environment have a widespread effect on the stability of the ice sheet (Payne *et al.*, 2004; Schoof, 2007; Goldberg *et al.*, 2009; Gagliardini *et al.*, 2010). Changes in this environment during the Late Pleistocene can be used as an analogy for what is currently happening in the Antarctic Peninsula.

2.1 Glacial History

2.1.1 Eocene to Pleistocene Expansion: A brief history

The Antarctic Ice Sheet existence has been traced back to the Middle to Late Eocene, impacting global climate since the Late Cenozoic through eustasy and driving ocean circulation (Barrett, 1991; Denton *et al.*, 1991; Flower & Kennett, 1994; Anderson, 1999; Barker *et al.*, 2007). West Antarctic glaciation initially began with the growth of the island arc ice caps, filling in the rift basins with glacial marine sediments, which facilitated the expansion of the Antarctic ice sheet across the West Antarctic continent and continental shelf (Anderson, 1999). There is debate as to when the ice sheet initially grounded on the West Antarctic continental shelf. Bart and Anderson (1995) state that it occurred during the Miocene, while others (Larter & Barker, 1989) argue that grounding did not take place until the Plio-Pleistocene. Deep-sea foraminiferal, oxygen isotope records, and seismic reflections indicate that fluctuation

in ice volume and position occurred during the Pliocene. Uplift of the Trans Antarctic Mountains (TAM) segregated the ice sheet into East and West, providing a physiographic barrier for glacial drainage. There is agreement that the configuration of the Antarctic Ice Sheet (separation into West Antarctic Ice Sheet (WAIS), East Antarctic Ice Sheet (EAIS), and ice expanded onto continental shelves) was completed by 1.8 Ma, during a major cooling event (Anderson, 1999).

During the Pleistocene the WAIS had advanced and retreated from the continental shelf in response to changes in global eustacy driven by Northern Hemisphere ice sheets. Correlation between the Vostok and global isotope records indicate an in-phase relationship between Southern and Northern Ice Sheets (Hollin, 1962; Thomas & Bentley, 1978; Denton *et al.*, 1991; Anderson, 1999; Ingólfsson, 2004). The Pleistocene section of the Antarctic Peninsula continental shelf seismic facies shows thin, discontinuous glacial marine deposits interbedded with multiple till sheets (Shipp & Anderson, 1994; Bart & Anderson, 1995). These deposits support ice sheet reconstructions indicating ice extending onto the Antarctic Peninsula continental shelf (Nakada *et al.*, 2000; Anderson, 1999; Bentley & Anderson, 1998; Anderson *et al.*, 2002).

2.1.2 Pleistocene Retreat: A detailed history of study area

There is extensive research on Last Glacial Maximum (LGM) reconstruction and retreat history of the WAIS (c.f. Anderson *et al.*, 1991; Shipp & Anderson, 1994; Anderson, 1999; Conway *et al.*, 1999; Anderson *et al.*, 2002; Canals *et al.*, 2002; Denton & Hughes, 2002; Ingólfsson, 2004; Evans *et al.*, 2005; Kilfeather *et al.*, 2011). Only the retreat history of Vega Trough/James Ross, Bransfield Basin, Anvers Trough/Biscoe Trough, and Marguerite Trough, the study area, (Fig. 1) will be summarized.

The ideal sediments for ice sheet retreat dating are those that were deposited near the grounding line, specifically from cores that sample the contact between glaciomarine

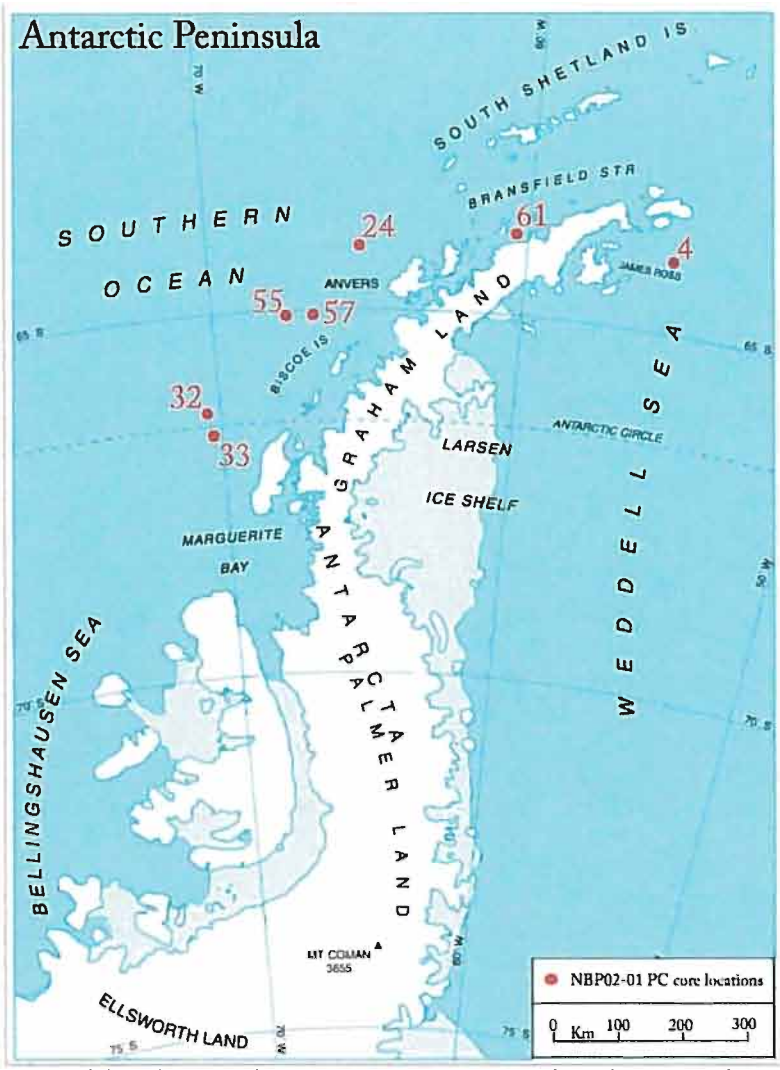

Fig. 1. Study area and locations of the NBP02-01 PC cores selected for sampling (modified from USAP, 2008).

sediments and underlying subglacial till. Whether radiocarbon dates are acquired from the lowest glaciomarine unit or from the lowest diatomaceous unit, they are minimum estimates of ice retreat. Retreat of grounding line, glaciomarine deposition, and onset of hemipleagic sedimentation revealing onset of open marine conditions must first occur, depending on which unit sample, prior to the radiocarbon date obtained (Anderson, 1999; Domack *et al.*, 1999; Anderson *et al.*, 2002; Heroy & Anderson, 2007). In addition to this time lag, there are uncertainties in radiocarbon ages with regards to the carbon reservoir effect. Temporal and spatial variability in the Antarctic carbon reservoir are caused by regional differences in ^{14}C depleted

deepwater upwelling, and input of ^{14}C-depleted CO^2 from melting ice. Corrections to radiocarbon dates obtained to account for this effect vary depending on the author, ranging from 750 to 2220 years (Domack *et al.*, 2001a; Anderson, 1999; Ingólfsson, 2004). Since variations in corrections occur within the same region, and it is not within the scope of this study to date grounding line retreat, all dates summarized are as they originally appear by each author with their individual corrections pre-applied, taken as a whole as minimum estimates of retreat. Dates presented by Heroy (2006) and Heroy and Anderson (2005, 2007) were obtained during the same cruise, with the cores used in this study.

2.1.2.1 Vega Trough/James Ross

Sediment cores and high-resolution seismic and multibeam records show an extensive glacial unconformity in the Vega trough extending to shelf break, transition from sediment-free zones in the Prince Gustav Channel, to flutes and lineations on the inner shelf, and a prominent grounding-zone wedge on the mid-shelf (Anderson *et al.*, 1992, Sloan *et al.*, 1995; Domack *et al.*, 2001a; Pudsey & Evans, 2001; Anderson *et al.,* 2002; Evans *et al.*, 2005; Heroy, 2006). Diamicton sampled in piston cores was interpreted as deformation till (Anderson, 1999). Radiocarbon dates from piston cores indicate that retreat of grounded ice from the outer shelf had occurred by 18,500 cal yr BP, with the inner shelf ice free by 12,000 cal yr BP (Heroy, 2006). Onshore radiocarbon dates reveal that deglaciation occurred prior to 7400 ^{14}C yr BP (Hjort *et al.*, 1997; Fig. 2).

2.1.2.2 Bransfield Basin

High-resolution seismic reflection profiles collected by Banfield and Anderson (1995) identify a glacial unconformity which extends to the continental shelf edge. Overlying this unconformity is a series of morainal ridges identifying the LGM within the troughs of the Bransfield Strait (Anderson *et al.*, 2002; Ingólfsson, 2004), as well as megascale glacial lineations identified by Canals *et al.* (2000) during a

swath bathymetry survey. Piston cores sampled ice-proximal glacial-marine sediment dating to 19,055 ^{14}C yr BP and 14,365 ^{14}C yr BP on the Trinity Peninsula shelf. This indicates that the ice retreated prior to 14,365 ^{14}C yr BP (Banfield and Anderson, 1995; Anderson *et al.*, 2002; Fig. 2).

2.1.2.3 Anvers Trough/ Biscoe Trough

Glacial landforms identified during surveys of Anvers Trough provide evidence of ice sheet extension to the outer shelf; flutes were identified on the inner shelf during a side-scan sonar survey (Pudsey *et al.*, 1994), as well as a grounding-zone wedge on the outer shelf (Larter & Vanneste, 1995). Heroy (2006) obtained radiocarbon dates of 15,090 cal yr BP and 16,230 cal yr BP from transitional glacial-marine sediments, and 15,650 cal yr BP from an iceberg-turbate in Anvers Trough (Fig. 2). Domack *et al.*'s (2001b) Palmer Deep radiocarbon stratigraphy of diatomaceous glacial-marine sediments indicates that ice retreated from this area around 13,000 yr BP (Anderson *et al.*, 2002).

The Heroy (2006) survey of Biscoe Trough obtained dates of 18,760 cal yr BP and 16,970 cal yr BP in the north, and 13,230 cal yr BP in the south, identifying a possible trend of glacial retreat initiating in the north and progressing southward (Fig. 2).

2.1.2.4 Marguerite Trough

Seismic studies, swath bathymetry, and sedimentological and petrographic analyses of piston cores identify a prominent glacial erosional surface with overlying till deposits that extend to the mid shelf. Glacial landforms transition from striations, flutes, and drumlins on the inner shelf to mega-scale glacial lineations extending seaward into a prominent grounding-zone wedge on the mid-shelf (Kennedy & Anderson, 1989; Pope & Anderson, 1992; Bart & Anderson, 1995; Anderson *et al.*, 2001; Heimstra, 2001; Anderson *et al.*, 2002; Ingólfsson, 2004). Pope and Anderson

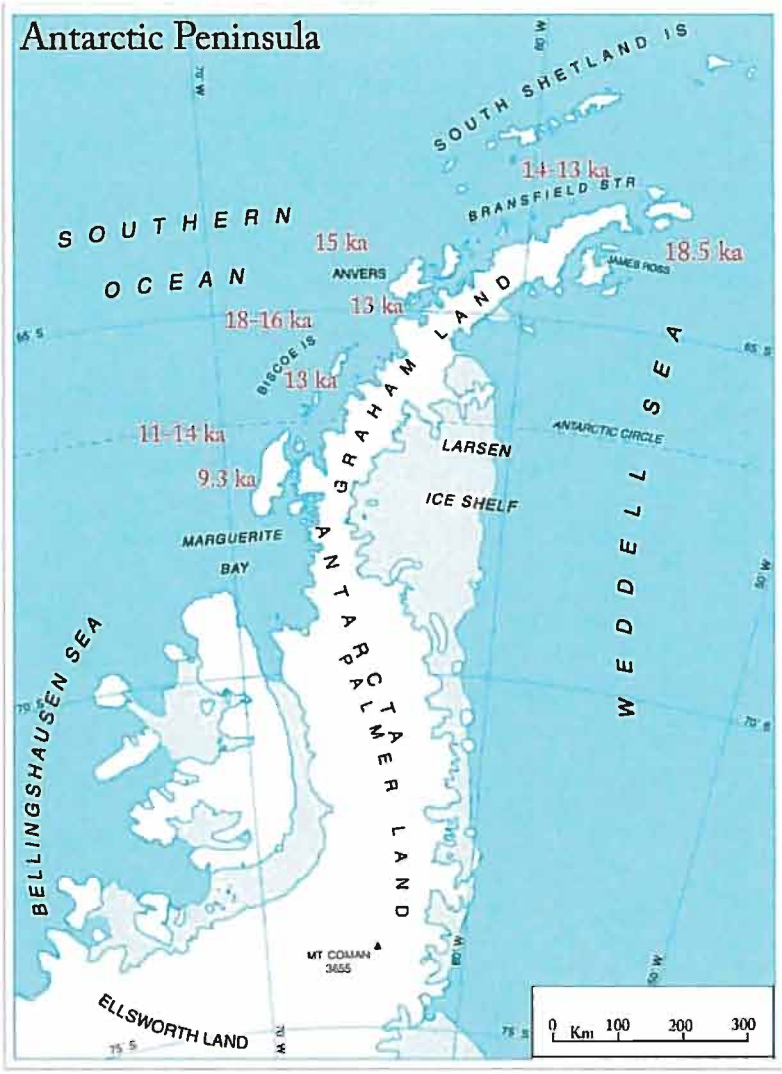

Fig. 2. Minimum dates of retreat from the various troughs on the Antarctic Peninsula, dates (in red) presented in ka BP (modified from USAP, 2008).

(1992) interpret glacial-marine sediment radiocarbon dates (of 12,190 – 11,125 ^{14}C yr cal BP) to indicate ice retreated from the prior to 12,000 yr BP, with the onset of open-marine conditions around 6000 ^{14}C yr BP (Harden *et al.*, 1992). Recent work by Kilfeather *et al.* (2011) indicates that ice-sheet retreat occurred earlier, by 14 ka BP, and rapid retreat from the outer- and mid-shelf of Marguerite Trough coincided with the sea-level rise of meltwater pulse 1a, grounding the ice-sheet on the inner shelf. Inner-shelf and grounding-line retreat occurred around 9.3 ka BP caused by the encroachment of Circumpolar Warm Deep Water onto the continental shelf (Kilfeather *et al.*, 2011).

2.1.3 Summary

The ice flow patterns, drainage, and retreat history varies from trough to trough indicating that the Antarctic Peninsula Ice Sheet (APIS) was comprised of the confluence of localized ice domes and ice stream systems responding to local conditions, rather than a dynamically coherent, concentric ice sheet (Ingólfsson, 2004). Retreat of ice, as suggested by radiocarbon date trends, occurred in a north to south progression along the Peninsula and a continuation of this trend is still occurring (Heroy & Anderson, 2005; Heroy, 2006). Retreat of ice from the outer-shelf has been dated as having occurred significantly earlier than current numerical, glaciological, and glacio-eustatic models predict, coinciding with meltwater pulse 1a and approximately in-phase with deglaciation in the Northern Hemisphere (Bard *et al.*, 1990; Kanfoush *et al.*, 2000; Nakada *et al.*, 2000; Huybrechts, 2002; Heroy & Anderson, 2005; Heroy, 2006; Heroy & Anderson, 2007; Kilfeather, *et al*, 2011). Alley *et al.* (2007) note that sedimentation stabilizes grounding line positions, and the variability of regional retreat could be linked to differing sedimentation rates, as well as physiographic variations from trough to trough.

2.2 Grounding Lines

Studies of modern marine-ending glacier grounding lines indicate that sedimentary deposits with different geometries are deposited in different glacial conditions (Cowan *et al.*, 1999; O'Brien *et al.*, 1999; Powell & Alley, 1997; Dahlgren, *et al.*, 2002; Taylor *et al.*, 2002; Schoof, 2007; Trusel *et al.*, 2010). Understanding what glaciological and climatological conditions produce these successions allow the interpretation of the marine sedimentological and stratigraphic record on continental shelves, such as those on the Antarctic Peninsula. Climate, glacial regime, and stability are the drivers of change in the glacial sedimentary record, regardless of glacier type. Climatic regime is linked to glacial regime and changes in one produces changes in the other, which are echoed in the sedimentary record. However, the sedimentary record, and the processes that produce it, plays an additional role in the

stability of marine-ending glaciers since it can change the local water depth at the grounding line, which in turn is a factor controlling grounding line movement and glacial stability. Therefore, interpretation of the sedimentary record can provide insight into both past glacial regimes as well as glacial stability (Powell & Alley, 1997).

2.2.1 Grounding Line Systems and Positions

2.2.1.1 Grounding Line Systems

Grounding line systems, as defined by Powell (1988), are the sedimentary depositional systems produced at grounding lines. Each system is distinguished by geometry, internal architecture, facies association, and process of formation. Since sediment accumulates in different geometries, or systems, depending on whether the grounding line is advancing, stable, or retreating, glacial behavior can be inferred based on the system produced. Maximum advance positions and standstill during retreat locations are the most commonly preserved grounding line system and analysis of these deposits can provide insight to the broader climatic conditions that triggered those paleoglaciological events (Powell & Alley, 1997; Powell & Domack, 2002).

Grounding line systems can be divided into those produced during stable conditions or advance and those produced during grounding line retreat. As the system produced during grounding line retreat is a sheet (of subglacial sediments interfingering with any type of pro-grounding-line deposit), only advance and standstill systems will be described in detail. Advance and standstill systems are subdivided by geometry – fan, morainal bank, and wedge. These geometries are produced through the interaction of different types of sediment transport to and release at the grounding line, shelf relief, and glacial termini type (Powell & Alley, 1997, Dahlgren, *et al.*, 2002). The two termini types of marine-ending glaciers are floating termini and grounded tidewater cliffs, the difference being the relationship of the calving line to the grounding line.

Where the two coincide, a tidewater cliff is formed. However if, the ice extends beyond the grounding line in a floating ice shelf then the calving line extends beyond the grounding line and the termini is termed as floating (Powell & Alley, 1997; Powell & Domack, 2002).

One of the major controls on sediment transport/release is the abundance of meltwater. When meltwater is abundant and transports fluvial sediment in large conduits to the grounding line fans are formed. Fans are geometries produced from point source deposition of subglacial or englacial meltwater channel sediments. They comprise subaquatic outwash, suspension settling deposits, and sediment gravity flow. Fans can be formed most commonly by a tidewater cliff and are produced during the initial stages of stability. Fans can grow into deltas during standstill, or overlapping of individual fans can produce a bank. They are a pro-grounding line landform with depositional structures similar to those found in fan deltas. Deformation structures are present if glacial pushing or ice rafting occurs, or during sediment gravity flow events (Powell & Alley, 1997; Lajeunesse & Allard, 2002; Powell & Domack, 2002).

Morainal banks also form when meltwater is abundant, but there are several differences between the two systems. Morainal banks can be formed by a variety of processes (instead of a single process such as the formation of fans) each forming a pro-grounding line landform similar to the end moraines formed by terrestrial glaciers. Morainal banks are produced most commonly at tidewater cliffs during advance or a standstill position. Morainal banks can aggrade to sea level as a tidewater cliff does not restrict the height of the bank. As previously stated, overlapping fans can produce a morainal bank. In this case of morainal bank formation, meltwater is transported in numerous small fluvial conduits which cause lateral dispersion of sediments (Powell & Alley, 1997; Powell & Domack, 2002). Sedimentary structures are similar to those found in fans, but sediment dispersal is from a multi-point source, or subglacial meltwater discharge could also occur as sheet flows. Some morainal banks can be formed by pushing pro-grounding line sediments

during advance. Those formed by push comprise pro-grounding line lithofacies that were subsequently deformed. Other banks are formed by the squeezing of subglacial sediments out beyond the grounding line. These comprise subglacial sediments possibly containing multi-event deformation structures. Sediments undergo deformation during the squeezing process and if glacial advance occurs then deformation is by glacial push. Morainal banks can also form by frontal-dumping and/or rock and grain fall of supraglacial debris during the calving process (Powell & Alley, 1997; Seramur *et al.*, 1997; Anderson, 1999; Powell & Domack, 2002). These are how morainal banks form by a single process, but an end-member bank could be formed by any combination of these processes, resulting in a bank composed of chaotic mixtures of gravel, diamicton, and mud facies (Powell & Alley, 1997). By looking at the internal architecture of morainal banks, and not just the geometry of the landform, the process of formation can be determined.

Wedges have been suggested to be more of a subglacial process than a definitive terminus type by Powell & Alley (1997). They state that subglacial diamicton is transported to the grounding line in a laterally continuous sheet which, once released at the grounding line, is redistributed via gravity flows forming a wedge shaped deposit. As sediment is continually being transported to and released at the grounding line the sediment wedge aggrades. This continual process produces a deforming sediment layer that thickens down-glacier, producing a wedge shaped landform; the smaller volumes of confined meltwater facilitate the subglacial deformation process. Subglacial sediment deformation occurs when basal water cannot be effectively drained, causing an increase in basal water pressure and reduction in sediment strength, allowing the sediment to be more easily deformed (Boulton & Hindmarsh, 1987). The end member landform produced during advance or stable conditions is determined by termini type. In the presence of a tidewater cliff or a basal crevasse, the aggradation is pushed into bank form, producing a push/squeeze morainal bank. If the terminus is floating, then the sediment wedge aggrades until contact with the base of the floating terminus is achieved. The grounding line then advances to where terminus grounded to the aggraded sediment and starts deforming the sediment as

advance continues (Anderson *et al.*, 1992; Bart & Anderson 1995; Vanneste & Larter, 1995; Powell & Alley, 1997; Anderson, 1999; Powell & Domack, 2002). Since this grounding line system encompasses subglacial processes, such as deformation, and the geomorphic feature extends upglacier and is not strictly a pro-grounding line landform, it will be referred to henceforth as a grounding zone wedge, aptly named by other authors (Anderson, 1999). The formation and growth of grounding zone wedges and their re-erosion during advance, removes the obstacle that deep water and pre-existing bed topography might pose during glacial advance. This process effectively decreases grounding line water depth and facilitates glacial advance onto the continental shelf (Dahlgren *et al.*, 2002; Alley *et al.*, 2007; Anandakrishnan *et al.*, 2007).

A simple geographical division based on meltwater abundance can be applied to where grounding line systems can be found; grounding zone wedges are formed with limited confined volumes of meltwater in deforming beds and morainal banks are formed with abundant channelized meltwater that can reach the grounding line by multiple means. The abundance of free flowing meltwater is usually found in temperate to subpolar glaciers where supraglacier water contributes to subglacial meltwater, with only subglacial inputs of meltwater to the deforming bed found in subpolar to polar glaciers. If morainal banks are only produced by subglacial deformational processes then they will also be found in subpolar or polar regions (Powell & Alley, 1997; Anderson, 1999; Powell & Domack, 2002).

2.2.1.2 Grounding line positions in the Antarctic Peninsula region from the LGM

Detailed studies have been conducted on the continental shelf of the Antarctic Peninsula which have yielded irrefutable evidence of grounded ice in the region (Pope & Anderson, 1992; Pudsey *et al.*, 1994; Larter & Vanneste 1995; Shipp & Anderson, 1997; Bentley & Anderson, 1998; Canals *et al.*, 1998; Canals *et al.*, 2000; Domack *et al.*, 2001a; Anderson *et al*, 2002; Heroy & Anderson, 2005; Heroy, 2006). The geophysical and geological data collected during these studies can be divided

into three categories (as follows with examples of encompassing data). Seismic data identify glacial unconformities, chaotic diamicton facies, bedrock erosional surfaces, morainal banks, and grounding zone wedges. Geomorphic data identify streamline features such as grooves, flutes, drumlins, megascale glacial lineations, and moraines with multibeam swath bathymetry and side-scan sonar. Finally, sedimentary data provide evidence of grounded ice by sampling stratigraphy containing subglacial diamicton with piston and kasten cores. To provide context for the subsequent micromorphological data (sedimentary data), a summary of the aforementioned data collected by previous authors in the study area is presented (Powell & Alley, 1997; Anderson, 1999; Heroy, 2006; Mosola & Anderson, 2006).

High resolution seismic data of the Pleistocene section on the Antarctic Peninsula continental shelf have identified subglacial and ice-proximal seismic facies (Banfield & Anderson, 1995; Anderson, 1999; Fretwell, 2005; Heroy, 2006). Two grounding-zone seismic facies, which overlie a glacial erosional surface, that have been identified are grounding line ridges and grounding zone wedges (Anderson, 1999). The thicknesses of the Pleistocene subglacial deposits on the continental shelf reinforce the idea that the dominant process in this region is deformation of subglacial sediment. This is supported by the lack of a source of supraglacial debris for the continental ice sheet and since any englacial debris is predominantly transported away from the grounding line via melt out from ice shelf or carried away by icebergs, which diminishes the fraction of supraglacial and englacial debris deposited in grounding line systems in the Antarctic (Powell & Alley, 1997).

Studies of the Vega Trough and off the coast of James Ross Island in the northwestern Weddell Sea have identified a prominent geomorphic landform on the middle continental shelf that overlies a glacial unconformity that extends to the shelf edge. This ~75m thick landform has been extensively mapped and interpreted as a grounding zone wedge formed during a prolonged stand-still using seismic and geomorphic data (Anderson *et al.*, 1992; Bentley & Anderson, 1998; Anderson, 1999;

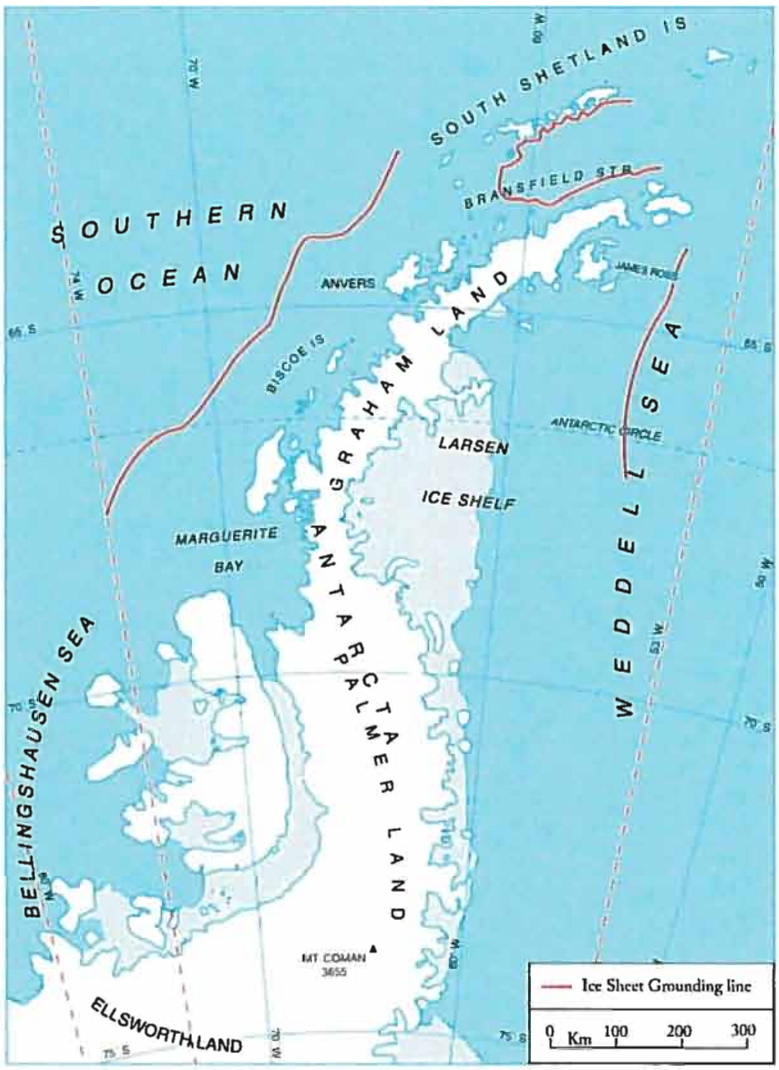

Fig. 3. Grounding line positions around the Antarctic Peninsula. A compilation of grounding line features identified by Pope and Anderson (1992), Pudsey *et al.* (1994), Larter and Vanneste (1995), Bart and Anderson (1996), Shipp and Anderson (1997), Bentley and Anderson (1998), Canals *et al.* (1998), Canals *et al.* (2000), Domack *et al.* (2001a), Anderson *et al.* (2002), Ó Cofaigh *et al.* (2002), Dowdeswell *et al.* (2004), Ingólfsson Ó. (2004), Fretwell (2005), Ó Cofaigh *et al.* (2005), Heroy (2006), and Heroy and Anderson (2007) (modified from USAP, 2008).

Pudsey & Evans, 2001; Heroy, 2006). Heroy (2006) obtained four cores in a transect across the grounding zone wedge, as well as additional seismic and geomorphic data, which sampled subglacial diamicton and was able to date the stratigraphic sequence to the LGM. With seismic, geomorphic, and sedimentary data this feature has been confidently identified as a LGM grounding zone wedge (Anderson *et al.*, 1992; Bentley & Anderson, 1998; Anderson, 1999; Heroy, 2006; Fig. 3).

Seismic, geomorphic, and sedimentary data have been collected in Bransfield Basin identifying ridges on the middle continental shelf overlying an unconformity that extends to the shelf break. These ridges have been interpreted as grounding line morainal banks formed during the LGM (Branfield & Anderson, 1995; Bentley & Anderson, 1998; Canals *et al.*, 2000; Heroy, 2006; Anderson *et al.*, 2002; Fig. 3). One of these ridges was sampled by Heroy (2006), who interpreted their diamicton composition as subglacial till. It was not in their scope of study to determine how the ridge was formed, only that its composition was subglacial till.

Similarly in Anvers Trough/Biscoe Trough, seismic, geomorphic, and sedimentary data have been collected, identifying glacial flutes on the inner shelf with a prograded, acoustically unstratified feature on the outer shelf off Anvers Island. In combination with LGM dates obtained from material stratigraphically overlying diamicton, the feature was interpreted as a grounding zone wedge formed by ice streams flowing over deforming subglacial diamicton (Pudsey *et al.*, 1994; Larter & Vanneste, 1995; Canals *et al.,* 1998; Domack *et al.*, 2001a; Anderson *et al.,* 2002; Heroy, 2006; Fig 1).

Numerous studies have been conducted in Marguerite Trough including seismic studies by Bart and Anderson (1996), swath bathymetry by Anderson *et al.* (2002), chirp subbottom profiler by Heroy (2006), and a micromorphological study of glacigenic cores by Hiemstra (2001). A glacial erosional surface was identified that underlies flutes, drumlins, and megascale glacial lineations that extend into a midshelf grounding zone wedge (Ó Cofaigh *et al.,* 2002; Dowdeswell *et al.*, 2004; Fretwell, 2005; Ó Cofaigh *et al.,* 2005b; Fig. 3). The sediment facies identified in the chirp subbottom profiler have been sampled and identified as 'soft' diamicton/deformation till that correlates with other "soft" diamicton facies sampled around the West Antarctic.

2.3 Stiff versus Soft Diamicton

The only access to the sediments from paleo-ice streams on the continental margin of the Antarctic is through coring. With the intention of reconstructing glacial history, macroscopic descriptions of diamictons sampled in cores, commonly massive and structureless, provided no means to determine the process of deposition. Often the only variability in the diamicton sampled in the core was shear strength, so this was used as a means to determine the process of deposition. Anderson (1999) identified two types of tills; stiff (tills with high shear strength) and soft (tills with low shear strength). The stiff tills were assumed to be deposited through lodgement which caused "overcompaction", thus increasing their shear strength, and soft tills were assumed to be deposited through deformation. Though Anderson (1999) stated that more detailed work to find other criteria to distinguish these till types was needed, the propagation of this division of depositional processes around the Antarctic based on "stiff" or "soft" has continued until very recently (Domack *et al.*, 1999; Shipp *et al.*, 1999; Anderson *et al.*, 2002; Heroy, 2006). With the application of micromorphological analysis to the cores sampled in the Antarctic the determination of emplacement by lodgement has been revised and the cause of the variation in shear strength been determined (Evans *et al.*, 2005; Ó Cofaigh *et al.*, 2005a, 2007; Reinardy *et al.*, 2011). It has been suggested that soft till represents a reworked homogenized version of underlying stiff till that has been dewatered, attributed to deformational processes and representing a transition from normal to streaming ice (Reinardy *et al.*, 2011). This interpretation is based on the identification of microstructures, and their associations, not purely on the variability of shear strength.

2.4 Micromorphology

2.4.0 Introduction

Glacial sediments go through a variety of processes and environments as they are mobilized, transported, and deposited (cf. Evans *et al.*, 2006). A sedimentary

signature of those conditions, stress histories, and processes are recorded within the structure of the sediment. Since the recognition of the deforming subglacial bed and its role in glacier movement (Boulton, 1986), there has been considerable debate on the identification and classification of the various sediment end members, and ultimately the sedimentary signatures that represent them (Boulton, 1979; Dreimanis, 1989; van der Meer *et al.*, 2003; Evans *et al.*, 2006; Menzies *et al.*, 2006, 2010). Identifying sometimes subtle differences in the characteristics of sediments can determine the depositional environment and can impact, for example, the recognition of a grounding line by properly identifying subglacial or proximal grounding-line sediments (Licht *et al.*, 1999).

While standard techniques of analyzing glacial sediments (grain size/petrographic analysis, gamma density, macroscopic observations, magnetic susceptibility, shear strength, x-radiographs radiographs) provide valuable information, they often destroy the sedimentary signatures in the process or focus on one component and not the relationships between the constituent elements and patterns of deformation. The ability to examine in detail the *in situ* structural components, arrangements, and composition of sediments, lithified and unlithified, is why a micromorphological analysis is becoming the technique of choice when seeking to understand the rheological conditions and stress applications occurring during deformation, deposition, and post-depositional processes. The micromorphology technique enables this detailed observation by impregnating and hardening the loose sediment, preserving the internal structures, and processing the sample into a thin section (van der Meer, 1996; Menzies, 2000; van der Meer *et al.*, 2003; Menzies *et al.*, 2010; Fig. 4).

Since this technique originated in pedology and was later adapted for the study of glacial sediments, the terminology used in micromorphology is rooted in that discipline (Kubiëna, 1938; Brewer, 1976). The nomenclature now draws from glacial and structural geology, as well as pedology, modifying and adapting terms to specifically describe the structures observed (Larsen *et al.*, 2007; Menzies *et al.*,

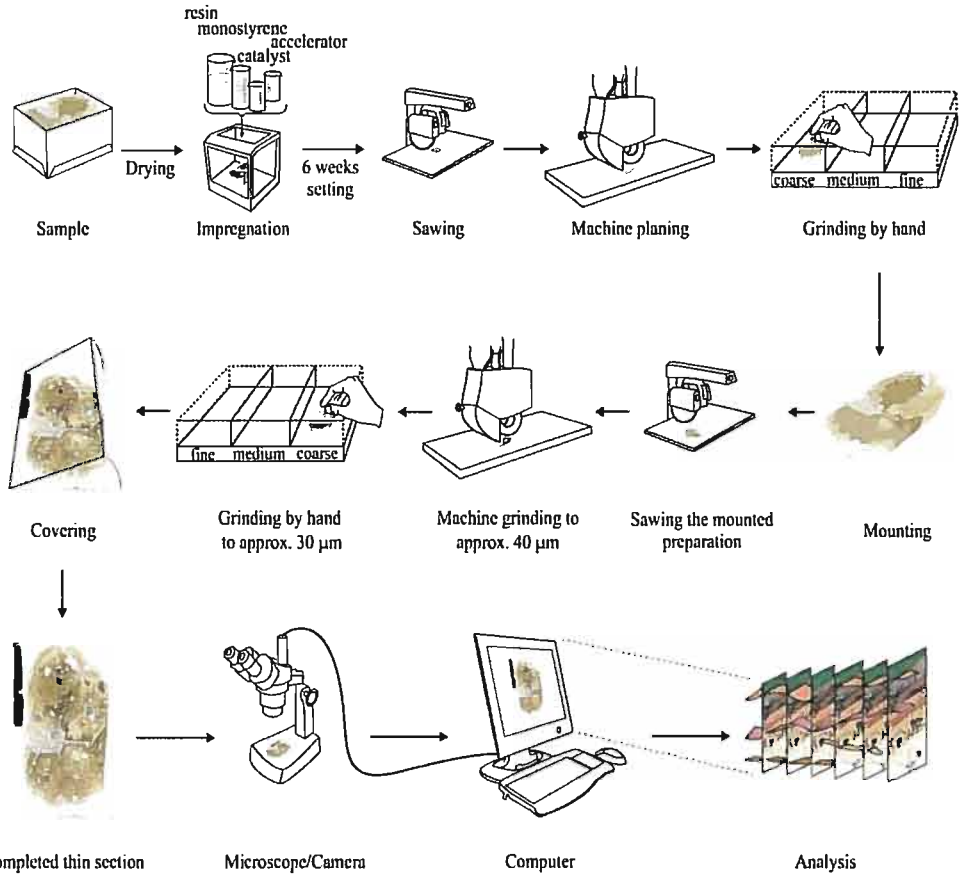

Fig. 4.Flow chart depicting steps involved in thin section processing. Illustrating impregnation, curing, two stage cutting and grinding, and image capture (modified from Menzies, 2000).

2010). Recognizing an array of microstructures in a macroscopically described massive/structure-less sediment, the strength of this analysis, is the major reason for the divergence in the terms used between the two scales. As the terminology is unique, a brief review and description of microstructures is given.

2.4.1 Terminology

Texture: Glacial geologists describe the texture of sediment in terms of the matrix and clast composition, where matrix is < 2 mm fraction and clasts the > 2 mm fraction. Since the average micromorphological sample is mounted on a 6 cm x 10 cm glass slide, the texture is described in terms of plasma and skeleton grains. Plasma is an all encompassing term referring to all the particles finer than 30 µm, the thickness of a

thin section, because in thin section it is not possible to discern these particles individually. Plasma is used as a synonym for matrix, as at the macroscopic scale, a matrix's particles are not individually discernable. Skeleton grains, like clasts, are the grain fraction that can be observed individually. All the grains that are larger than 30 μm are referred to as skeleton grains (van der Meer, 1993; Hiemstra and Rijsdijk, 2003; van der Meer *et al.,* 2003; Carr, 2004; Menzies, 2004; O Cofaigh *et al.*, 2005a). They are both described according to composition, distribution, size, shape and variability throughout the thin section.

Structure: The structures or microstructures observed are the various arrangements that skeleton grains and plasma form individually, or in combination, or discontinuities among these components, and are grouped into plasmic fabric, skelsepic plasmic fabric, and S-matrix (Menzies *et al.*, 2006; Fig. 5).

Plasmic fabric: Plasmic fabric is a category of structures formed by orientated clay particles that exhibit birefringence when viewed though crossed polarized light. The various types of plasmic fabrics (Fig. 5) develop as the sediment is deformed and the clay particles reorient to the stress field, and can vary from random orientations - omnisepic fabric - to a single preferential orientation - unistrial fabric (Fig. 6) (van der Meer, 1993; Carr, 2000; Menzies, 2000, 2004; Hiemstra & Rijsdijk, 2003; van der Meer *et al.,* 2003; O Cofaigh *et al.*, 2005b; Menzies *et al.*, 2006; Larsen *et al.*, 2007).

Skelsepic plasmic fabric: Skelsepic plasmic fabric (Fig. 5) is formed by the interaction between plasma and skeleton grains, when clay particles reorient parallel to skeleton grain edges (van der Meer, 1993; Menzies *et al.*, 2006; Fig. 6). Skelsepic plasmic fabric is originally a pedological term used to describe the structure caused by clay permeating through the soil profile. As the structure is observed in sediments that have been deformed the term remained, but it was suggested that this fabric could form as a result of deformation where the plasma particles were mechanically reoriented around skeleton grains as a result of shearing. Since either causation is correct, the interpretation of this structure, as with all structures, should be a result of

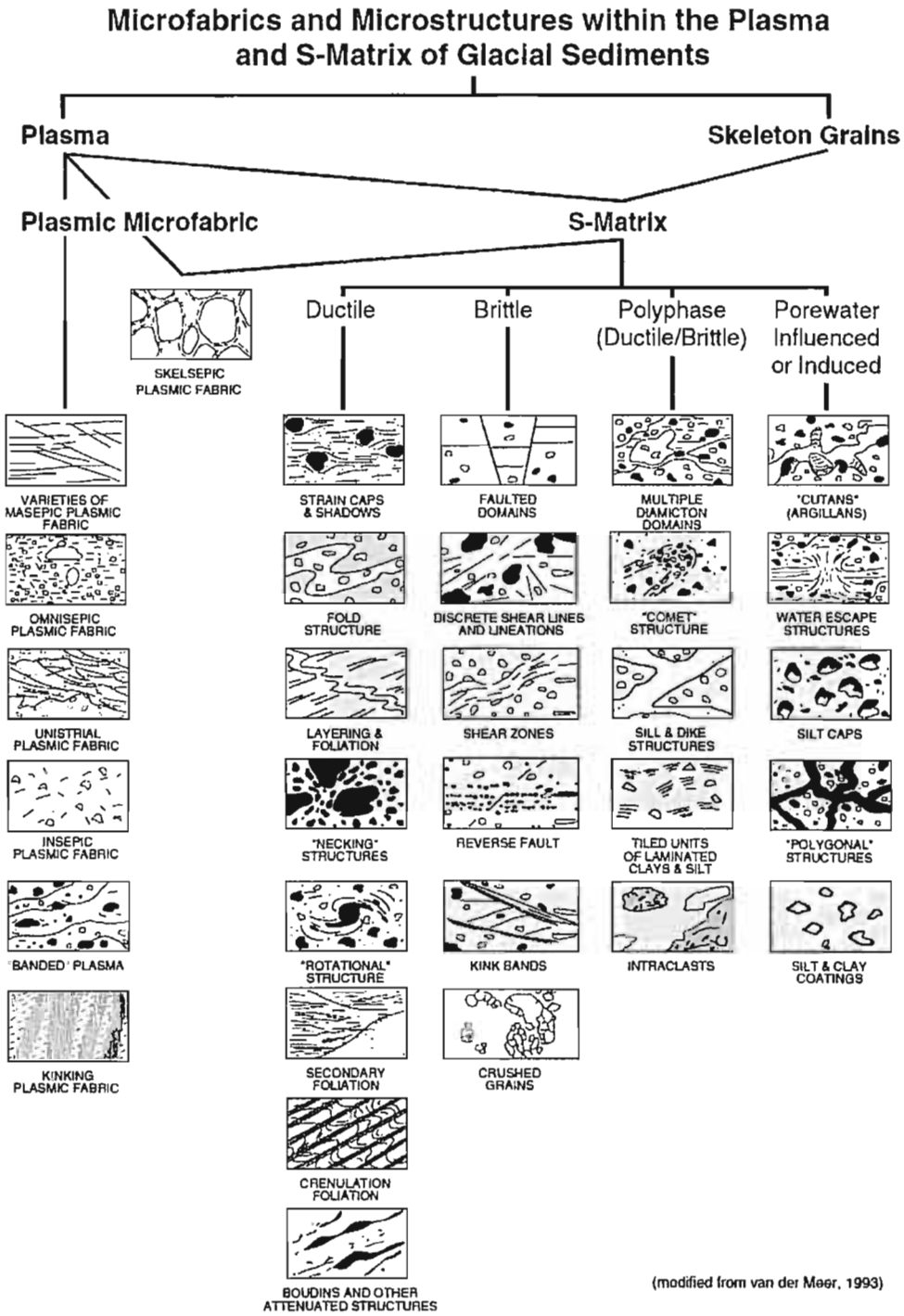

Fig. 5. Types of microstructure found in glacial sediments, grouped into plasmic fabric, skelsepic plasmic fabric, and S-matrix based on the various arrangements that skeleton grains and plasma form individually, or in combination, or discontinuities among these components (Menzies, 2000).

the combination of all the observed structure's characteristics (van der Meer, 1993, 1996; Menzies *et al.*, 2006; Larsen *et al.*, 2007).

S- matrix: S-matrix is a group of microstructures (Fig. 5) formed by both the plasma (<30 μm) and skeleton grains (>30 μm) when they are spatially associated and are indicative of deformational (ductile, brittle, and polyphase (brittle/ductile)) or porewater-induced formation (van der Meer, 1993; Menzies, 2000). Microstructures indicative of deformational formation (Fig. 6) have been artificially induced in experimental studies, illustrating their development and evolution as a result of increasing strain (Hiemstra & Rijsdijk, 2003; Thomason & Iverson, 2006).

Processing artifacts: During sample processing (Fig. 4) artifacts can be introduced into the sample. When samples are processed into thin sections they undergo a series of steps: sediments are dried, impregnated and cured, then go through a two-stage cutting, grinding process that results in a 30 μm thin section of sediment mounted on a glass slide to which a cover slip is then applied. The sample is then ready for analysis. At several stages, artifacts can be introduced affecting the final sample. If sediment drying is not done as slowly as possible, cracking and sample collapse can occur. If the resin has not completely cured, then partial removal of the sample can occur during grinding. Partial removal of the sample can also occur if the final grinding is uneven or results in a sample that is <30 μm thick. Bubbles can be introduced when the cover slip is added, resulting in circular structures. It is important to identify these possible artifacts and recognize that they are a result of poor sample preparation and are not microstructures. Artifacts can be greatly minimized or completely removed when sample preparation is done by an experienced technician.

2.4.2 Summary

By interpreting these microstructures together, as a set, one can begin to piece together the deformational events that occurred and the rheological conditions present during those events. As the conditions in the subglacial environment fluctuate, microstructures re-deform, overprint or completely destroy previous microstructures

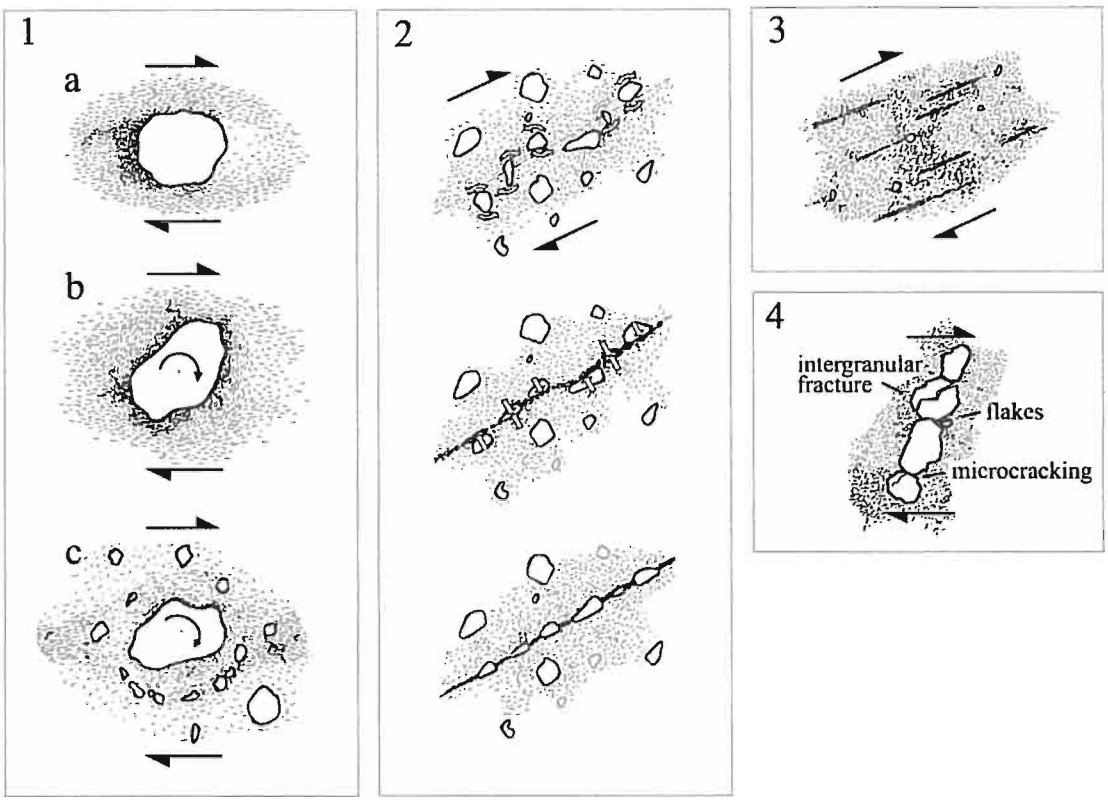

Fig. 6. Schematic illustrating microstructure development, dashes representing plasma particles around white skeleton grains (modified from Hiemstra and Rijsdijk, 2003 and Larsen *et al.*, 2007): (1) skelsepic plasmic fabrics development during deformation when a) a skeleton grain is immobile and clay particles reorient on the up-stress side of the skeleton grain but remain randomly oriented on the lee side. b) a skeleton grain rotates and the clay particles in the zone affected reorient. c) a central skeleton grain rotates, clay and skeleton grains in the zone affected reorient. (2) development of grain lineations. (3) development of unistrial plasmic fabric. (4) types of edge to edge grain crushing, intergranular fractures, flakes and microcracking.

allowing, when previous microstructures are not completely destroyed, the cycle of deformation to be determined (Menzies *et al.*, 2010).

Large outcrops of glacial sediments are rare given the extent of Late Pleistocene deposits, which mean that access is often limited to cores. With the recovery of a small amount of material in a core, limits are placed on the information that a macroscopic description can provide, as structures could be absent in the stratigraphic

sequence or just not sampled. Micromorphology, however, only requires a small amount of material for a complete analysis. It is in this situation, when the means of gathering information becomes limited, that the description a micromorphological analysis provides becomes invaluable (Carr, 1999).

Chapter 3 – Methodology

3.0 Introduction

During the 2002 Austral summer, Earth Science personnel from Rice University collected data aboard the *Nathaniel B. Palmer* (cruise NBP02-01) on the Antarctic Peninsula Shelf. This area contains stratigraphic records that are key to determining past ice sheet behavior and history of deglaciation (Heroy, 2006). Both geological and geophysical data were collected, including sediment cores, seismic records, and swath bathymetry data (Fretwell, 2005; Heroy, 2006). Geological samples were obtained using a piston core with a maximum penetration of 12 m (3 to 4 m was common). Of the cores collected during the NBP02-01 cruise, seven were selected (Fig. 1) on the basis of their proximity to the LGM grounding line environments of the WAIS.

3.1 Previous Analysis

The cores were analyzed by Fretwell (2005) and Heroy (2006) on a multi-sensor core scanner, photographed, and X-radiographed at the Antarctic Research Facility at Florida State University. Cores were measured for magnetic susceptibility, attenuated gamma counts and shear strengths. The grain size, texture, color, sorting, and mineralogy were also described. The cores were then sampled for radiocarbon dating, grain size, and foraminifera (Fretwell, 2005; Heroy, 2006).

This standard technique employed by Fretwell (2005) and Heroy (2006) to analyze the diamicton units in the cores resulted in the interpretation of the units as deformation or lodgment till. As there was insufficient information from the descriptions to determine the subglacial and rheological conditions in the grounding line environment, the cores were sub-sampled for micromorphological analysis.

3.2 Micromorphology sampling

As micromorphological analysis examines the internal architecture of sediment, samples cannot be taken from disturbed material as the structures are then no longer *in situ.* Given that some intervals of the cores had been disturbed, samples were limited to the sections that weren't, resulting in 2 or 3 samples per core (totaling 18) (Table 1).

Samples were collected in Kubiëna boxes, which have two removable lids and a hinged side, and were cut into the core using a trowel or knife as to leave the sample undisturbed and intact. The boxes were labeled with identification numbers and direction of core top. In other micromorphological sampling all orientations are measured in relation to the sample outcrop. However, this type of coring process did not record the orientation of the cores, thus removing any directional information other than to top or bottom of the core. The samples were then transported to the micromorphology laboratory (Brock University) to be processed for thin sectioning (Fig. 4).

Samples went through a slow air-drying period to avoid sample cracking and disintegration. Once dry, the samples were placed in an epoxy resin immersion bath, allowing the resin to permeate the sediments either under gravity or by low level pressure applied in a vacuum chamber (<15 mm Hg). Due to the varying size, porosity, and permeability, sample impregnation took at least 2 weeks. Subsequent to impregnation was a period of curing, which is essential for the resin to harden, allowing the sample to be cut without damaging the internal sedimentary structures. To expedite the curing process, samples were placed in a 40-50 °C oven for a further 2-3 weeks. Once cured, the samples went through a two-stage cutting and grinding process to produce a mounted 30μm thin section (Kemp, 1985; Menzies, 2000, 2001, 2004; Taylor, 2005).

Table 1
Sample location, core ID, and sample interval.

Sample Id	Ship	Cruise	Core ID	Type[a]	Water Depth (m)	Core Location	Latitude (S) (decimal degrees)	Longitude (W) (decimal degrees)	Core Length (cm)	Lab No.[b]	Sample Depth Interval (cm)
1	Palmer	NBP02-01	4	PC	385	Vega Trough	63.9802	54.9861	240	BU 09	110-120
2	Palmer	NBP02-01	4	PC	385	Vega Trough	63.9802	54.9861	240	BU 10	160-170
3	Palmer	NBP02-01	61	PC	591	Bransfield West	63.8893	60.3188	766	BU 18	710-720
4	Palmer	NBP02-01	61	PC	591	Bransfield West	63.8893	60.3188	766	BU 19	758-768
5	Palmer	NBP02-01	24	PC	557	Anvers Trough	64.0877	65.4860	312	BU 06	200-210
6	Palmer	NBP02-01	24	PC	557	Anvers Trough	64.0877	65.4860	312	BU 07	250-260
7	Palmer	NBP02-01	24	PC	557	Anvers Trough	64.0877	65.4860	312	BU 08	290-300
8	Palmer	NBP02-01	57	PC	732	Bisco Trough	65.1112	66.8987	326	BU 15	100-110
9	Palmer	NBP02-01	57	PC	732	Bisco Trough	65.1112	66.8987	326	BU 16	150-160
10	Palmer	NBP02-01	57	PC	732	Bisco Trough	65.1112	66.8987	326	BU 17	250-260
11	Palmer	NBP02-01	55	PC	587	Bisco Trough	65.1257	67.7489	393	BU 11	170-180
12	Palmer	NBP02-01	55	PC	587	Bisco Trough	65.1257	67.7489	393	BU 12	246-256
13	Palmer	NBP02-01	55	PC	587	Bisco Trough	65.1257	67.7489	393	BU 13	310-320
14	Palmer	NBP02-01	32	PC	547	Marguerite Trough	66.3610	70.6324	362	BU 01	50-60
15	Palmer	NBP02-01	32	PC	547	Marguerite Trough	66.3610	70.6324	362	BU 02	250-260
16	Palmer	NBP02-01	32	PC	547	Marguerite Trough	66.3610	70.6324	362	BU 03	307-317
17	Palmer	NBP02-01	33	PC	590	Marguerite Trough	66.6497	70.5311	80.5	BU 04	45-55
18	Palmer	NBP02-01	33	PC	590	Marguerite Trough	66.6497	70.5311	80.5	BU 05	65-78

[a] PC = Piston Core

[b] BU = Brock University

Once the thin sections were produced, they were analyzed under a Leitz M420 petrological microscope, using plane and cross-polarized light to identify textural and structural characteristics of the sample. A microscope-mounted Nikon Digital Sight DS-Fi1 camera was used to capture images, at magnifications of x6 and x10, of each sample using Nikon imaging software, NIS Elements BR 3.0, for use in producing detailed descriptions of each thin section. The Nikon imaging software was used to obtain measurements of area, length, width, circularity, and roughness of individual skeleton grain, as well as unbiased differentiation of texturally distinct zones of plasma for each thin section. This research software provided a highly accurate and efficient alternative to acquiring these measurements manually.

Micromorphological descriptions of the thin sections were conducted in a series of steps. The site location and sample lithofacies are described. For this study these descriptions are those made by Fretwell (2005) and Heroy (2006). As the samples for thin sectioning were collected by Earth Science personnel from Rice University, no personal descriptions of the lithofacies could be made. The thin sections are then described as a whole microscopically, and undergo a textural and structural analysis. The textural analysis consists of a description of the skeletal and plasma fractions. Skeletal grain composition, size ranges, distribution, and particle shape and form are noted. The plasma is described in terms of its texture, density, and distribution, as well as plasmic fabric type, distribution, and strength. The structural analysis consists of descriptions of voids (ratio, type, and distribution), microfabric (horizontal or vertical), and structures (sedimentary, deformational, any diagnostic features for specific environments, diagenesis, and post-depositional alteration) (Menzies, 2000, 2001).

Chapter 4 – Descriptions

4.0 Introduction

The original purpose of the core collection by Fretwell (2005) and Heroy (2006) during the NBP02-01 cruise was to determine ice sheet retreat and onset of open marine conditions. As such, the identification of the diamicton/subglacial units enabled the authors to date the lower most glacial marine sediments that directly overlaid these units. The determination of the origin of the diamicton/subglacial units in the cores collected was not within their scope of research and therefore those units were only briefly described. The units identified as diamicton/subglacial will focused upon in this study building upon the research of the overlying sediments in order to determine the depositional processes occurring at the grounding line.

Samples for micromorphological analysis were collected from units identified as diamictons in Fretwell (2005) and Heroy (2006) from the cores selected for this study. Sampling was restricted to 2 or 3 samples per identified diamicton unit in each core; recovered unit thickness and disturbances limited the number of samples. Core locations and sample depth intervals are summarized in Table 1.

Since access to the core archive was unavailable, Fretwell's (2005) and Heroy's (2006) unit descriptions will serve as a macroscopic unit description for this study. Heroy (2006) provided two unit descriptions, one a sediment description and the other a description of the X-radiograph of the unit; Fretwell (2005) did not include a X-radiograph description. These two descriptions do not always correlate but both are included in the macroscopic unit description. Correlations between the macroscopic sediment description, X-radiograph description and micromorphological description will be discussed in a later chapter.

4.1 Core 4

Core 4 sampled a 'wedge' feature identified in the Vega Trough in the Northwestern Weddell Sea by Heroy (2006). The piston core recovered a core length of 240 cm in a water depth of 385 m. A diamicton unit was sampled from 60 cm to the end of the core (EOC) at 240 cm; no lower boundary to this unit was retrieved. Descriptions of the diamicton unit were divided into a sediment description and an x-radiograph description by Heroy (2006).

The sediment description given for 60-240 cm identified a dark grey pebble rich diamicton (Munsell color 5Y 4/1), with increasing sand/pebble content and 'stiffness' down core. The x-radiographs description for the 60-240 cm unit was broken into subsections: (a) 60-70 cm contained 25% pebble content, that had random fabric and orientation, (b) 70-105 cm also contained 25% pebble content and random fabric, but was slightly 'brighter' which was stated to be due to a probable increase in sand content or compaction, (c) 105-240 cm was the 'brightest' unit but with only 20-25% pebble content (Heroy, 2006).

Two samples were collected from this core for analysis at the interval of 110-120 cm (sample 1) (Fig. 7) and 160-170 cm (sample 2) (Fig. 7). Both of these samples fall into Heroy's (2006) description as dark grey pebble rich diamicton (sediment description), with a pebble content of 20-25%, and possible high sand content and/or compaction (x-radiograph description).

X-radiographs of core 4 were obtained as a means to compare Heroy's (2006) macroscopic sediment and x-radiograph descriptions to the overview description of the thin section samples from this core. Sample 1 stratigraphically overlies sample 2 and though both were obtained from the same unit Heroy (2006) identified, they are visually distinct and dissimilar. Looking at sample 1 as a whole, there is an increase in the predominance of larger clasts/skeleton grains in the 115-120 cm section compared to the 110-115 cm section. The thin section of sample 2 is from the same

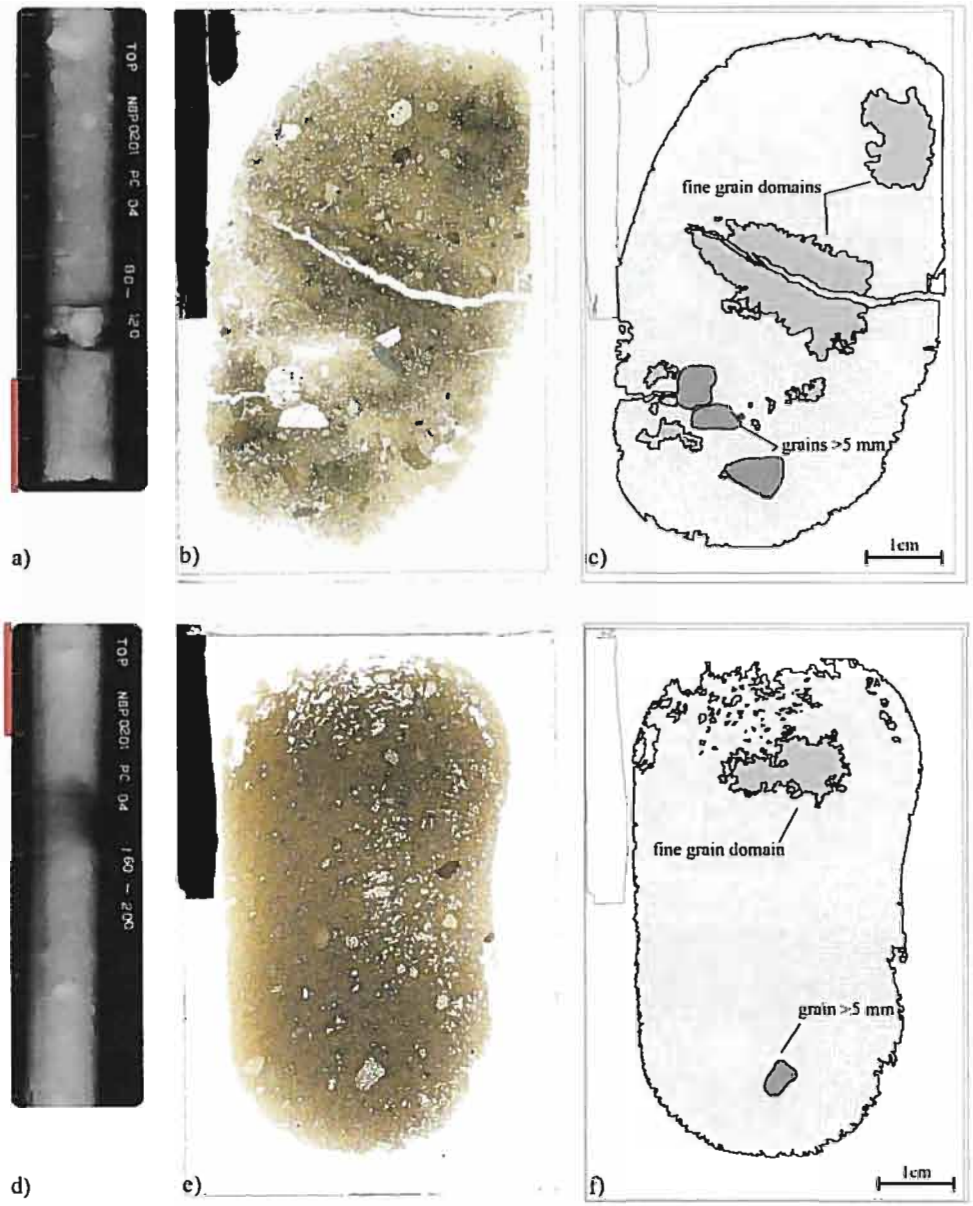

Fig. 7. Overview of samples 1 and 2 from Core 4. a) x-radiograph of section 80-120 cm of core 4, containing sample 1 at interval 110-120 cm highlighted by red bar. b) thin section of sample 1. c) overview of sample 1 displaying locations of fine grain domains and skeleton grains over 5 mm. d) x-radiograph of section 160-200 cm of core 4, containing sample 2 at interval of 160-170 cm highlighted by red bar. e) thin section of sample 2. f) overview of sample 2 displaying location of fine grain domain and skeleton grain over 5 mm (AMGRF, 2002).

unit as sample 1 but further down core. As a whole, both samples are texturally distinct from each other. Sample 2 is coarser grained than sample 1, with fewer fine

grain domains and fewer skeleton grains over 5 mm. Sample 2 contains a more uniform clast shape and size than sample 1, with less variation in lithology.

4.1.1 Detailed description of Sample 1

Texture: The thin section shows a number of fine (clay) grained domains in a predominantly coarse (medium silt) grained sample. These fine-grain domains (Fig. 7c) differ in shape and size throughout the sample. The uppermost fine-grained domain (Fig. 7c and Fig. 8a) is semi-spherical in shape with irregular boundaries. While visually distinct from the surrounding coarse-grained plasma, the boundary, in places, is hard to determine as it appears that the fine-grained domain slowly diffuses into the coarser grained domain. It is for this reason that Nikon imaging software is used to determine domain boundaries impartially. Large fine-grained domains are present in the middle of the thin section, separated by a void. This void transects the sample; it is most likely an artifact created during thin section production and not a microstructure. The fine-grained domains that are both above and below this void are identified as a single domain and will be referred to henceforth as a single domain. The fine-grained domain occurring in the middle of the thin section is oblong in shape, and is identified using the Nikon imaging software. Below this is another processing artifact; partial removal of the sample due to uneven grinding has made it impossible to identify any structures in this portion of the thin section. In the lower third of the thin section there are multiple smaller fine-grained domains (Fig. 7c). All of these domains have irregular boundaries and are identified using Nikon imaging software. There are three skeleton grains over 5 mm, all located in the bottom third of the sample. The sample contains multiple skeleton grain lithologies (see Heroy, 2006, for lithology composition). The shape of skeleton grains range from rounded to angular, with sub-angular being the predominant shape. There is no difference in the dominant shape between the different skeleton grain size fractions. The larger size fractions of skeleton grains are predominantly in the lower half of the sample, with nine skeleton grains over 3 mm in the lower half, and 3 in the upper half. There are intraclasts of another diamicton present in the sample (one shown in Fig. 8b).

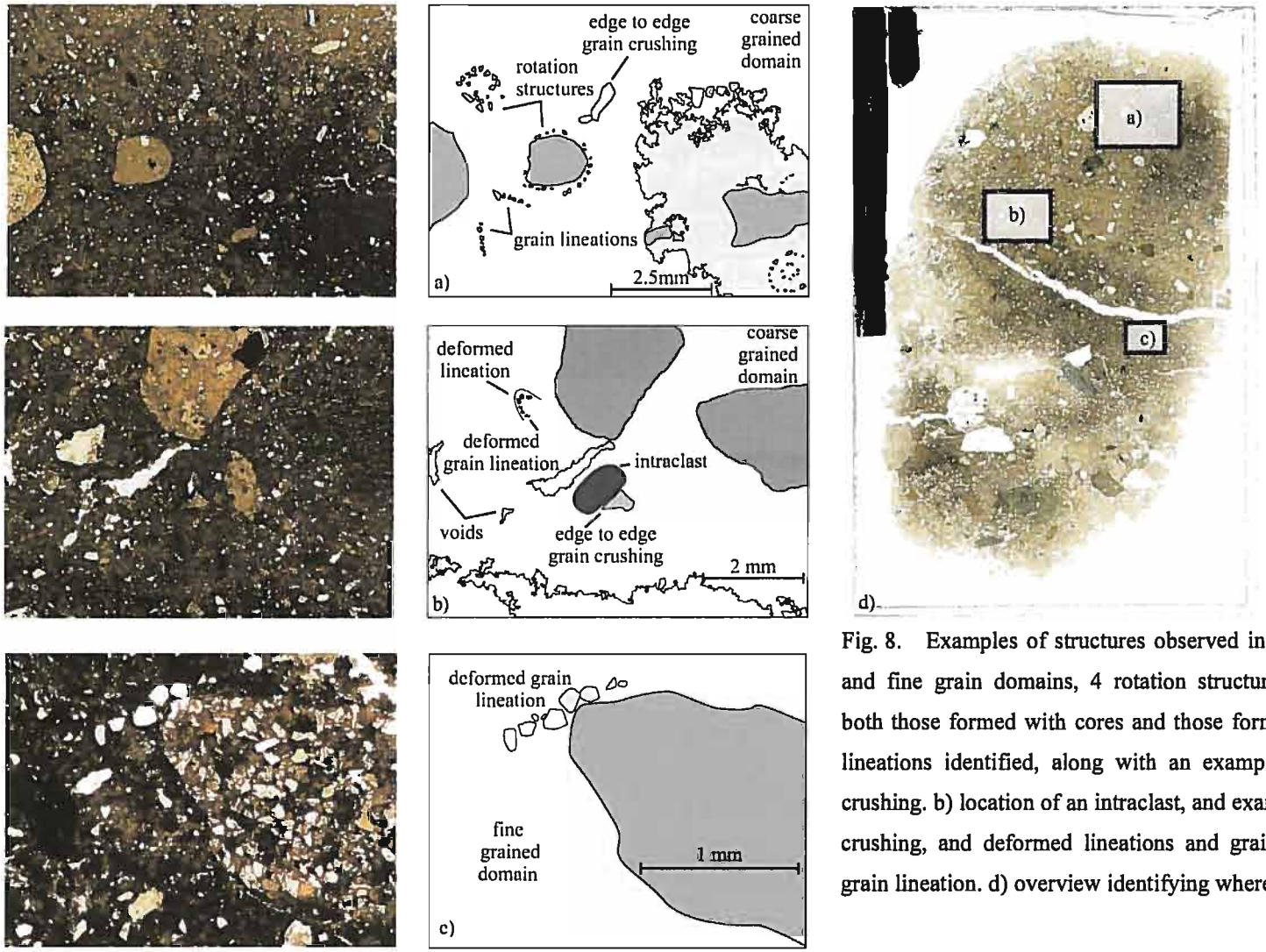

Fig. 8. Examples of structures observed in sample 1. a) Both coarse and fine grain domains, 4 rotation structures highlighted displaying both those formed with cores and those formed without, several grain lineations identified, along with an example of edge to edge grain crushing. b) location of an intraclast, and example of edge to edge grain crushing, and deformed lineations and grain lineations. c) deformed grain lineation. d) overview identifying where each example is located.

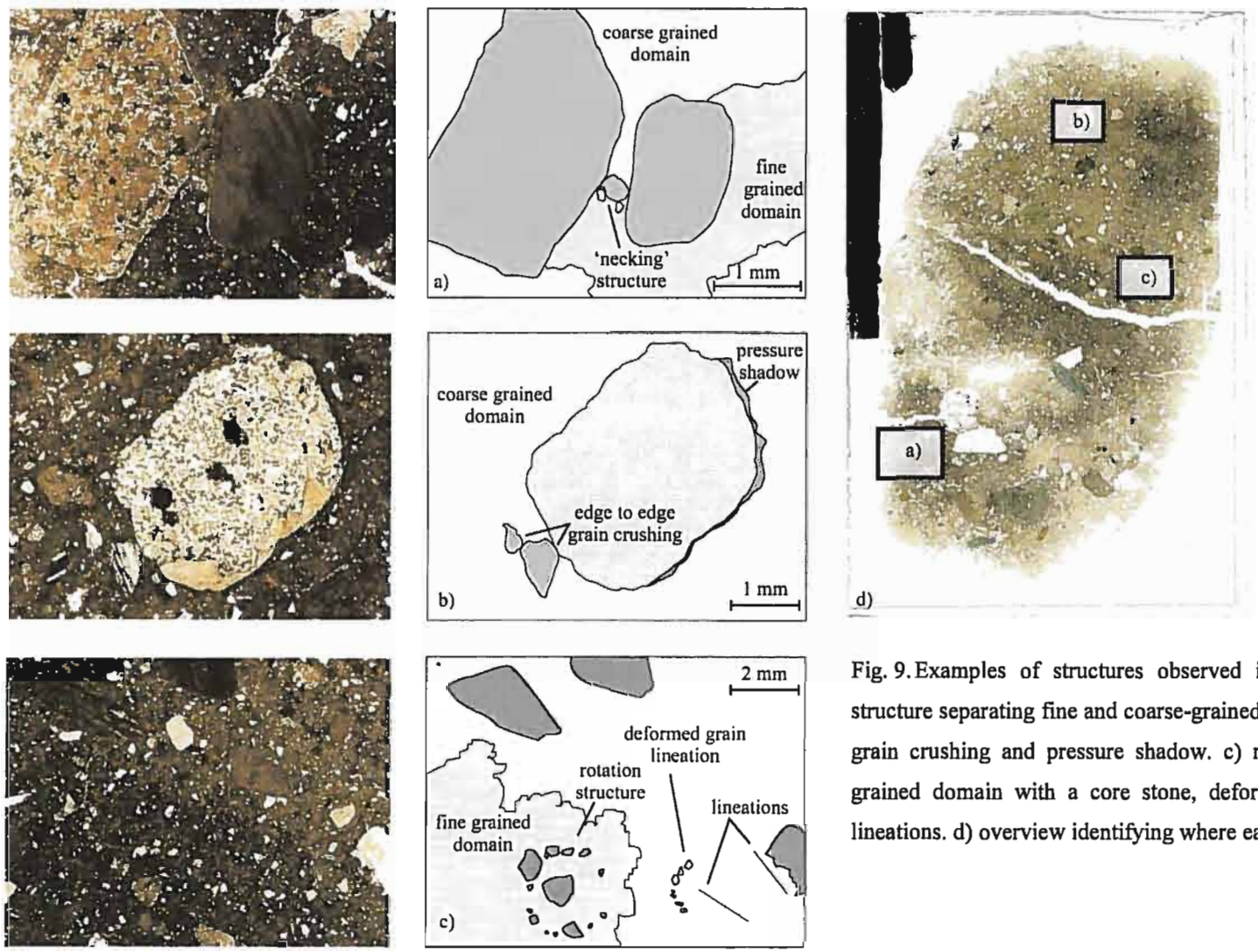

Fig. 9. Examples of structures observed in sample 1. a) necking structure separating fine and coarse-grained domains. b) edge to edge grain crushing and pressure shadow. c) rotation structure in fine-grained domain with a core stone, deformed grain lineation, and lineations. d) overview identifying where each example is located

Structure: The structures observed in the thin section are ductile deformational structures and brittle deformational structures; no porewater structures are identified. All of the structures observed occur in both the fine and coarse-grained domains. Figures 8 and 9 contain examples of the structures identified in the thin section that will be described in detail as follows. Multiple rotational structures are located in both the coarse and fine-grained domains. Some contained core stones (Fig. 8a, and 9c), and some did not (Fig. 8a). Plasmic fabric is predominantly skelsepic to bimasepic and several pressure shadows were identified (Fig. 8b, and 9b-c). There is an abundance of grain lineations, mostly short distance, in both the fine and coarse-grained domains. Some of the grain lineations have been deformed, suggesting multi-event ductile deformation. Figure 9a is an example of one of two necking structures identified in the thin section. Edge to edge grain crushing is the only brittle deformational structure identified (Fig. 8a-b and 9a-b).

4.1.2 Detailed description of Sample 2

Texture: Sample 2 is coarse (coarse silt) grained with a single fine (clay) grained domain (Fig. 7f). The fine grain domain is oblong in shape with irregular boundaries that diffuse into the coarse grain domain; identified with Nikon imaging software. The thin section contains several voids in the central portion of the right side of the sample; identified as processing artifacts created during thin section production and not microstructures (Fig. 7e). The coarse grain domain surrounding these voids does contain microstructures that appear not to have been affected during processing. Therefore, the microstructures that are identified in this portion of the sample are still analyzed. Since the location of all domains and microstructures is noted, the interpretation of these structures will take into account their proximity to the processing artifacts. There is only one skeleton grain over 5 mm in the sample, located in the bottom of the thin section. The sample is dominated by the finer fraction of skeleton grains with only a few skeleton grains (17 total) over 1 mm. The finer fraction of skeleton is predominantly composed of the same lithology, with varying lithologies primarily in the larger size fraction. The shape of the skeleton

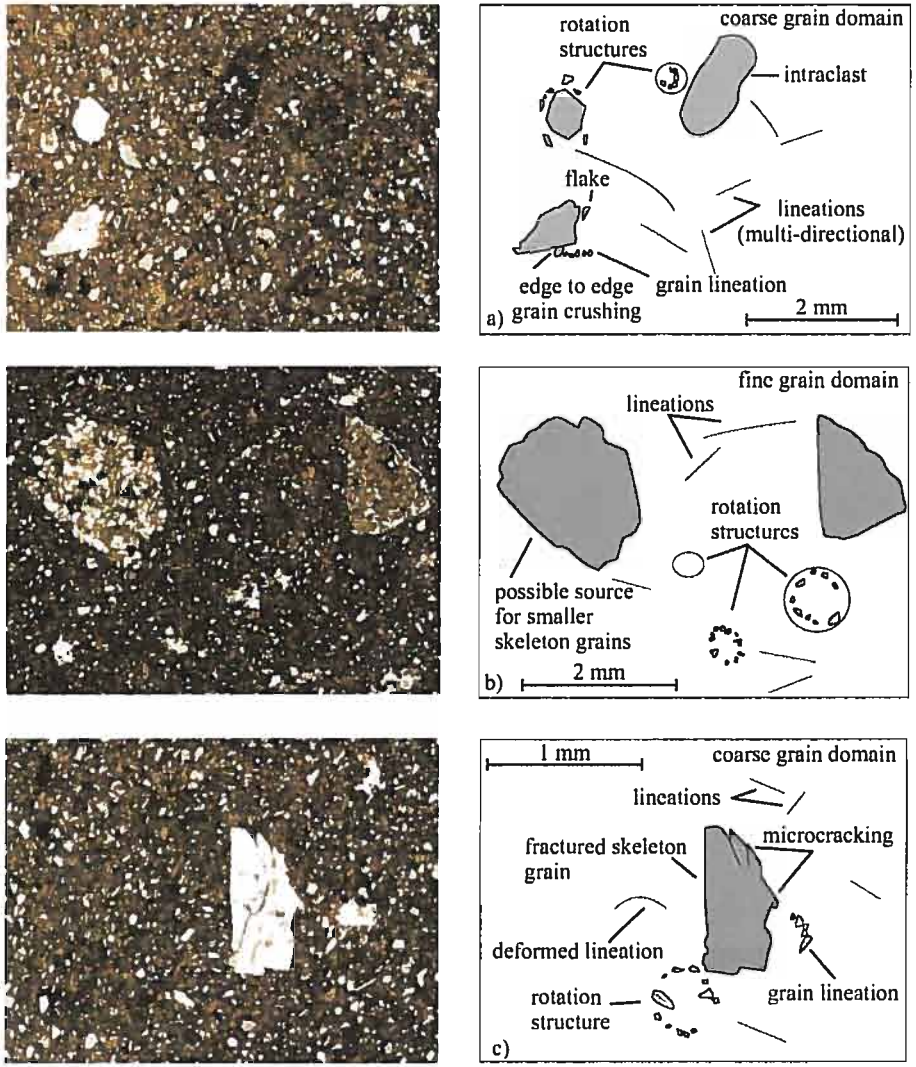

Fig. 10. Examples of structures observed in sample 2. a) structures in a coarse grain domain - rotation structures, lineations in multiple directions, edge to edge grain crushing, grain lineation. b) structures in a fine grain domain - rotation structures, lineations. c) fractured skeleton grain, rotation structures, grain lineations, lineations, deformed lineations. d) overview identifying where each example is located.

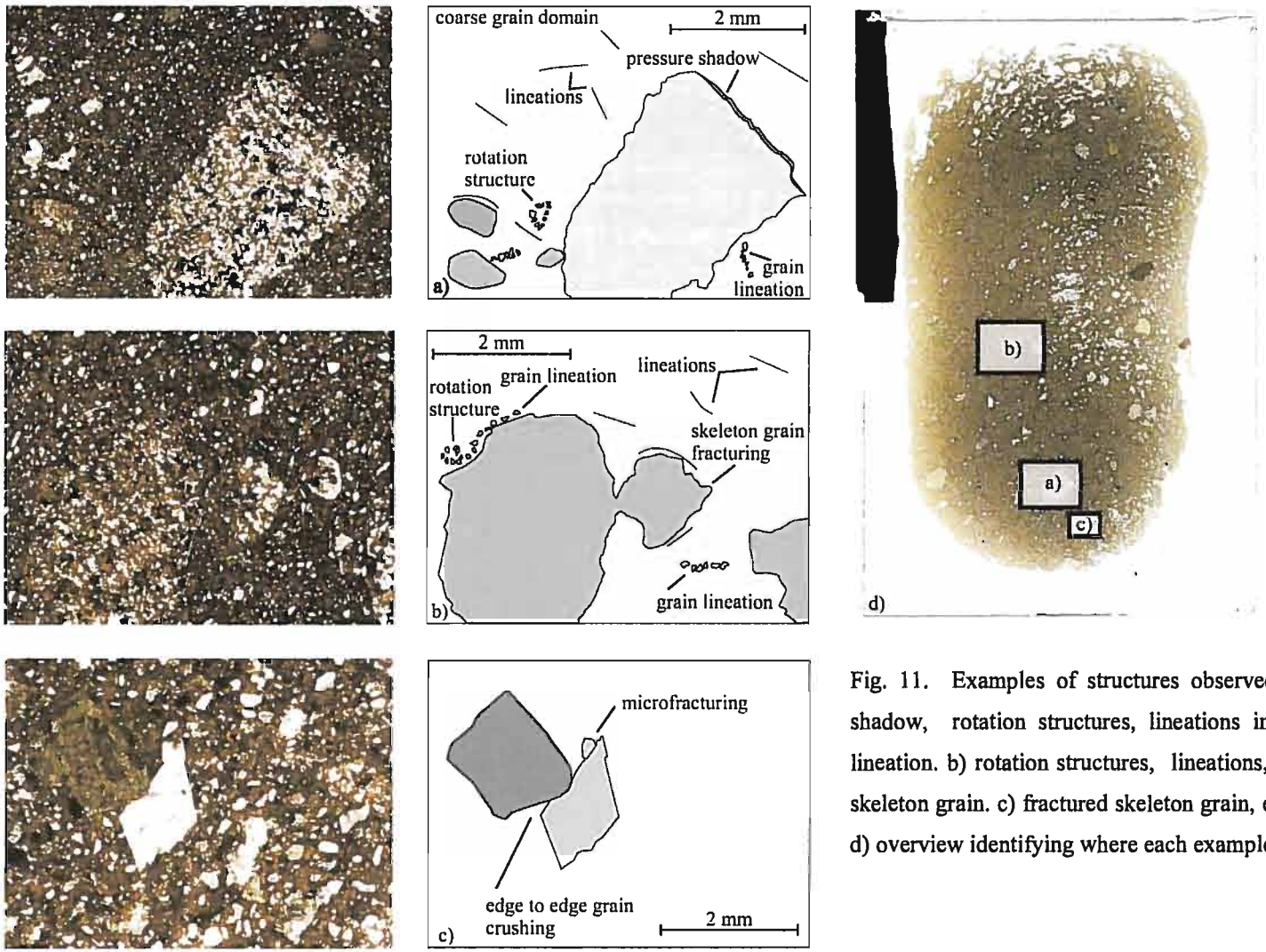

Fig. 11. Examples of structures observed in sample 2. a) pressure shadow, rotation structures, lineations in multiple directions, grain lineation. b) rotation structures, lineations, grain lineations, fracturing skeleton grain. c) fractured skeleton grain, edge to edge grain crushing. d) overview identifying where each example is located.

grains does not follow this division; rounded to angular grains are present in both fractions, with sub-angular being the common shape in both. There are intraclasts of another diamicton present in the sample (one shown in Fig. 10a)

Structure: The structures observed in the thin section are ductile deformational structures and brittle deformational structures, with no porewater structures identified. All of the structures observed occur in both the fine and coarse-grained domains. Figures 10 and 11 contain examples of the structures identified in the thin section that will be described in detail as follows. Lineations are the most abundant microstructure in the sample; they are short distance and mulit-directional (Fig. 10a-c and 11a-b). Some of the lineations have been deformed, suggesting multi-event deformation (Fig. 10c). Grain lineations are the second most common microstructure observed in the sample (Fig. 10a, c, and 11a-b), also short distance and multi-directional. Multiple rotational structures are observed with (Fig. 10a) and without (Fig. 10b-c) core stones. Plasmic fabric is weakly bimasepic and pressure shadows had developed (Fig. 11a). Skeleton grains show evidence of brittle deformation in the form of edge to edge grain crushing (Fig. 10a and 11c), microcracking, and fractures (Fig. 10c, and 11b-c). Some of the larger skeleton grains ares identified as having possibly undergone comminution, producing the smaller skeleton grain size fraction (Fig. 10b, and 11a-b). Figure 11c shows an example of skeleton grain undergoing edge to edge grain crushing with another skeleton grain of slightly larger size. The smaller skeleton grain is angular in shape with a microcrack that is almost intragranular which would produce a smaller skeleton grain if brittle deformation had continued. Figure 10c also shows a larger skeleton grain with microcracks surrounded by smaller skeleton grains of the same lithology, as does Figure 11b.

4.2 Core 61

Core 61 sampled the mid-trough of the Orleans Trough in the Western Bransfield Basin, collected by Heroy (2006). The piston core recovered a core length of 768 cm in a water depth of 591 m. A diamicton unit was sampled from 656 cm to the EOC at

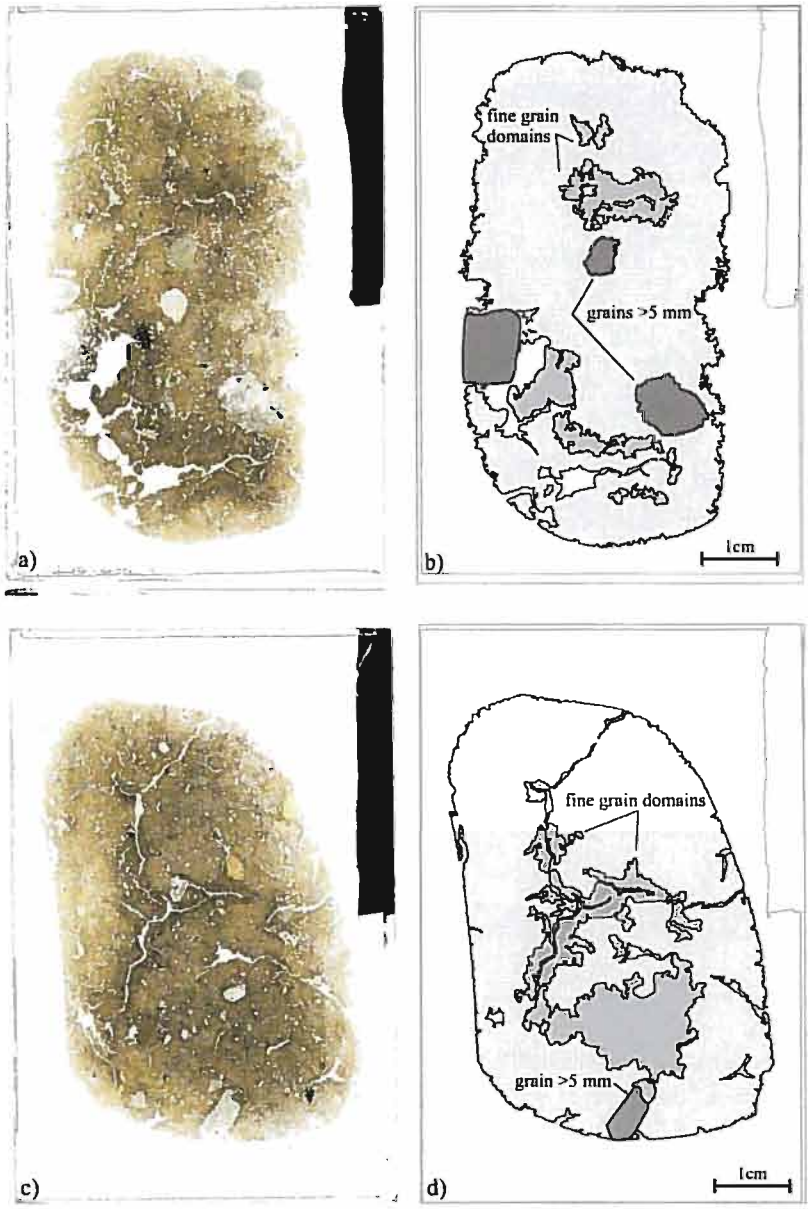

Fig. 12. Overview of samples 3 and 4 from Core 61. a) thin section of sample 3. b) overview of sample 3 displaying locations of fine grain domains and skeleton grains over 5 mm. c) thin section of sample 4. d) overview of sample 4 displaying location of fine grain domains and skeleton grain over 5 mm (AMGRF, 2002).

768 cm; no lower boundary to this unit was retrieved. Descriptions of the diamicton unit were also divided into a sediment description and an x-radiograph description (Heroy, 2006). Heroy's descriptions of the unit from 656 cm to the EOC are of a black stiff pebbly diamicton (sediment description), and as a unit of diamicton

containing 25-30% clast content, 3-8 mm with 1.5 cm common clast size (x-radiograph description).

Two samples were collected from this core for analysis at the interval of 710-720 cm, and 758-768 cm. Both samples are derived from the diamicton or black stiff pebbly diamicton unit.

No X-radiographs of core 61 were available to be compared to Heroy's (2006) macroscopic sediment and x-radiograph descriptions. The descriptions Heroy (2006) gave will be compared to the overview descriptions without reference to an x-radiograph for missed information. Sample 3 stratigraphically overlies sample 4 and both are texturally similar to each other. They are coarse-grained containing fine-grained domains and skeleton grains over 5 mm. Sample 3 contains three skeleton grains over 5 mm in the middle and lower portions of the sample, where sample 4 contains one skeleton grain over 5 mm in the bottom of the sample. The two samples, at this scale, appear to have come from the same unit. Heroy (2006) applied the descriptor 'stiff' to this unit; a more detailed description is needed to determine if any microstructures can be associated with it.

4.2.1 Detailed description of Sample 3

Texture: The sample is coarse (medium silt) grained with multiple fine (clay) grain domains that differ in size and shape (Fig. 12b). The boundaries of the fine grain domains diffuse into the coarse grain domain except in one instance. The uppermost fine grain domain has a sharp boundary on the left hand side of the domain that intersects with an intraclast but becomes diffuse on the right hand portion of the domain (Fig. 13a). All domain boundaries are identified with Nikon imaging software. There are several voids in the sample with the largest occurring in the lower portion of the sample. These are most likely processing artifacts produced during creation of the thin section and are not microstructures. There are three skeleton

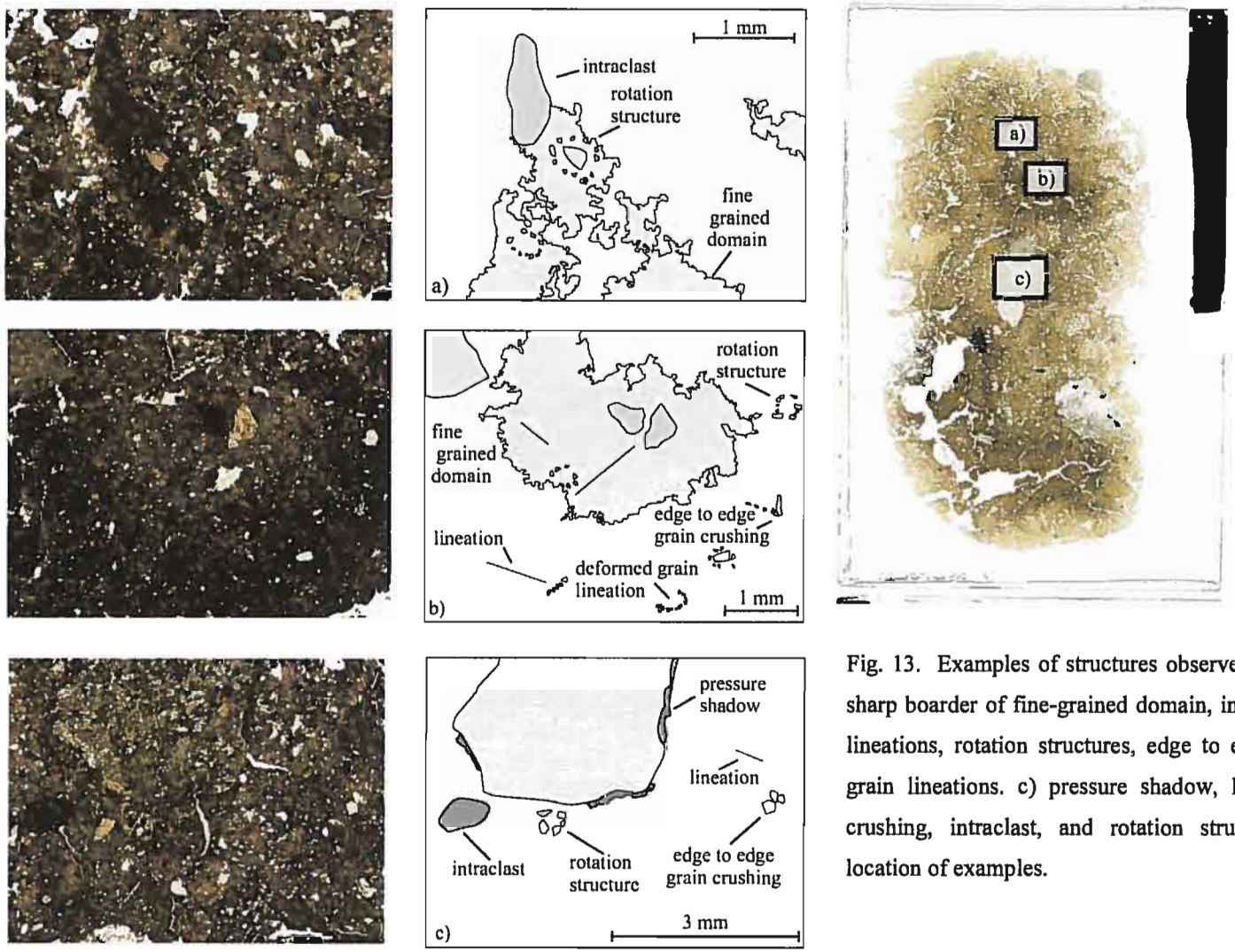

Fig. 13. Examples of structures observed in sample 3. a) diffuse and sharp boarder of fine-grained domain, intraclast, rotation structures. b) lineations, rotation structures, edge to edge grain crushing deformed grain lineations. c) pressure shadow, lineation, edge to edge grain crushing, intraclast, and rotation structure. d) overview showing location of examples.

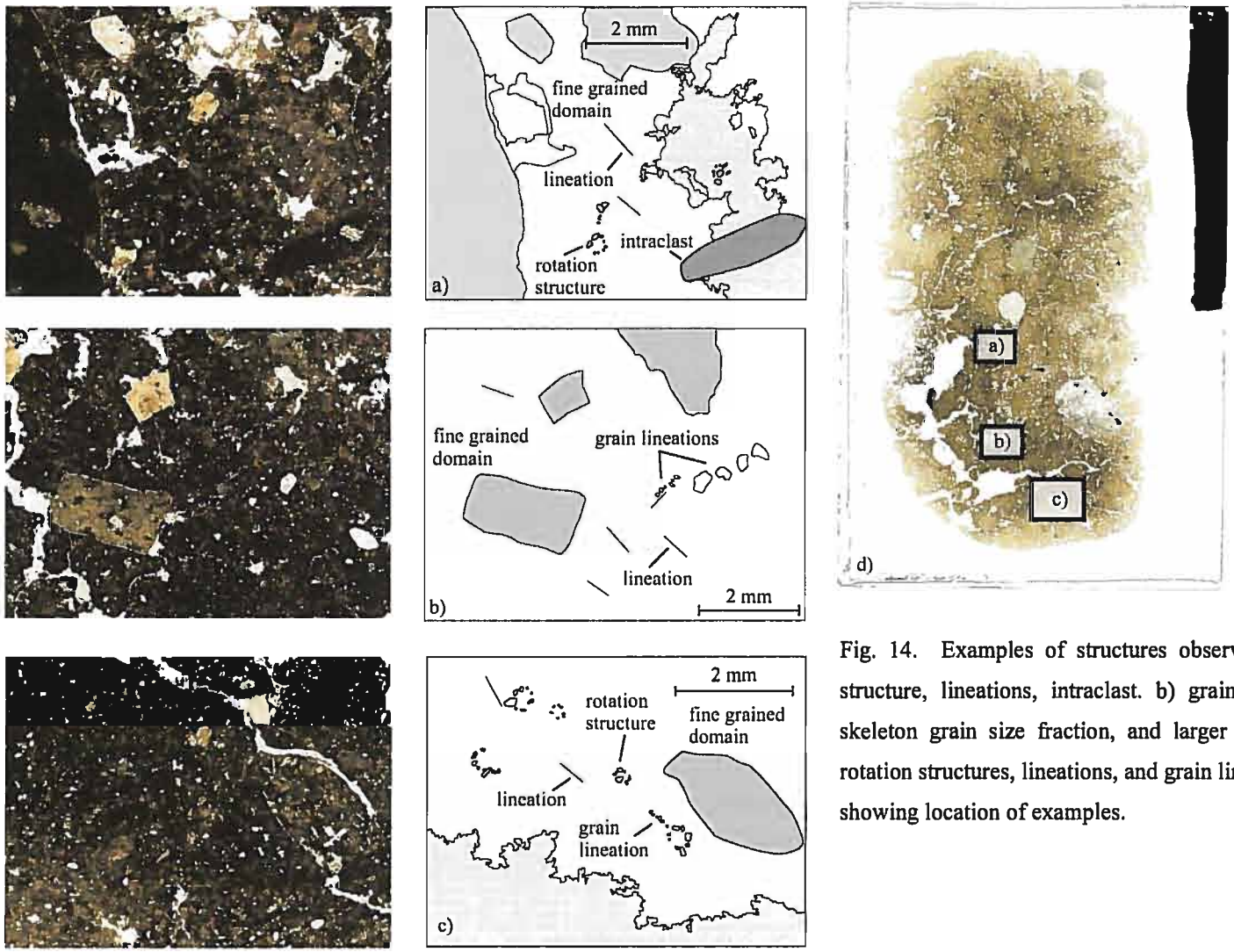

Fig. 14. Examples of structures observed in sample 3. a) rotation structure, lineations, intraclast. b) grain lineations formed by finer skeleton grain size fraction, and larger size fraction, lineations. c) rotation structures, lineations, and grain lineations. d) overview showing location of examples.

grains over 5 mm in the sample, the largest occurring in the bottom of the sample. The larger fractions of skeleton grains are mainly in the lower portion of the sample. Skeleton grain shape ranges from rounded to angular with the predominant shape being subangular. The sample contains multiple skeleton grain lithologies that are found in all the skeleton grain size fractions (see Heroy, 2006, for lithological analysis). There are intraclasts of another diamicton present in the sample (Fig. 13a, c, and 14a).

Structure: The structures observed in the thin section are ductile deformational structures and brittle deformational structures; no porewater induced structures are identified. All structures observed are located in both the fine and coarse grain domains. Figures 13 and 14 contain examples of the structures identified in the thin section described in detail below. There are abundant lineations and grain lineations in this sample. Both are short distance and multi-directional (Fig. 13b, c and 14a-c). The grain lineations are predominantly formed by the finer size fraction of the skeleton grains, with the exception of one (Fig. 14b). With the exception of pressure shadows (Fig. 13b) and the single grain lineation (Fig. 14b), the larger skeleton grain fraction didn't form any microstructures. Rotation structures are observed with and without core stones. Some lineations and grain lineations have been deformed, suggesting multi event deformation. Edge to edge grain crushing did occur (Fig. 13b-c), but is considered to be minor as only a few were observed.

4.2.2 Detailed description of Sample 4

Texture: The sample is coarse (medium silt) grained with multiple fine (clay) grained domains. There is a large semi-circular fine-grained domain in the bottom of the sample with a smaller columnar fine-grained domain radiating upwards off the left side. The columnar fine-grained domain is split in two by a void that continues along the length of the domain. This void or crack in the sample is a processing artifact. The columnar fine-grained domain branches in the middle of the sample (as does the void); with one domain continuing to the upper portion of the sample, and one

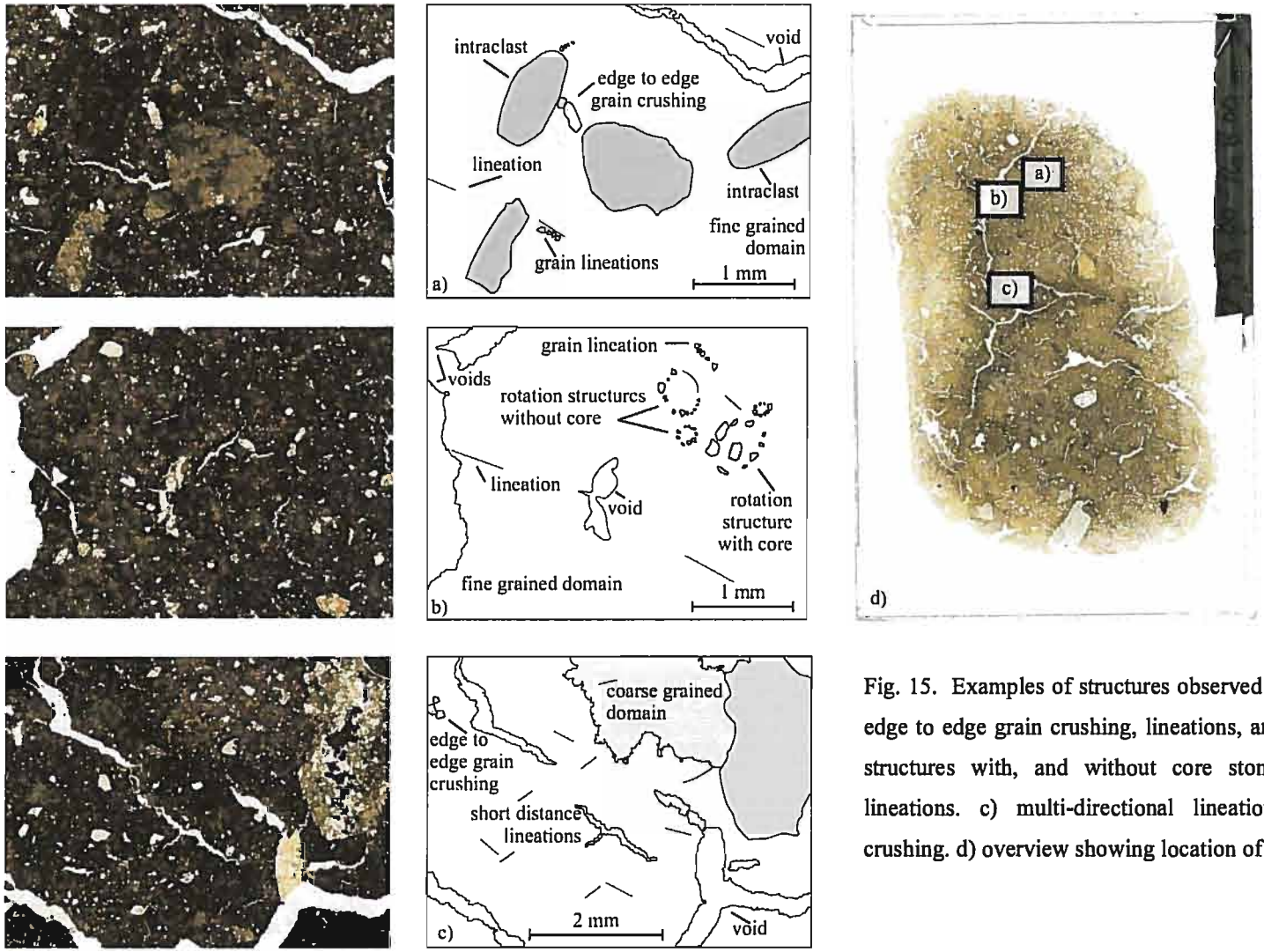

Fig. 15. Examples of structures observed in sample 4. a) intraclasts, edge to edge grain crushing, lineations, and grain stacks. b) rotation structures with, and without core stones, lineations, and grain lineations. c) multi-directional lineations, edge to edge grain crushing. d) overview showing location of examples.

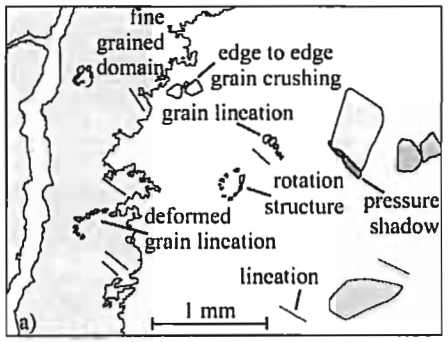

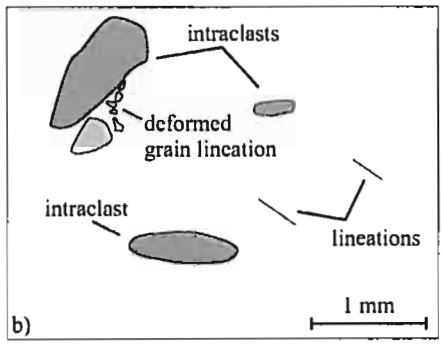

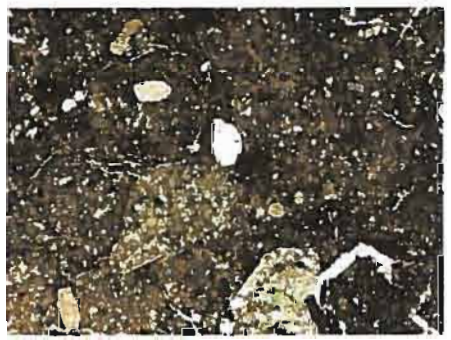

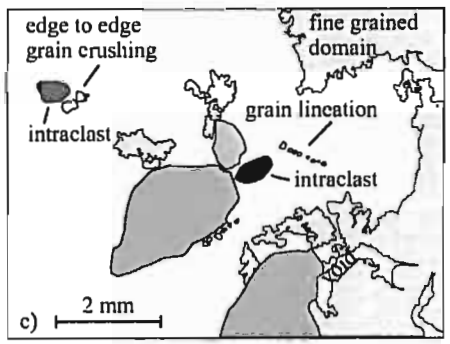

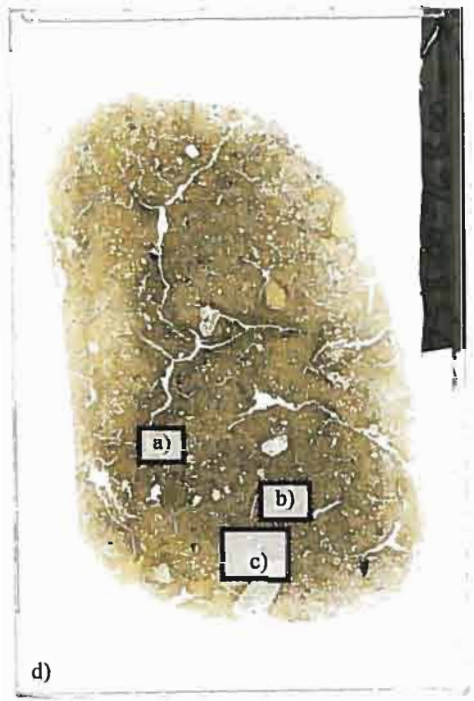

Fig. 16. Examples of structures observed in sample 4. a) rotation structures, deformed grain lineations, pressure shadow, edge to edge grain crushing, lineations. b) intra clasts, lineations, and deformed grain lineations. c) edge to edge grain crushing, grain lineations, and intraclasts. d) overview showing location of examples.

domain continuing horizontally across the sample (Fig. 12d). The boundaries of the fine grain domains are diffuse and were identified using Nikon imaging software. There is only one skeleton grain over 5 mm in the sample and it is situated at the bottom of the sample. The larger fraction of skeleton grains are found throughout the sample. The sample contains multiple lithologies; with the larger skeleton grain size fraction having a greater variety of lithologies than the smaller skeleton grain size fraction (see Heroy, 2006, for a lithological analysis). Skeleton grains range from rounded to angular, with the most subangular being the most common shape. There are several intraclasts of another diamicton present in the sample (Fig. 15a, 16b-c).

Structure: The structures observed in thin section are ductile deformational and brittle deformation structures, with no porewater induced structures observed. All the structures occur in both the fine and coarse-grained domains. Figures 15 and 16 contain examples of the structures identified in this sample. Lineations and rotation structures are the most abundant microstructure in this sample. The lineations are short distance and multi-directional (Fig. 15a-c, and 16a-b). Rotation structures are observed with and without core stones (Fig. 15b). Short distance grain lineations are common (Fig. 15a-b, and 16a-c). Some have been deformed (Fig. 16a-b), indicating multi-event deformation. Plasmic fabric is bimasepic and only a few pressure shadows occurred (Fig. 16a). Edge to edge grain crushing did occur (Fig. 15a, c, and 16a, c) but is considered a sporadic microstructure.

4.3 Core 24

Core 24 sampled a 'wedge' feature in the mid-trough off of Anvers Island, collected by Heroy (2006). The piston core recovered a core length of 314 cm in a water depth of 557 m. A diamicton unit was sampled from 200 cm to the EOC at 314 cm; no lower boundary to this unit was retrieved. Descriptions of the diamicton unit were also divided into a sediment description and an x-radiograph description by Heroy (2006), which contained contradictions.

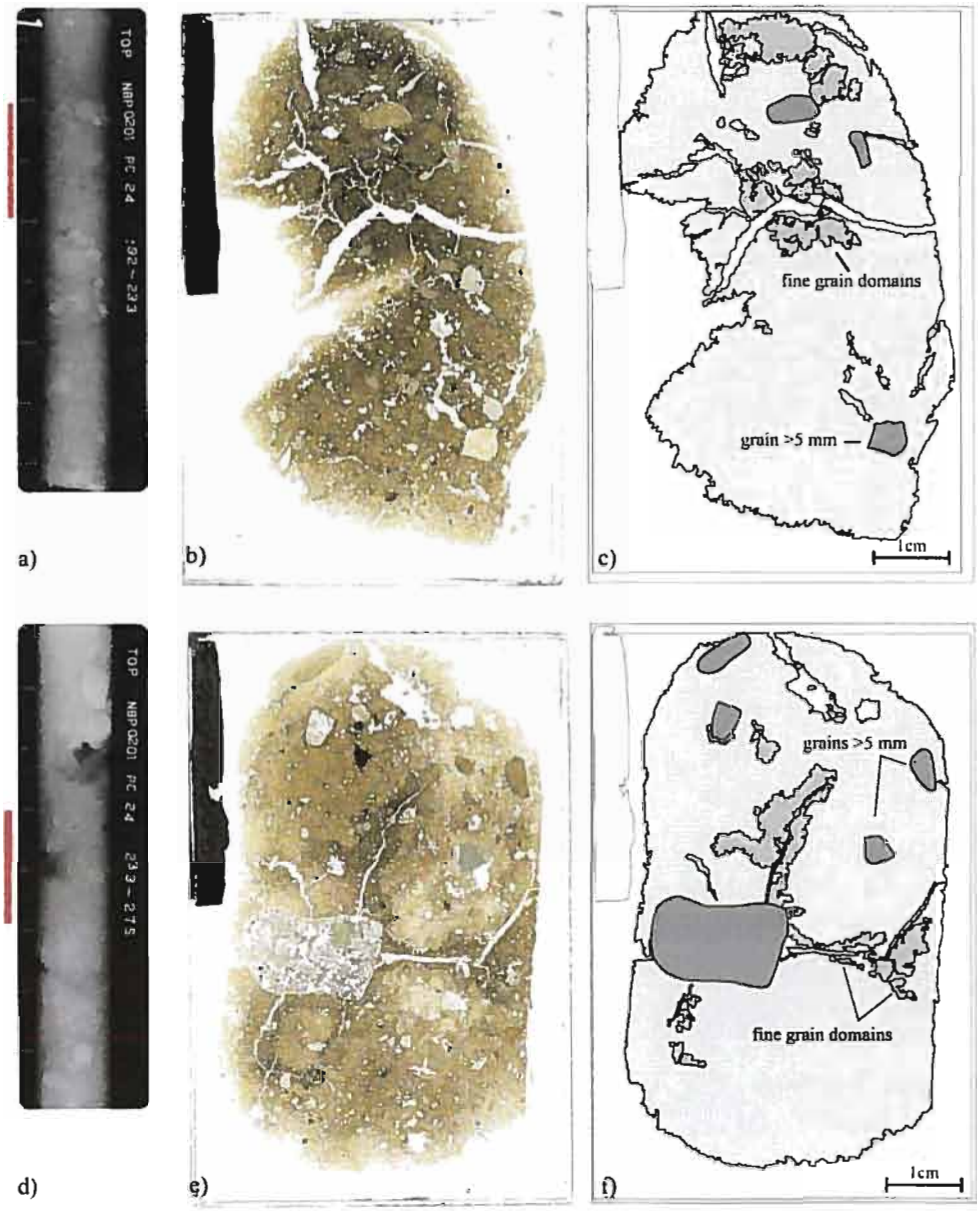

Fig. 17. Overview of samples 5 and 6 from Core 24. a) x-radiograph of section 192-233 cm of core 24, containing sample 5 at interval 200-210 cm highlighted by red bar. b) thin section of sample 5. c) overview of sample 5 displaying locations of fine grain domains and skeleton grains over 5 mm. d) x-radiograph of section 233-275 cm of core 24, containing sample 6 at interval of 250-260 cm highlighted by red bar. e) thin section of sample 6. f) overview of sample 6 displaying location of fine grain domains and skeleton grains over 5 mm (AMGRF, 2002).

Heroy's (2006) sediment description of the unit from 200-314 cm was that it was a dark grey sandy mud (no Munsell color) with increasing pebble content down core to 30%. The x-radiograph description of the same unit, 200-314 cm, was a pebbly

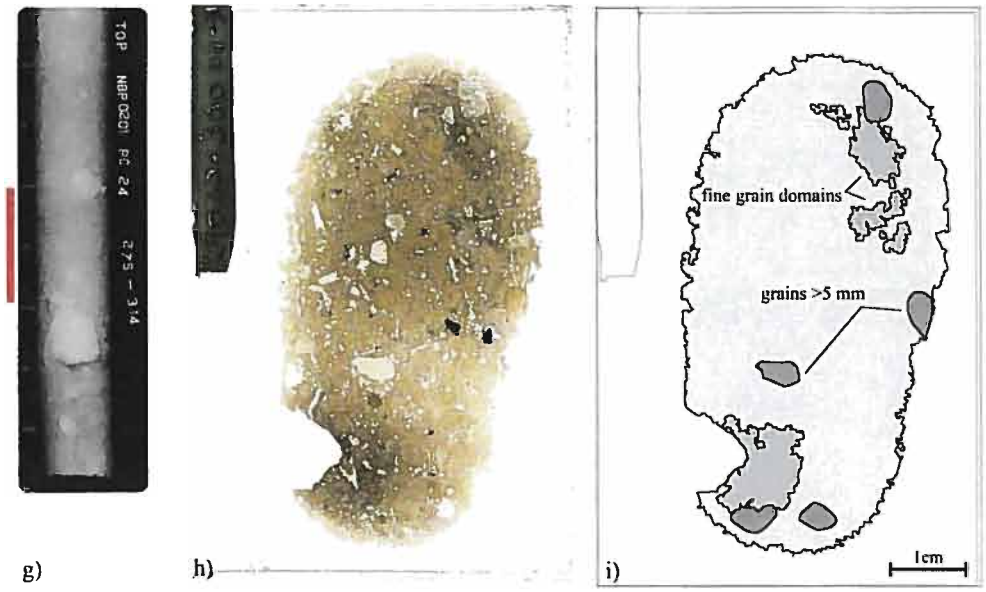

Fig. 18. Overview of sample 7 from Core 24. a) x-radiograph of section 275-314 cm of core 24, containing sample 7 at interval 290-300 cm highlighted by red bar. b) thin section of sample 7. c) overview of sample 7 displaying locations of fine grain domains and skeleton grains over 5 mm (AMGRF, 2002).

diamicton with 30-50% pebble content of 2-10 mm average size, the largest being 4.5 cm, with no laminations present in the unit. Three samples were collected from this core for analysis at the interval of 200-210 cm (sample 5), 250-260 cm (sample 6), and 290-300 cm (sample 7). All samples fall into the same macroscopic descriptions that Heroy (2006) gave for this unit.

X-radiographs of core 24 were obtained as a means to compare Heroy's (2006) macroscopic core descriptions to the overview description of the thin section samples from this core. Sample 5 stratigraphically overlies sample 6 which overlies sample 7, and though all were obtained from the same 'unit' there are some dissimilarities that would suggest otherwise. Texturally sample 5 (Fig. 17a-c), sample 6 (Fig. 17d-f) and sample 7 (Fig. 18a-c) are similar; coarse-grained with fine-grained domains. What differentiates them is the distribution of the fine-grained domains. In samples 6 and 7 the fine grain domains are randomly distributed or sporadic. Sample 5, however, has a top to bottom distribution. The thin sample goes from a fine-grained domain at the top to a coarse-grained domain, then a fine-grained domain in the middle of the

sample to a coarse-grained domain at the bottom, which contains more skeleton grains than the previous coarse-grained domain. There are also lithologies present in sample 5 in abundance that are near absent in samples 6 and 7. Increasing pebble content down core is not observed in the sample overview, as sample 7 does not contain more skeleton grains than sample 5

4.3.1 Detailed description of Sample 5

Texture: The sample is coarse (medium to coarse silt) grained with multiple fine (clay) grained domains. The fine-grained domains are in the upper half of the sample, and can be grouped into two major clusters, with a few sporadic domains dispersed between the two clusters. The upper cluster, located at the top of the sample, contains a horizontal domain that nearly transects the top of the sample with three smaller semi circular domains that arc downwards off the bottom right side. Voids, processing artifacts, separate these domains, and will henceforth be referred to as a singular fine-grained domain. The second major cluster, located in the middle of the sample a third of the way down, is comprised of several smaller fine grain domains that together form a circular shape. A large void that transects the sample, also transects this circular cluster of fine grain domains. This void is most likely a processing artifact. Processing artifacts are prevalent in this thin section, with multiple cracks, and partial removal of the sample in the middle left side of the sample due to over-grinding. All of the fine grain domains have irregular, diffuse boundaries and are identified with Nikon imaging software (Fig. 17). There are three skeleton grains over 5 mm, randomly distributed in the sample. The skeleton grains range from rounded to angular in shape, with the most common shape being sub-angular. The skeleton grains are composed of multiple lithologies that are found in all skeleton grain size fractions. In addition to intraclasts of another diamicton, there are skeleton grains of a lithology not found in the other samples of this core (top right corner of Fig. 19b).

Structure: The structures observed in the thin section are mostly ductile deformational structures, with one type of brittle deformational structure; no porewater structures

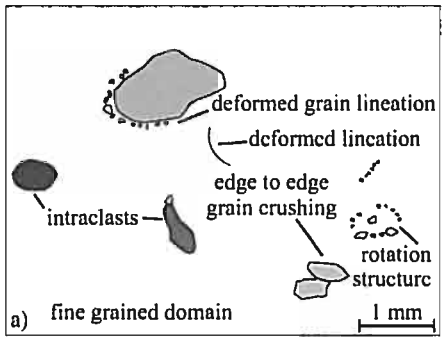

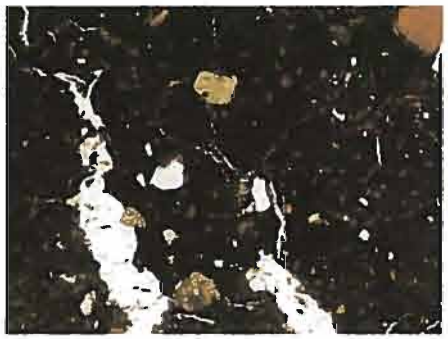

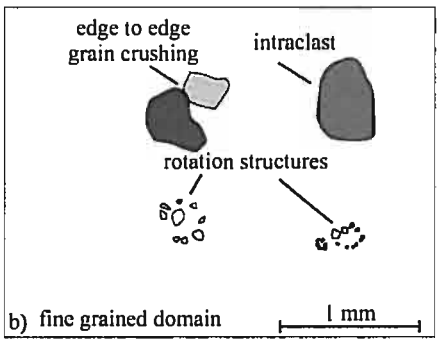

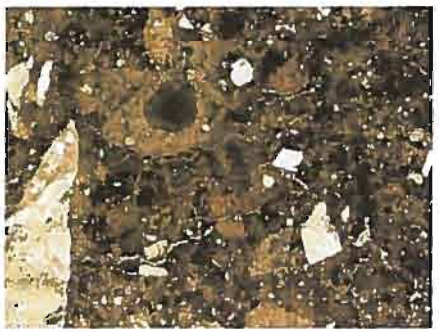

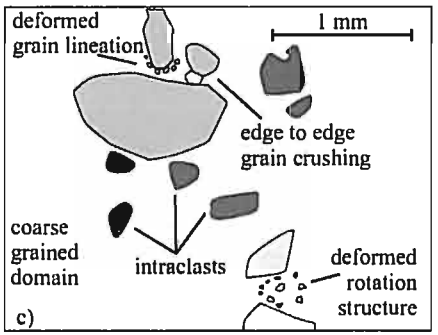

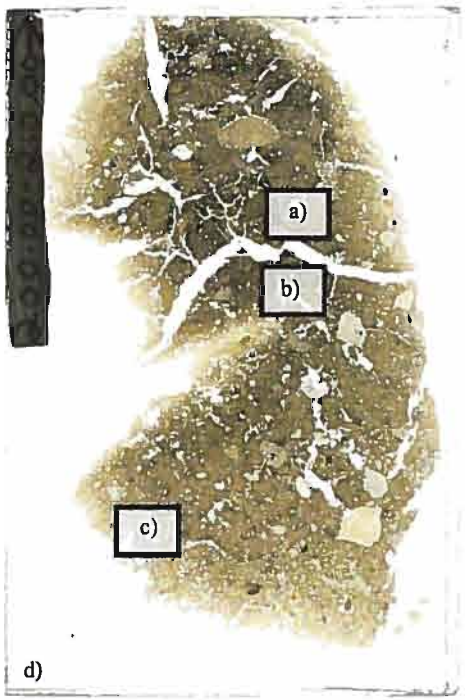

Fig. 19. Examples of structures observed in sample 5. a) deformed lineations and grain lineations, rotation structures, edge to edge grain crushing and intraclasts. b) edge to edge grain crushing, rotation structures and intra clasts. c) deformed grain lineations, edge to edge grain crushing, intraclasts, deformed rotation structure. d) overview showing location of examples.

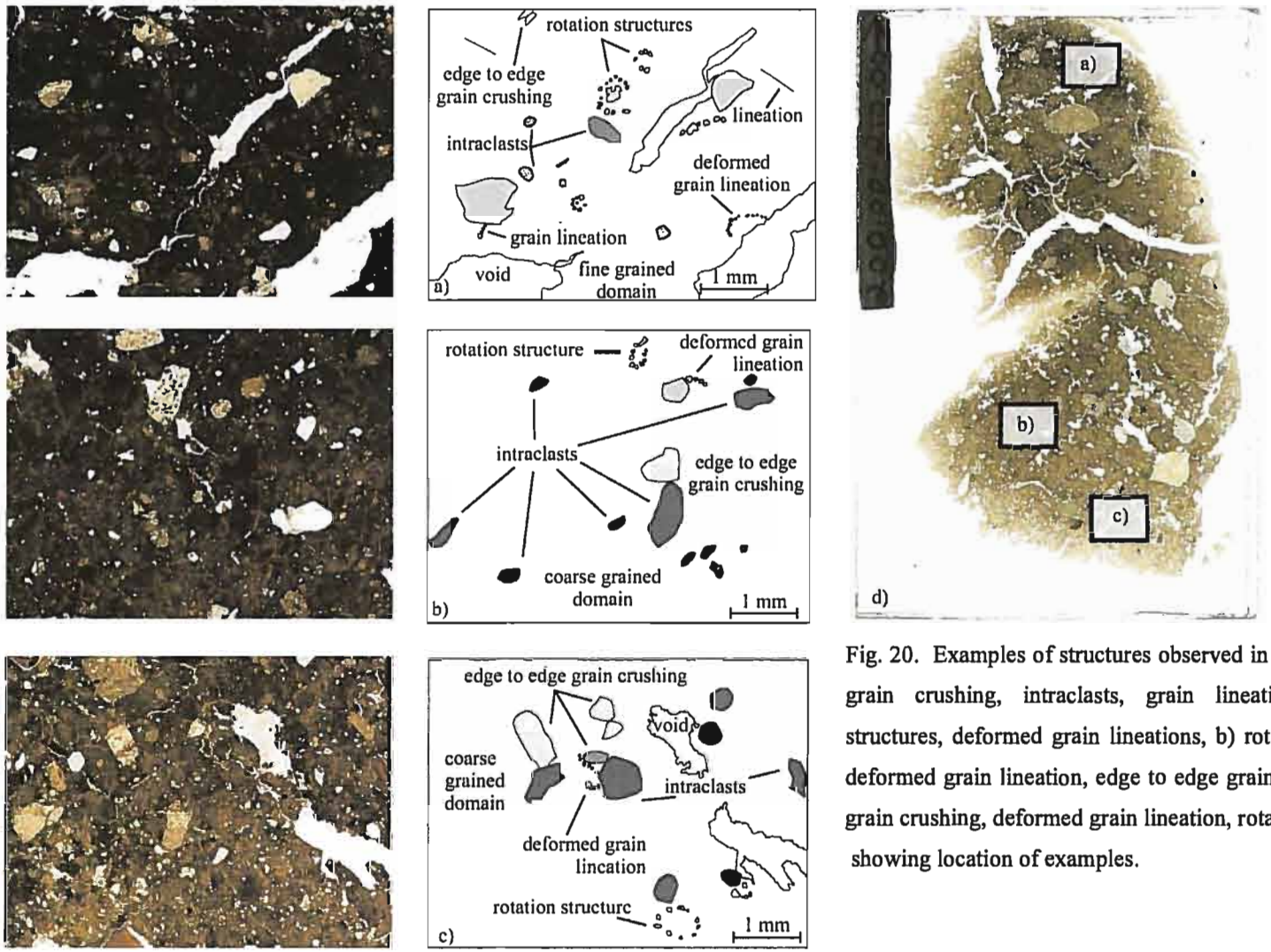

Fig. 20. Examples of structures observed in sample 5. a) edge to edge grain crushing, intraclasts, grain lineations, lineations, rotation structures, deformed grain lineations, b) rotation structure, intraclasts, deformed grain lineation, edge to edge grain crushing. c) edge to edge grain crushing, deformed grain lineation, rotation structure. d) overview showing location of examples.

were identified. All the structures are observed in both the fine and coarse-grained domains. Figures 19 and 20 contain examples of the structures identified in the thin section that are described in detail below. Grain lineations, rotation structures, and edge to edge grain crushing are the most common structures observed. The grain lineations are short and multi-directional; some have been subsequently deformed (Fig. 19a, and 20a-c). Rotation structures mostly occur in the finer grain size fraction, with and without core stones (Fig. 19a-c). There is a prevalence of intraclasts that formed microstructures, including grain crushing, grain lineations, and rotation structures (Fig 19a-b and 20b-c). Short distance lineations, a brittle deformation structure, are observed but were infrequent (Fig 19a, and 20a); some have been deformed suggesting multi-event deformation.

4.3.2 Detailed description of Sample 6

Texture: The sample is coarse (medium silt) grained with multiple fine (clay) grained domains radiating out from the largest skeleton grain in the sample, located in the middle left of the sample. The fine grain domains contain voids that radiate outwards from the largest skeleton grain; it is thought that these voids are formed during sample preparation, with uneven drying causing a crack in the densest portions of the sample (Fig. 17). The boundaries of the fine grain domains are easily identified in most cases, but Nikon imaging software is used to define them as a few are diffuse, and for consistency. There are five skeleton grains over 5 mm; four are similar in size ~7.5 mm, with the largest being 1.643 cm. Skeleton grain shape ranges from rounded to angular, with subangular being the most common. The skeleton grains are composed of multiple lithologies found in all size fractions, but the smaller size fraction contains less variability than the larger fraction. Intraclasts of another diamicton are present in the sample (21a-b, and 22a-b).

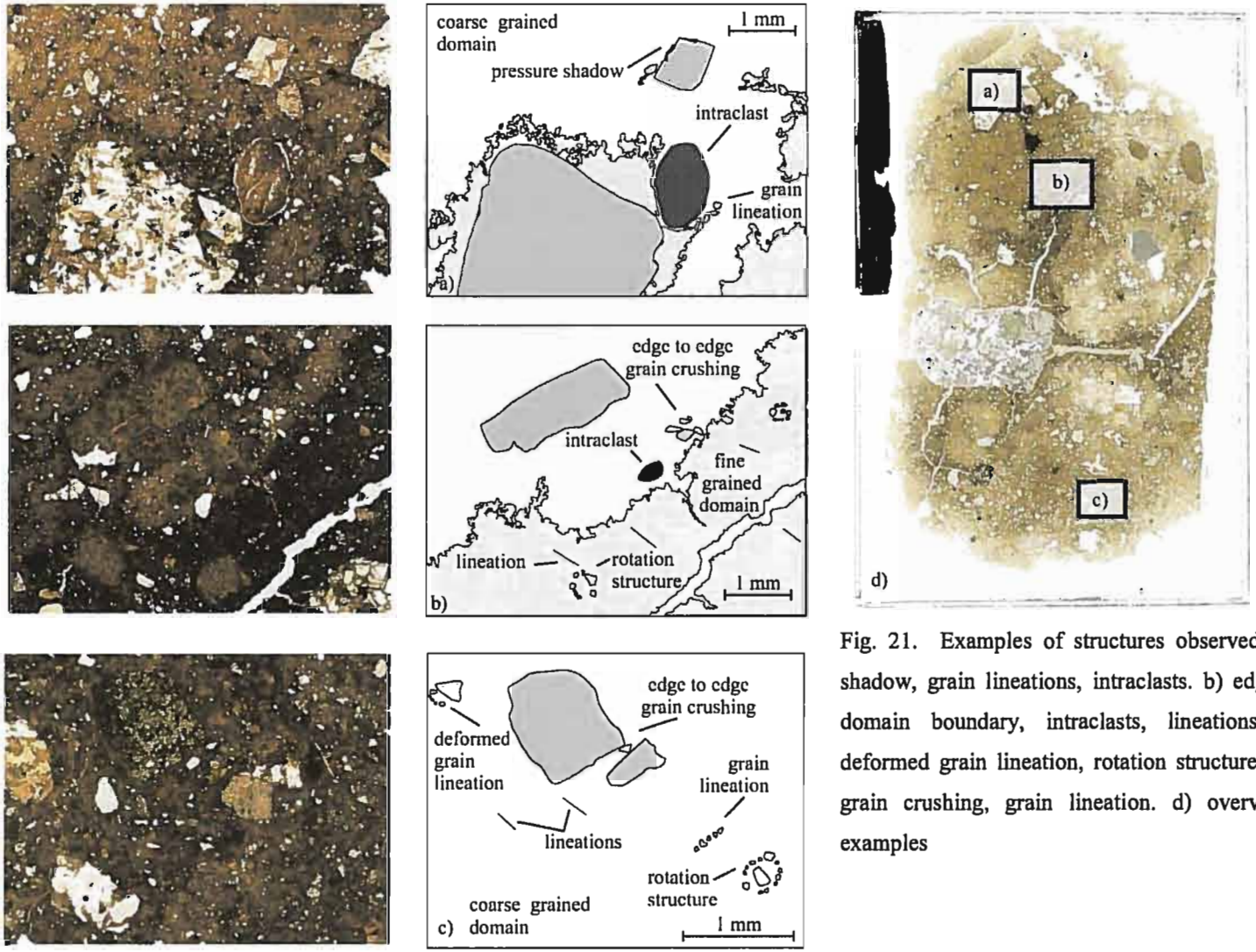

Fig. 21. Examples of structures observed in sample 6. a) pressure shadow, grain lineations, intraclasts. b) edge to edge grain crushing, domain boundary, intraclasts, lineations, rotation structures. c) deformed grain lineation, rotation structures, lineations, edge to edge grain crushing, grain lineation. d) overview showing location of examples

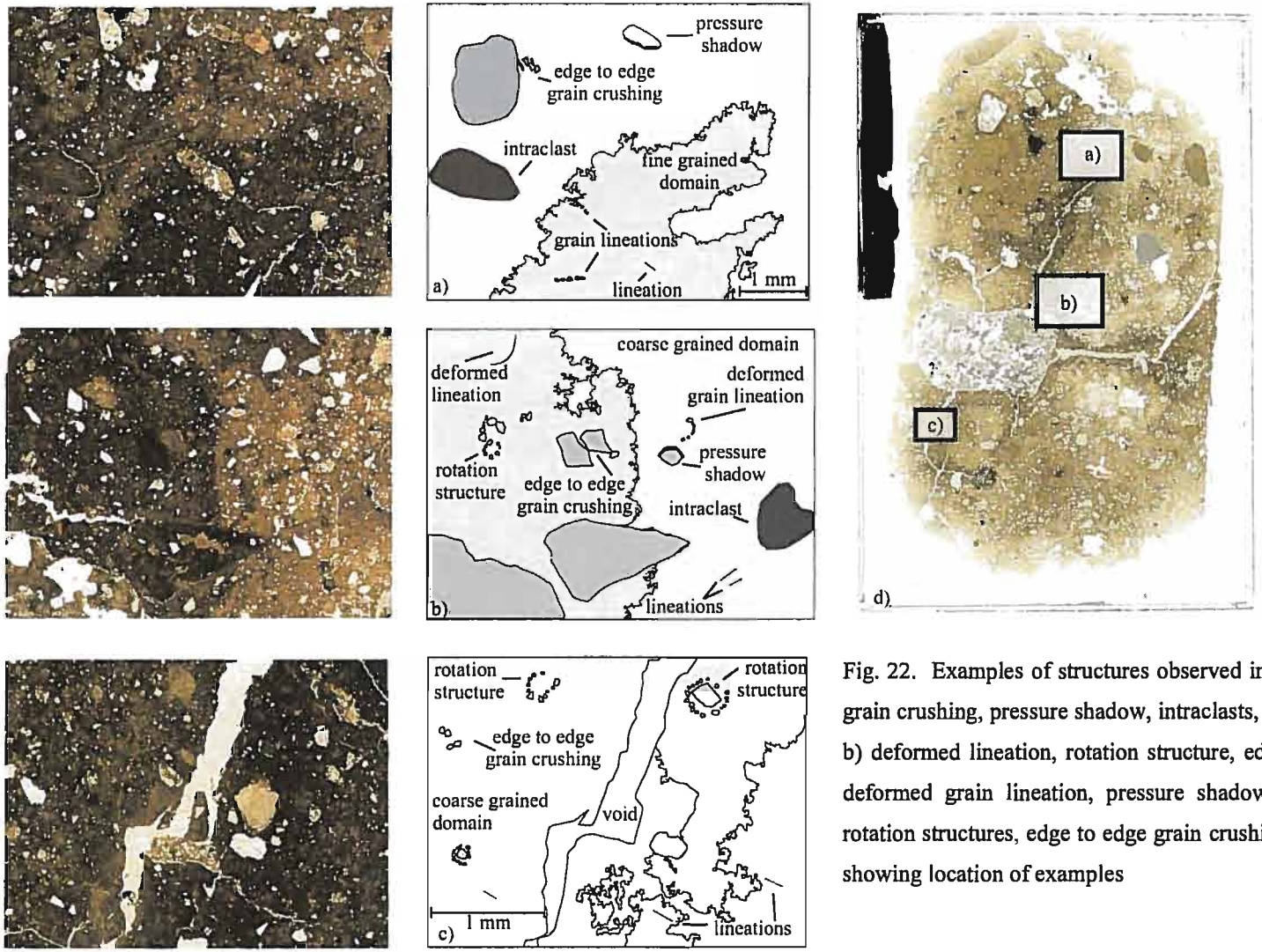

Fig. 22. Examples of structures observed in sample 6. a) edge to edge grain crushing, pressure shadow, intraclasts, grain lineations, lineations. b) deformed lineation, rotation structure, edge to edge grain crushing, deformed grain lineation, pressure shadow, lineation, intraclasts. c) rotation structures, edge to edge grain crushing, lineations. d) overview showing location of examples

Structure: The structures observed in the thin section are ductile deformational and brittle deformational structures; no porewater induced structures were observed. All structures occur in both the coarse and fine grain domains. Figures 21 and 22 contain examples of the structures identified in the sample that will be described in detail below. The most abundant microstructure observed are lineations and grain lineations. Both are short distance and multi-directional (Fig. 21a-c, and 22a-c). Some of the grain lineations and lineations are found deformed, indicating multi-event deformation (Fig. 22b). Rotation structures, with and without core stones, are common (Fig. 21c, and 22b-c). Edge to edge grain crushing is observed (Fig. 21b-c, and 22a-c). Pressure shadows do occur infrequently (Fig. 21a, and 22a-b).

4.3.3. Detailed description of Sample 7

Texture: The sample is coarse (medium to coarse silt) grained with multiple fine (clay) grain domains. The fine grain domains are semi-circular in shape and are located in the top right and bottom left of the sample. The boundaries are diffuse and irregular, and are identified using Nikon imaging software. There are five skeleton grains over 5 mm, randomly distributed throughout the sample (Fig. 18). Skeleton grains range from rounded to angular in shape, with subangular the most common. The sample contains multiple lithologies found in all size fractions, although the smaller size fraction contains less variety of lithologies (see Heroy, 2006, for lithological analysis of entire diamicton section of core). There are intraclasts of another diamicton present in the sample (Fig. 23b, 24a, and c).

Structure: The microstructures observed in thin section are ductile and brittle deformational structures, with no porewater induced structures were observed. All structures occur in both the coarse and fine grain domains. Figures 23 and 24 contain examples of the microstructures observed that will be discussed in detail as follows. Lineations and grain lineations are the most abundant microstructure observed. Both are observed to be short distance, multi-directional, and some had undergone

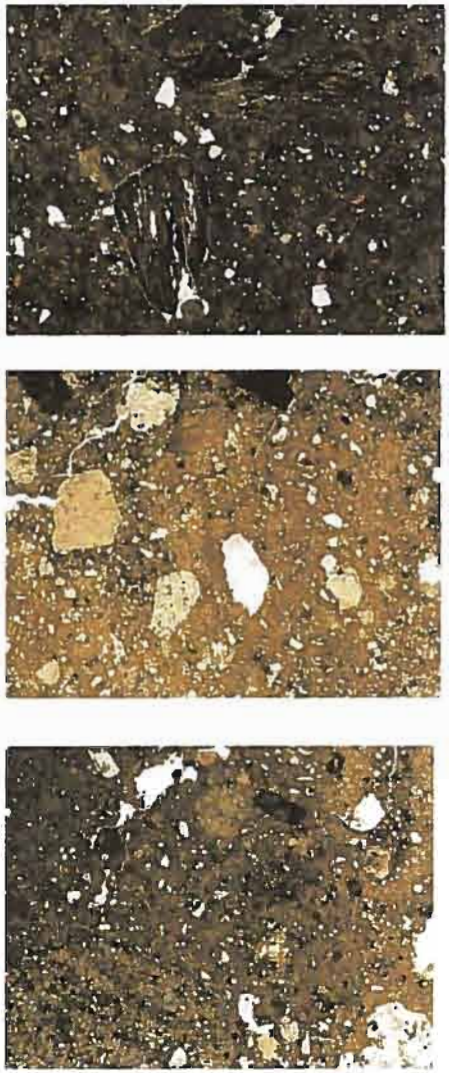

Fig. 23. Examples of structures observed in sample 7. a) edge to edge grain crushing, grain lineations, rotation structures, lineations. b) rotation structures, edge to edge grain crushing, grain lineation, lineation, intraclast. c) rotation structures, grain lineations, deformed grain lineations, lineations. d) overview showing location of examples

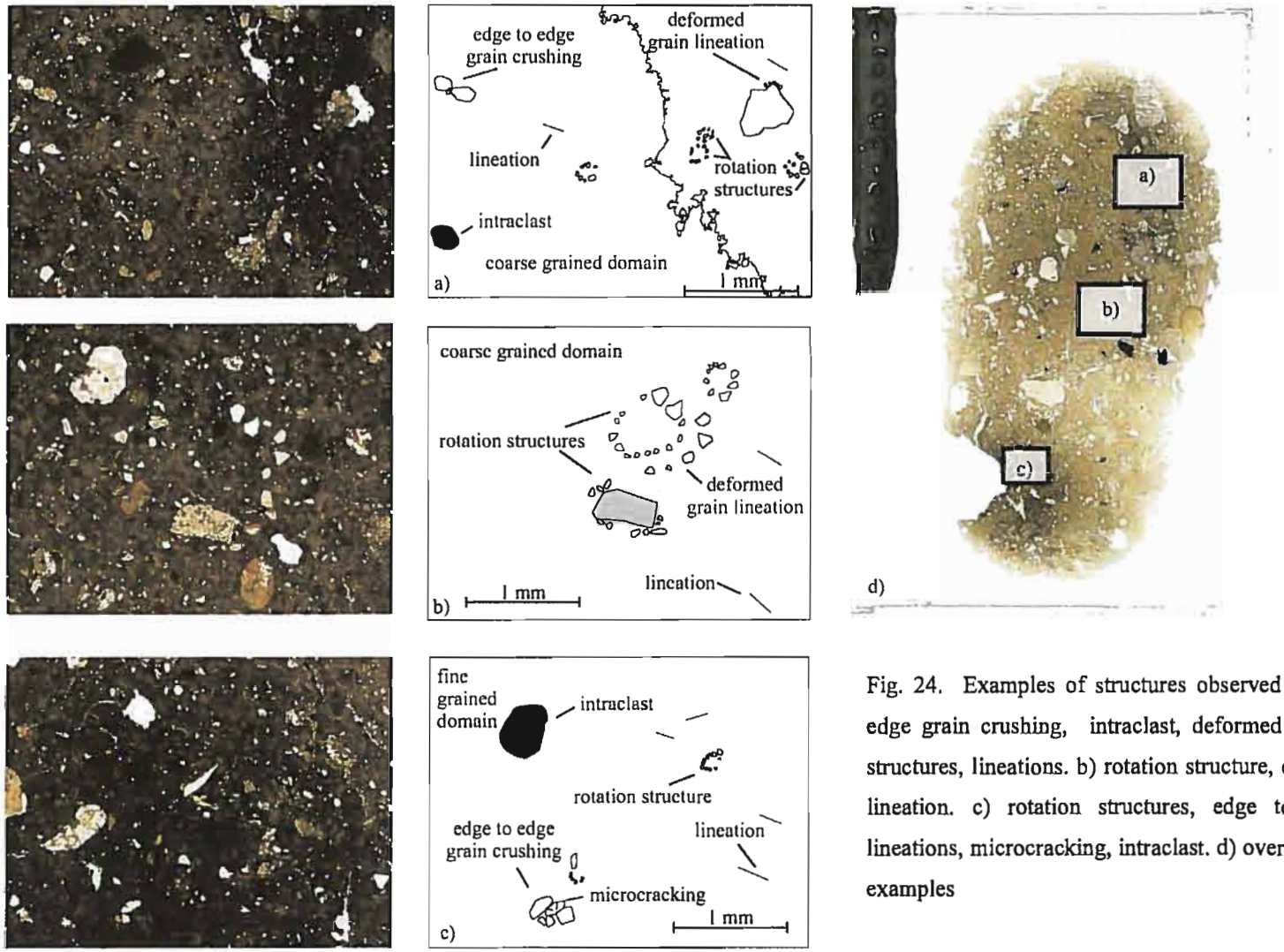

Fig. 24. Examples of structures observed in sample 7. a) edge to edge grain crushing, intraclast, deformed grain lineation, rotation structures, lineations. b) rotation structure, deformed grain lineation, lineation. c) rotation structures, edge to edge grain crushing, lineations, microcracking, intraclast. d) overview showing location of examples

subsequent deformation (Fig. 23a-c, and 24a-c). Rotational structures are observed with and without core stones (Fig. 23a-c, and 24a-c). Edge to edge grain crushing is common. Noted examples of this structure are found in Fig. 23b, and Fig. 24c. The former shows a skeleton grain embedded in an intraclast, and is believed to have been in the process of dividing the intraclast in two. The latter shows edge to edge grain crushing that resulted in microcracks in one of the skeleton grains.

4.4 Core 57

Core 57 sampled the inner shelf of Bisco Trough and was collected by Heroy (2006). The piston core recovered a core length of 324 cm in a water depth of 732 m. A diamicton unit was sampled from 69 cm to the EOC at 324 cm; no lower boundary to this unit was retrieved. Descriptions of the diamicton unit were also divided into a sediment description and an x-radiograph description by Heroy (2006).

Heroy (2006) describes the sediment from 69-110 cm as soft grey diamicton with a sharp upper contact that grades at the unit's lower contact into a sandy pebbly mud layer between 110-120 cm. This then grades into a soft grey diamicton that continues to the EOC, gradually increasing in stiffness down core. Heroy's (2006) x-radiograph description is of a pebbly clast supported mud is described at 54-80 cm; 15 cm up-core of where the soft grey diamicton is stated to be and extending into the 'soft grey diamicton' unit, so a separate unit is not being identified. From 80-95 cm are laminated sand and mud. Then from 95 cm to EOC is a pebble rich diamicton, with 30-50% clast content, showing neither fabric nor laminations.

Three samples were collected from this core for analysis at the interval of 100-110 cm (sample 8), 150-160 cm (sample 9), and 250-260 cm (sample 10). Sample 8 is described by Heroy (2006) as sampling a soft grey diamicton unit or a pebble rich diamicton. The unit from which both samples 9 and 10 are derived from is described as soft grey diamicton with increasing stiffness down core, and as a pebble rich diamicton.

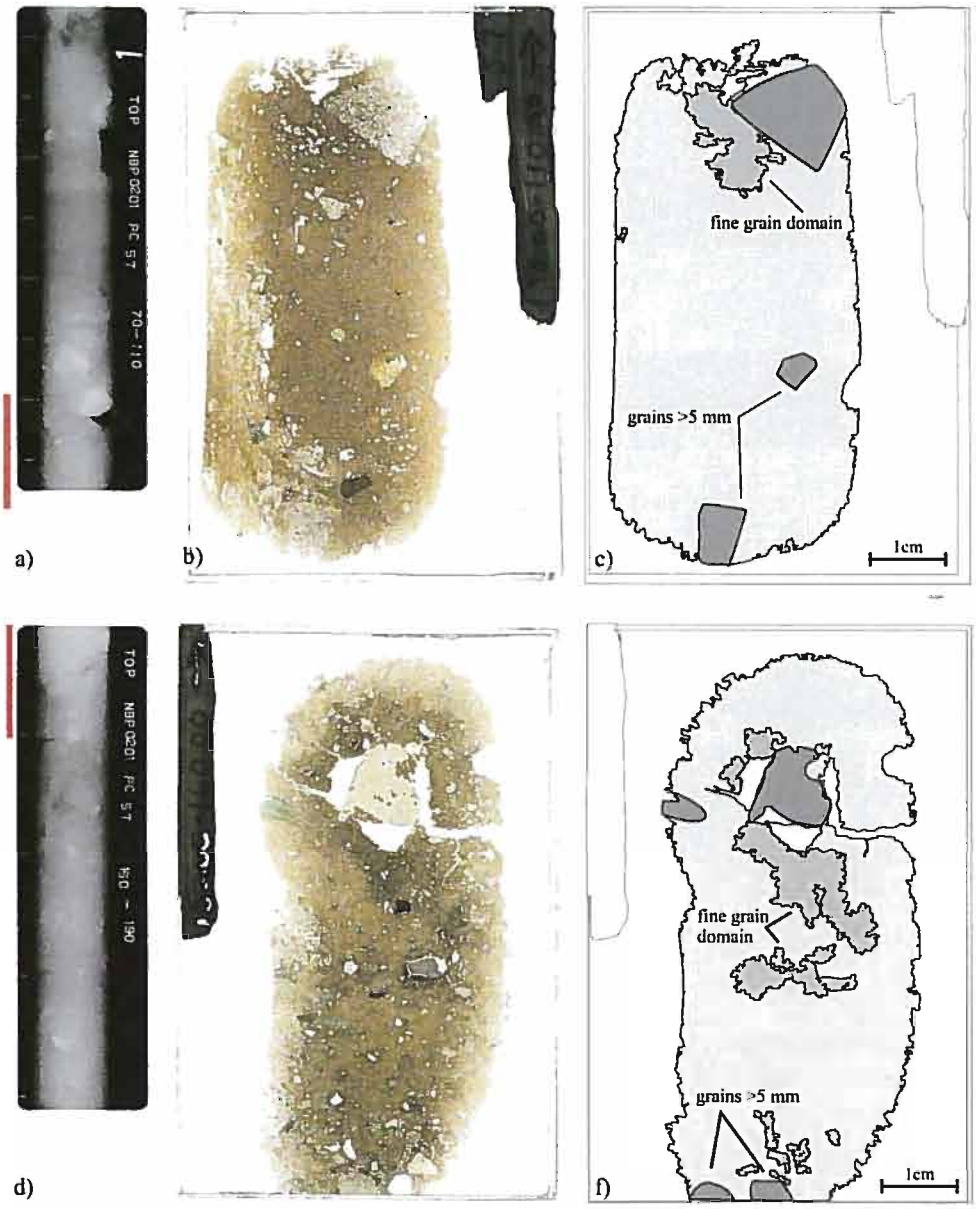

Fig. 25. Overview of samples 8 and 9 from Core 57. a) x-radiograph of section 170-110 cm of core 57, containing sample 8 at interval 100-110 cm highlighted by red bar. b) thin section of sample 8. c) overview of sample 8 displaying locations of fine grain domain and skeleton grains over 5 mm. d) x-radiograph of section 150-190 cm of core 57, containing sample 9 at interval of 150-160 cm highlighted by red bar. e) thin section of sample 9. f) overview of sample 9 displaying location of fine grain domains and skeleton grains over 5 mm (AMGRF, 2002).

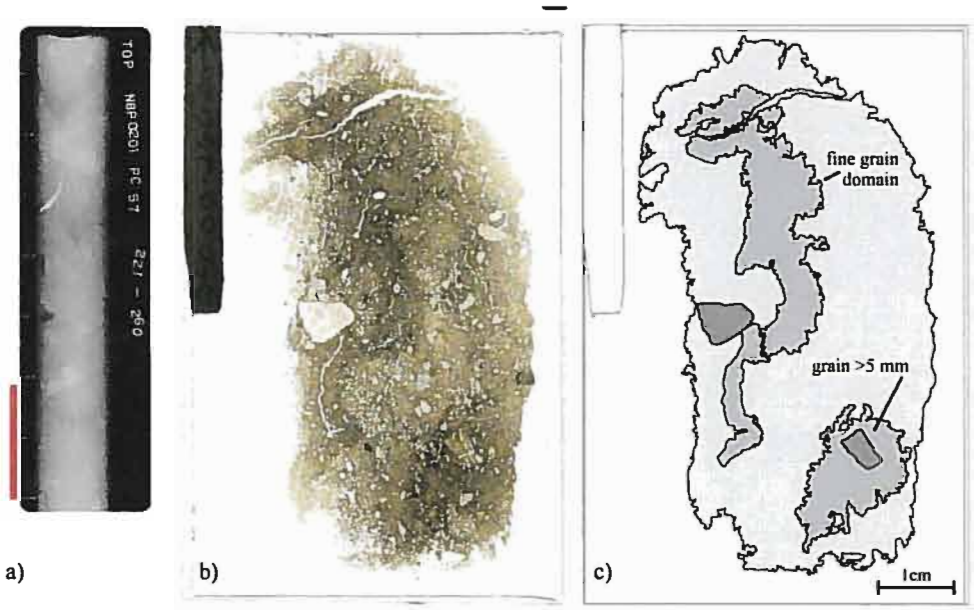

Fig. 26. Overview of sample 10 from Core 57. a) x-radiograph of section 221-260 cm of core 57, containing sample 10 at interval 25-260 cm highlighted by red bar. b) thin section of sample 10. c) overview of sample 10 displaying locations of fine grain domains and skeleton grains over 5 mm (AMGRF, 2002).

X-radiographs of core 57 were obtained as a means to compare Heroy's (2006) macroscopic core, and x-radiograph descriptions to the overview description of the thin section samples from this core. Sample 8 stratigraphically overlies sample 9 which overlies sample 10, and according to Heroy (2006) all samples come from units described as soft grey diamicton/pebble rich diamicton. Sample 8 is visually distinct and dissimilar in all regards from samples 9 and 10 as if they have been sampled from separate units (Fig. 25 and 26). Sample 8 is comparatively coarser grained than samples 9 and 10, with fewer fine grain domains, a more uniform clast shape and size, and less variation in skeleton grain lithology.

4.4.1 Detailed description of Sample 8

Texture: Sample 8 is coarse (coarse silt) grained with a single fine (clay) grained domain (Fig. 25c). The fine grain domain is located at the top of the sample, on the left of the largest skeleton grain in the sample. The fine grain domain has irregular boundaries that diffuse into the coarse grain domain and Nikon imaging software is

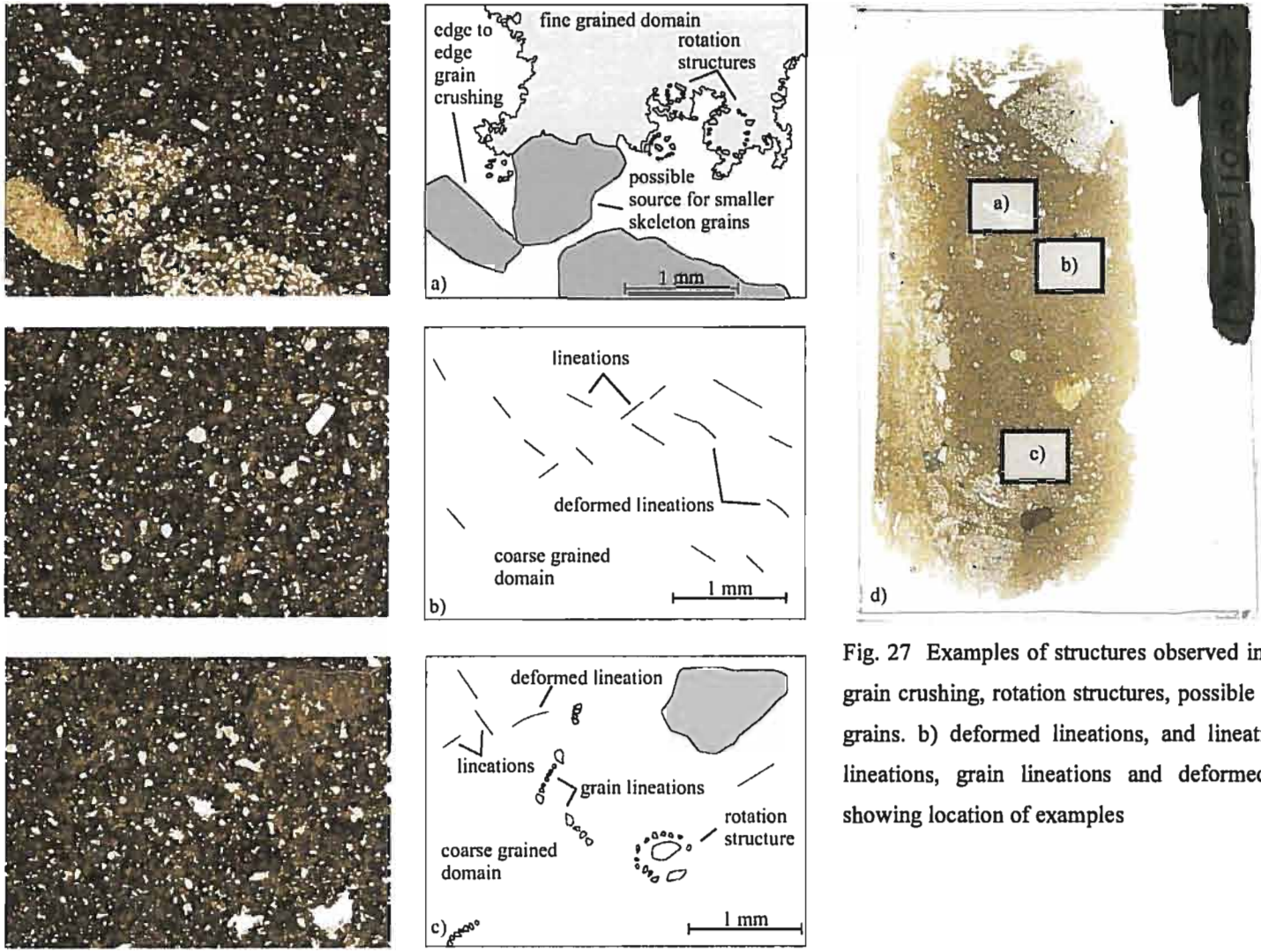

Fig. 27 Examples of structures observed in sample 8. a) edge to edge grain crushing, rotation structures, possible source for smaller skeleton grains. b) deformed lineations, and lineations. c) rotation structure, lineations, grain lineations and deformed lineations. d) overview showing location of examples

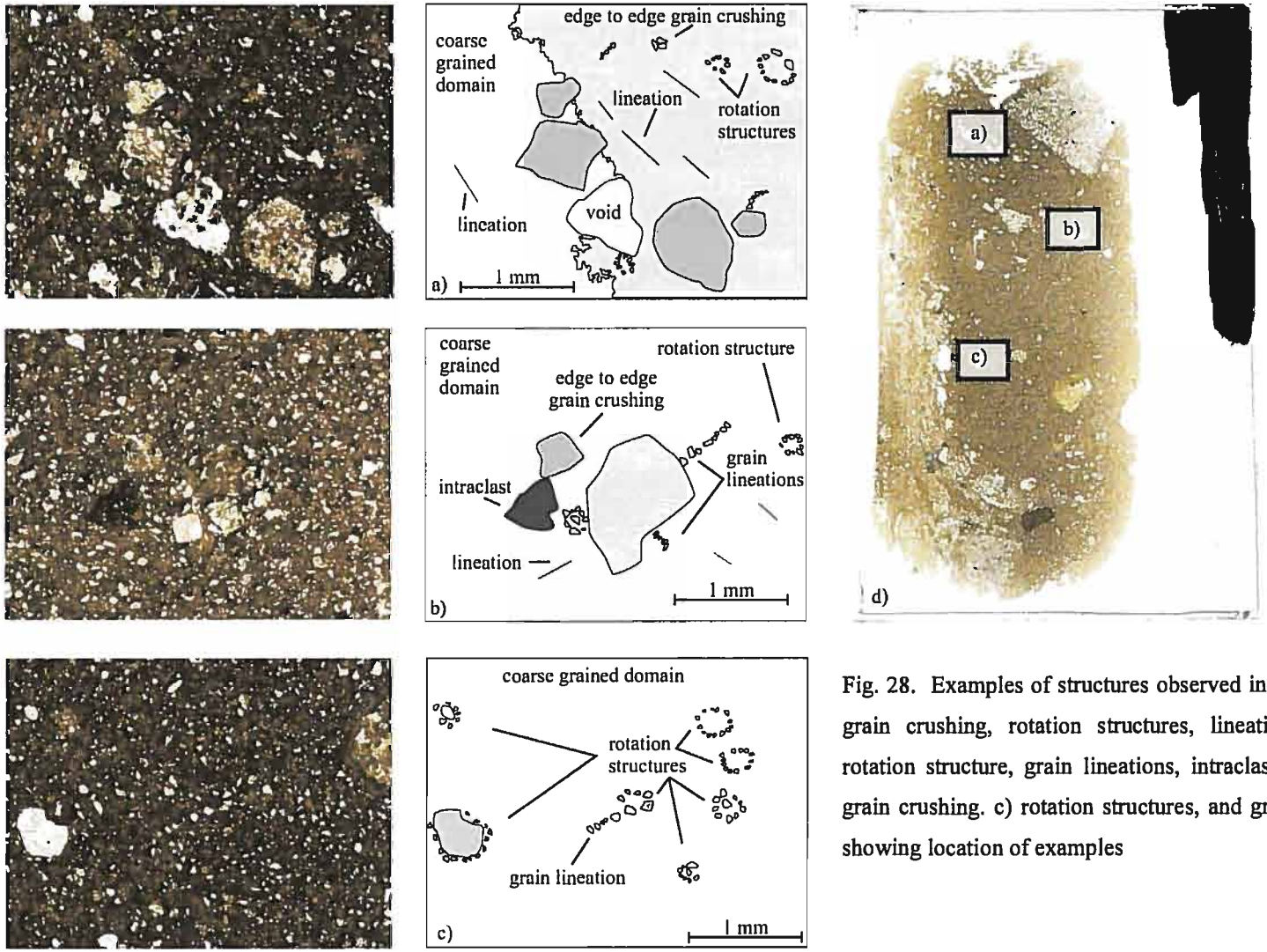

Fig. 28. Examples of structures observed in sample 8. a) edge to edge grain crushing, rotation structures, lineations, grain lineations. b) rotation structure, grain lineations, intraclast, lineation, edge to edge grain crushing. c) rotation structures, and grain lineation. d) overview showing location of examples

used to define them. The thin section contains several voids along the left side of the sample and extend halfway across the bottom. Theses voids are processing artifacts created during thin section production, probably due to over grinding, and are not microstructures. There are three skeleton grains over 5 mm in the sample and are randomly distributed. The skeleton grains in the sample can be divided into large and small grain size fractions. There are only 18 skeleton grains ≥1 mm, making the sample dominated by the finer fraction of skeleton grains. The variation in lithology also differs in the grain size fractions; the larger grain size fraction contains the most variety of skeleton grain lithology, with the small grain size fraction only containing a few lithologies. The shape of the skeleton grains does not vary between size fractions. Skeleton grain shape ranges from rounded to angular with subangular the most frequent shape. There are intraclasts of another diamicton present in the sample (Fig. 28b).

Structures: The structures observed in the sample are ductile and brittle deformational structures, with no porewater induced structure. All of the structures observed occur in both the coarse and fine grain domains. Figures 27 and 28 contain examples of the structures identified in the thin section that will be described in detail as follows. Lineations and grain lineations are respectively the most and second most common microstructures (Fig. 27b, c, and 28a-c). They are both short distance, multi-directional, and some were subsequently deformed suggesting multi-event deformation (Fig. 27b, c). Multiple rotational structures are observed, with and without core stones (Fig. 28c). Edge to edge grain crushing is common; some of the larger skeleton grains are identified as having possibly undergone comminution producing the smaller skeleton grain size fraction (Fig. 27a).

4.4.2 Detailed description of Sample 9

Texture: The sample is coarse (medium silt) grained with multiple fine (clay) grain domains that differ in size and shape (Fig. 25f). The boundaries of these fine

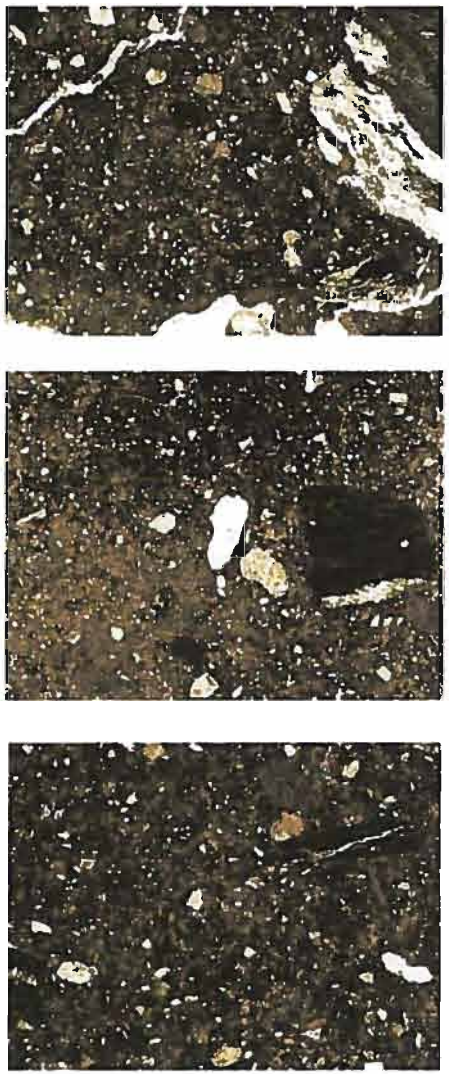

Fig. 29. Examples of structures observed in sample 9. a) edge to edge grain crushing, rotation structures, lineations, grain lineations. b) rotation structure, grain lineations, intraclast, edge to edge grain crushing. c) rotation structure, edge to edge grain crushing, deformed grain lineations, deformed lineations, lineations, and grain lineation. d) overview showing location of examples

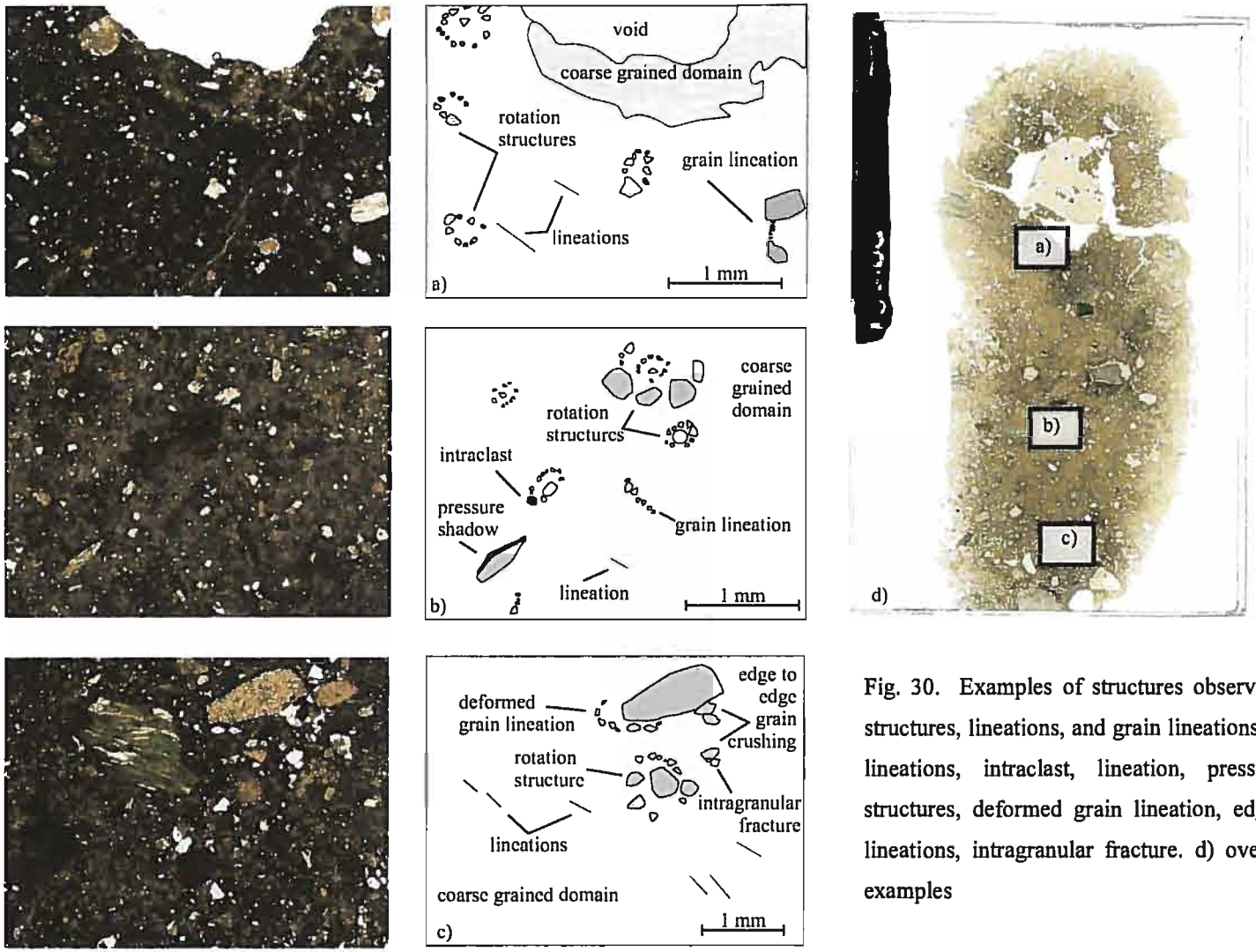

Fig. 30. Examples of structures observed in sample 9. a) rotation structures, lineations, and grain lineations. b) rotation structure, grain lineations, intraclast, lineation, pressure shadow. c) rotation structures, deformed grain lineation, edge to edge grain crushing, lineations, intragranular fracture. d) overview showing location of examples

grain domains diffuse into the surrounding coarse grain domain and were identified using Nikon imaging software. The largest fine grain domain is located just below the largest skeleton grain in the sample, located near the top of the sample. This large skeleton grain is surrounded by voids which branch out to either side of the sample. The voids are believed to be processing artifacts created during sample production. Unfortunately, the complete picture of how the large skeleton grain and the surrounding fine grain domains (in addition to the one below there are two fine grain domains to the left of the skeleton grain and the voids) interacted was lost in the missing sediment. In the center of the sample there is a semi-linear fine-grained domain, as well as some small sporadic fine grain domains located near the bottom of the sample. There are four skeleton grains over 5 mm in the sample; two near the top of the sample, including the largest, and two at the bottom. It is important to note that there is a higher concentration of the larger skeleton grains, or grains from the larger skeleton grain size fraction, at the bottom of the sample. Skeleton grain shape ranges from rounded to angular with subangular being the most common. A variety of skeleton grain lithologies occur in all size fractions, including intraclasts of another diamicton (Fig. 29b-c, and 30b).

Structure: All structures observed in the thin section are ductile and brittle deformational structures. No pore water induced structures were observed. The structures identified are found in both the fine and coarse grain domains. Figures 29 and 30 contain examples of the structures identified that will be discussed in detail as follows. There are abundant grain lineations in the sample, as well as rotation structures. Grain lineations are short distance, multi directions, and some have undergone subsequent deformation suggesting multi-event deformation (Fig. 29a-c, and 30a-c). Rotation structures are observed with and without core stones (Fig. 30a-c). Figure 30b highlights a rotation structure complex composed of two rotation structures with one occurring inside the other. Lineations are also common; they are short distance, multi-directional, and had undergone subsequent deformation as well (Fig. 29a, and c). There are a couple pressure shadows (Fig. 30b). Edge to edge grain crushing is observed, with one instance of intragranular microfracturing occurring as

a result (Fig. 30c). Both pressure shadows and edge to edge grain crushing are considered to be minor microstructures occurring infrequently.

4.4.3 Detailed description of Sample 10

Texture: The sample is coarse (coarse silt) grained with multiple large fine (clay) grain domains. The fine grain domains can be separated into a cluster, and a single fine-grained domain. The cluster consists of the two columnar fine-grained domains on the left side of the sample, and the two horizontal fine-grained domains at the top of the sample. This cluster is considered a single fine-grained domain as the voids in the sample caused the Nikon imaging software to identify a boundary. If the voids had been encompassed by the fine grain domain then no boundary would have been identified. The voids are processing artifacts formed during thin section production and are prevalent in this sample. The single fine grain domain, at the bottom right of the sample, is semi-spherical and encompasses one of the two skeleton grains over 5 mm. Skeleton grains range in shape from rounded to angular, with subangular being the most common. The skeleton grains are composed of multiple lithologies that are observed in all skeleton grain size fractions, including intraclasts of another diamicton (Fig. 31a, c, and 32c).

Structure: The structures identified in the sample are ductile and brittle deformational structures; no porewater induced structures were observed. All structures occur in both the fine and coarse-grained domains. Figures 31 and 32 contain examples of the structures observed in the sample that have been described in detail as follows. The most common microstructures observed are grain lineations, then rotation structures. The grain lineations are short distance and multi-directional. They have also been observed to have undergone subsequent deformation and include edge to edge grain crushing (Fig. 31a-b and 32a-c). Rotation structures are observed with and without core stones (Fig. 31a-c, and 32a, c). Figure 31c contains an example of a rotation structure forming between two larger skeleton grains. It appears that another rotation structure is forming around it involving the larger skeleton grains, and might be the

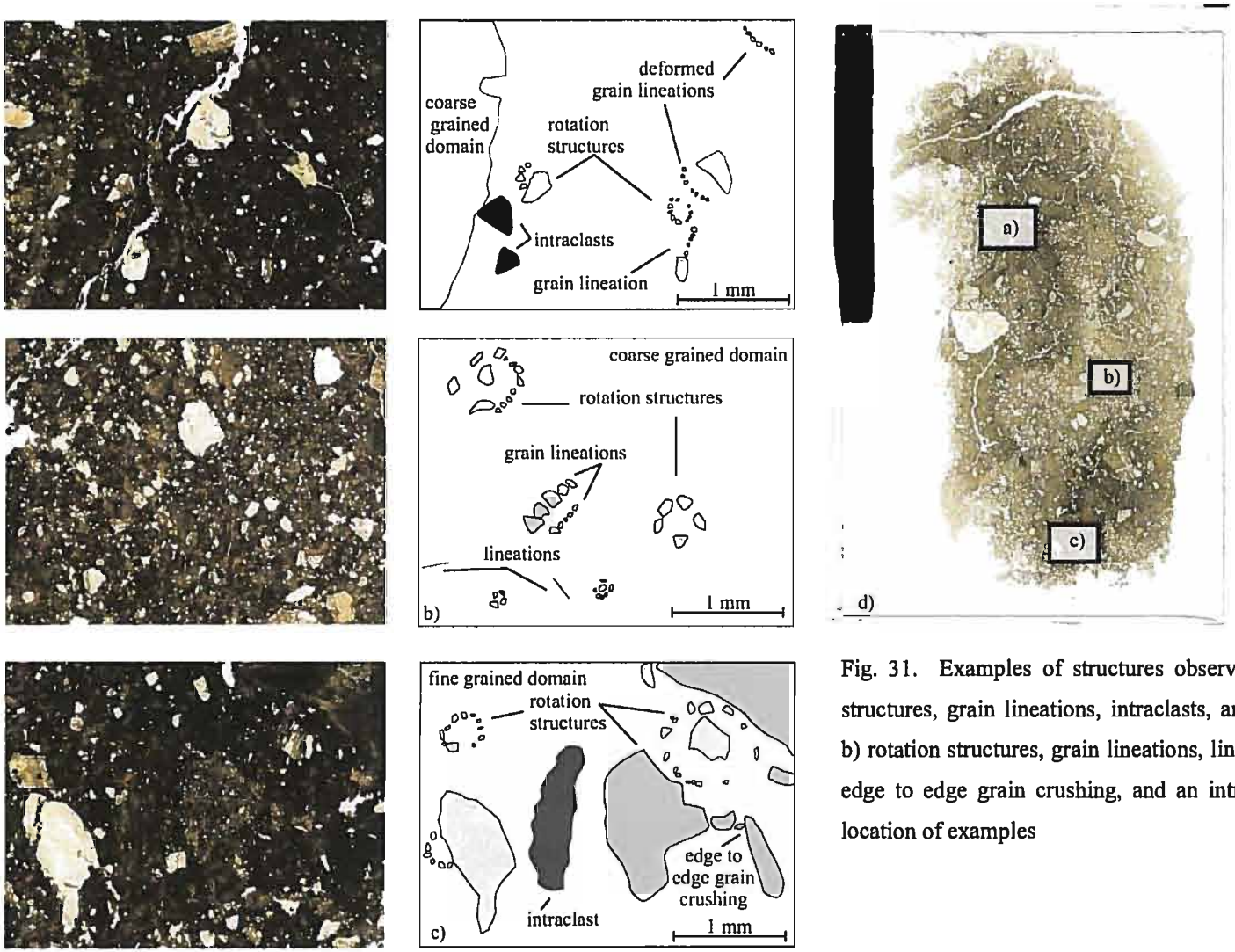

Fig. 31. Examples of structures observed in sample 10. a) rotation structures, grain lineations, intraclasts, and deformed grain lineations. b) rotation structures, grain lineations, lineations. c) rotation structures, edge to edge grain crushing, and an intraclast. d) overview showing location of examples

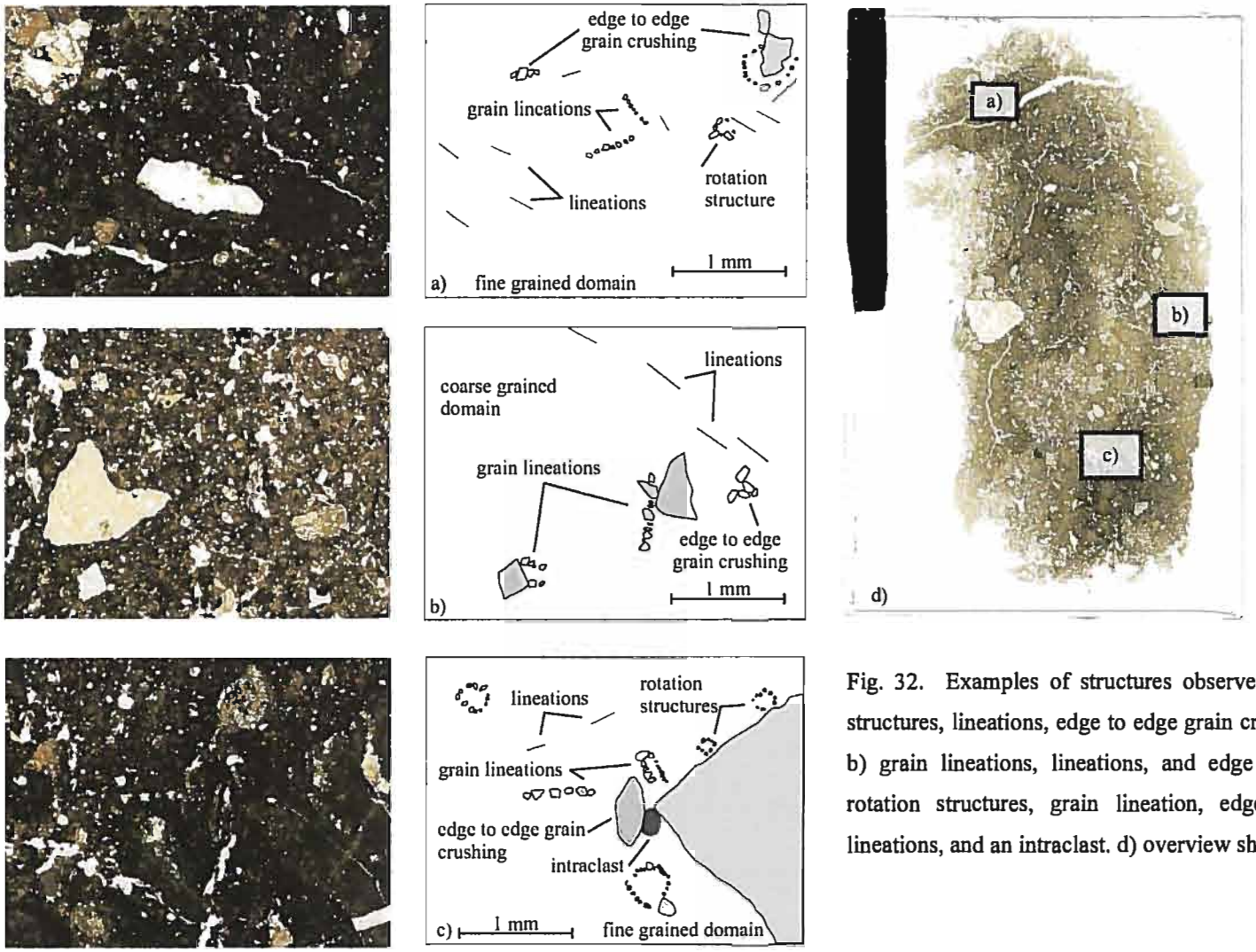

Fig. 32. Examples of structures observed in sample 10. a) rotation structures, lineations, edge to edge grain crushing, and grain lineations. b) grain lineations, lineations, and edge to edge grain crushing c) rotation structures, grain lineation, edge to edge grain crushing, lineations, and an intraclast. d) overview showing location of examples

cause of the edge to edge grain crushing observed. Lineations are also common in this sample (Fig. 31b, 32a-c), and are short distance and multi-directional. Edge to edge grain crushing is observed but not as frequently as the other microstructures (Fig. 31c, 32a-c).

4.5 Core 55

Core 55 sampled the outer shelf of Bisco Trough and was collected by Heroy (2006). The piston core recovered a core length of 384 cm in a water depth of 587 m. A diamicton unit was sampled from 155 cm to the EOC at 384 cm; no lower boundary to this unit was retrieved. Descriptions of the diamicton unit were also divided into a sediment description and an x-radiograph description by Heroy (2006).

In the sediment description, Heroy (2006) identifies a soft gray diamicton from 155-285 cm that overlies a very stiff dark grey mud (no Munsell color) from 285 cm to the EOC. The x-radiograph description given shows no distinction of units from 153 cm to the EOC, no laminations nor layering, variable pebble content from 30-50%, 3-4 mm average, 2 cm common, as well as variable brightness (a diamicton is assumed as the sediment type from the sediment description). The accompanying sediment diagram shows a single unit from 153 cm to the EOC. It is unknown if the unit starts at 153 cm or 155 cm, and if there is a gradational upper contact at 285 cm then it is not indicated.

Three samples were collected from this core for analysis at the interval of 170-180 cm (sample 11), 246-256 cm (sample 12), and 310-320 cm (sample 13). Two of the samples are soft grey diamicton, and the other is very stiff dark grey mud, determined by the sediment descriptions that Heroy (2006) gave.

X-radiographs of core 55 were obtained as means to compare Heroy's (2006) macroscopic core and x-radiographs descriptions to the overview description of the thin section samples from this core. The x-radiograph confirms Heroy's (2006) x-

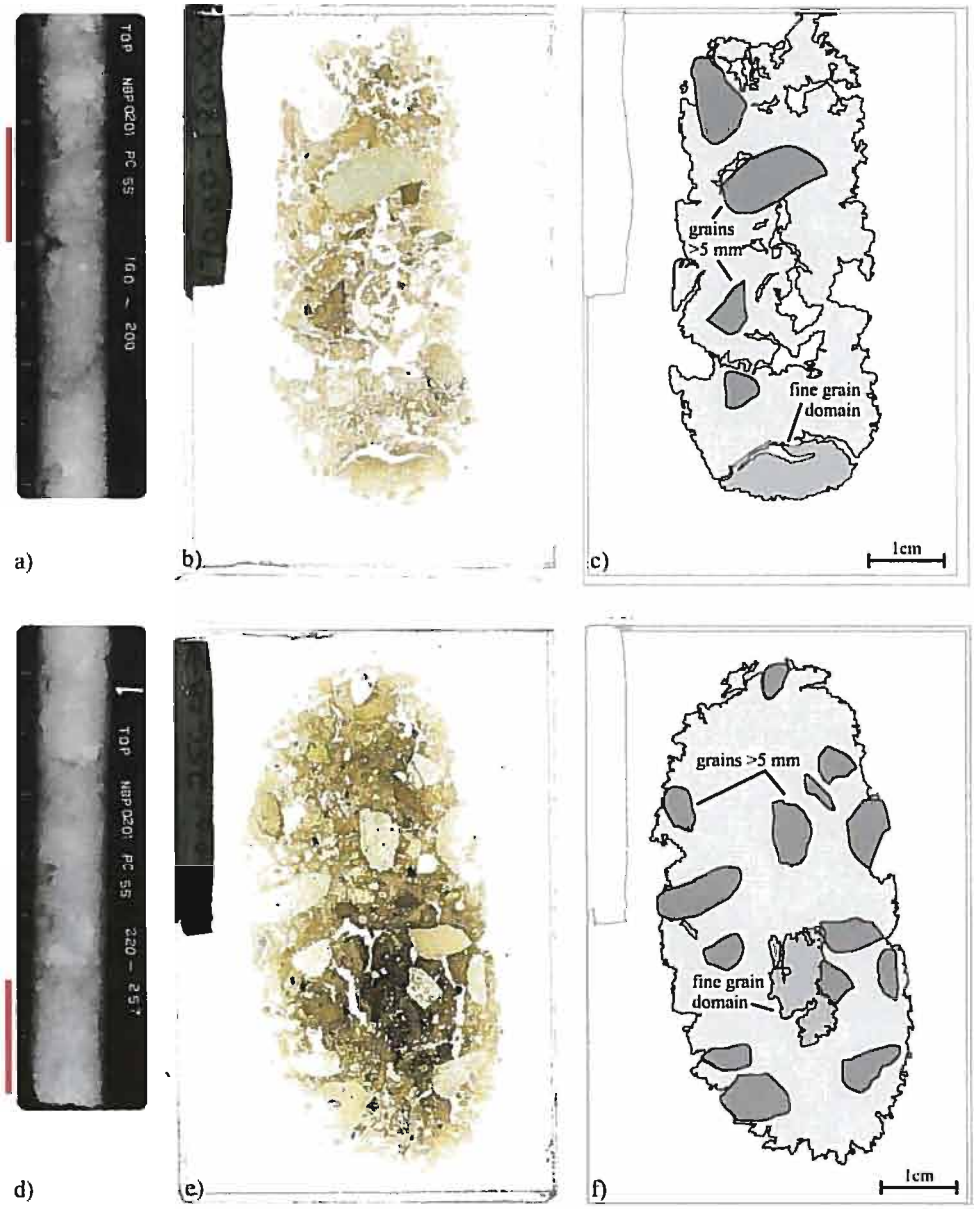

Fig. 33. Overview of samples 11 and 12 from Core 55. a) x-radiograph of section 160-200 cm of core 55, containing sample 11 at interval 170-180 cm highlighted by red bar. b) thin section of sample 11. c) overview of sample 11 displaying locations of fine grain domains and skeleton grains over 5 mm. d) x-radiograph of section 220-257 cm of core 55, containing sample 12 at interval of 246-256 cm highlighted by red bar. e) thin section of sample 12. f) overview of sample 12 displaying location of fine grain domain and skeleton grains over 5 mm (AMGRF, 2002).

radiograph description that the diamicton unit starts at 153 cm. Briefly looking at samples 11, 12 and 13 (Fig. 33, and 34), samples 11 and 12 appear similar, and they are distinct from sample 13 based solely on skeleton grain content. Samples 11 and

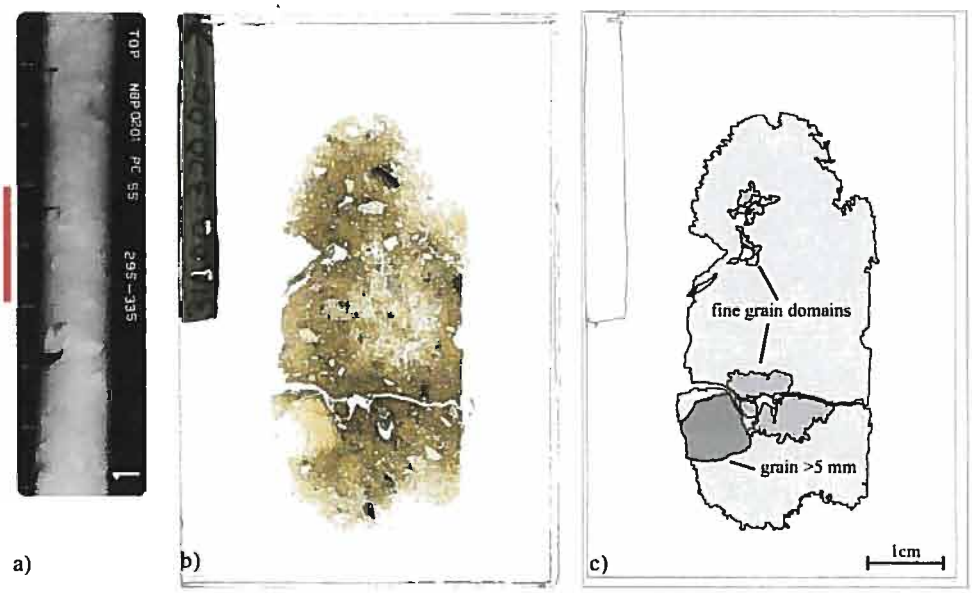

Fig. 34. Overview of sample 13 from Core 55. a) x-radiograph of section 295-335 cm of core 55, containing sample 13 at interval 310-320 cm highlighted by red bar. b) thin section of sample 13. c) overview of sample 13 displaying locations of fine grain domains and skeleton grain over 5 mm (AMGRF, 2002).

12 contain a higher larger-skeleton grain-size fraction than sample 13 does. As samples 11 and 12 are described, in Heroy's (2006) sediment description, as coming from a separate unit than sample 13, then one could cautiously say the differences observed would support a separate unit for sample 13. An interesting note is that the fine-grained domain identified in sample 11 is fine-grained in terms of that samples texture, but it is the same texture that samples 12 and 13 are comprised of, and is labeled as coarse-grained in those samples as they in turn contain finer grained domains. 'Brightness' was a descriptor used in Heroy's (2006) x-radiograph description of a singular unit it described, it is noted that all three samples come from areas with a different 'brightness'.

4.5.1 Detailed description of Sample 11

Texture: The sample is coarse (coarse silt) grained with a fine (coarse to medium silt) grained domain encompassing the lower end of the sample (Fig. 33). While the

boundaries of the fine-grained domain are determined using Nikon imaging software, they are visually distinct. It appears that the skeleton grains directly above, or on, the domain boundary are partially embedded. The fine grained domain is marginally texturally distinct from the rest of the sample, but contains no skeleton grains from the large size fraction. That is a marked difference from the remaining sample which is dominated by skeleton grains from the large size fraction. Perhaps this domain could be a separate unit, as differences between it and the remaining sample are not solely textural; further discussion of this possibility will be left to a subsequent chapter once all descriptions have been made. As previously stated, the sample contains a prevalence of skeleton grains from the larger size fraction, though only 4 are over 5 mm. The shape of the skeleton grains range from rounded to angular with subangular being the most common in all skeleton grain size fractions. There is a variety of lithologies in this sample in both the large and small grain size fractions, including intraclasts of another diamicton (Fig. 35a, 36a-c). Voids or processing artifacts are, unfortunately, prevalent in this sample.

Structure: The structures observed in the thin section are ductile and brittle deformational structures, with no porewater induced structures observed. Not all the structures are observed in both the fine and coarse-grained domains. The fine grained domain does contain ductile and brittle deformational structures, but these are only formed by the small skeleton grain size fraction, and only lineations, rotation structures, and grain lineations were observed. In the small fine-grained domain only a few structures are identified but, of those, lineations are the most common. They are short distance and multi-directional (only one shown in Fig. 35c). A few rotation structures are identified with (Fig. 35c) and without core stones. Only a couple grain lineations are observed; they are short distance and multi-directional. In the coarse-grained domain, grain lineations and rotation structures are the most common microstructure observed. Grain lineations are short distance and multi-directional (Fig. 35a-c, and 36a-c). Rotation structures mostly contained core stones (Fig. 35a, and 36b). Edge to edge grain crushing is common and is observed in other microstructures, such as rotation structures, grain lineations, and skeleton grains

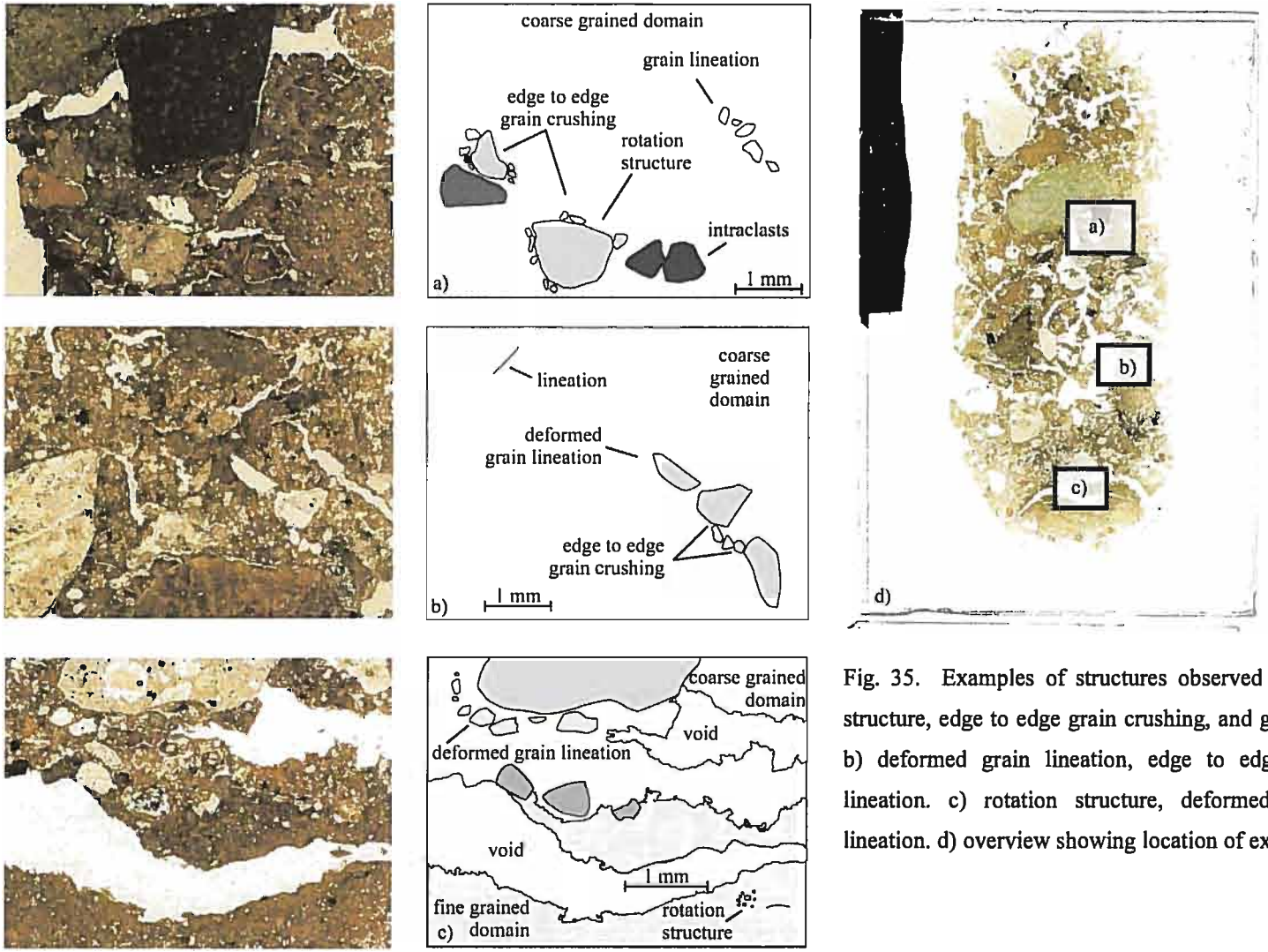

Fig. 35. Examples of structures observed in sample 11. a) rotation structure, edge to edge grain crushing, and grain lineations, intraclasts. b) deformed grain lineation, edge to edge grain crushing, and a lineation. c) rotation structure, deformed grain lineation, and a lineation. d) overview showing location of examples

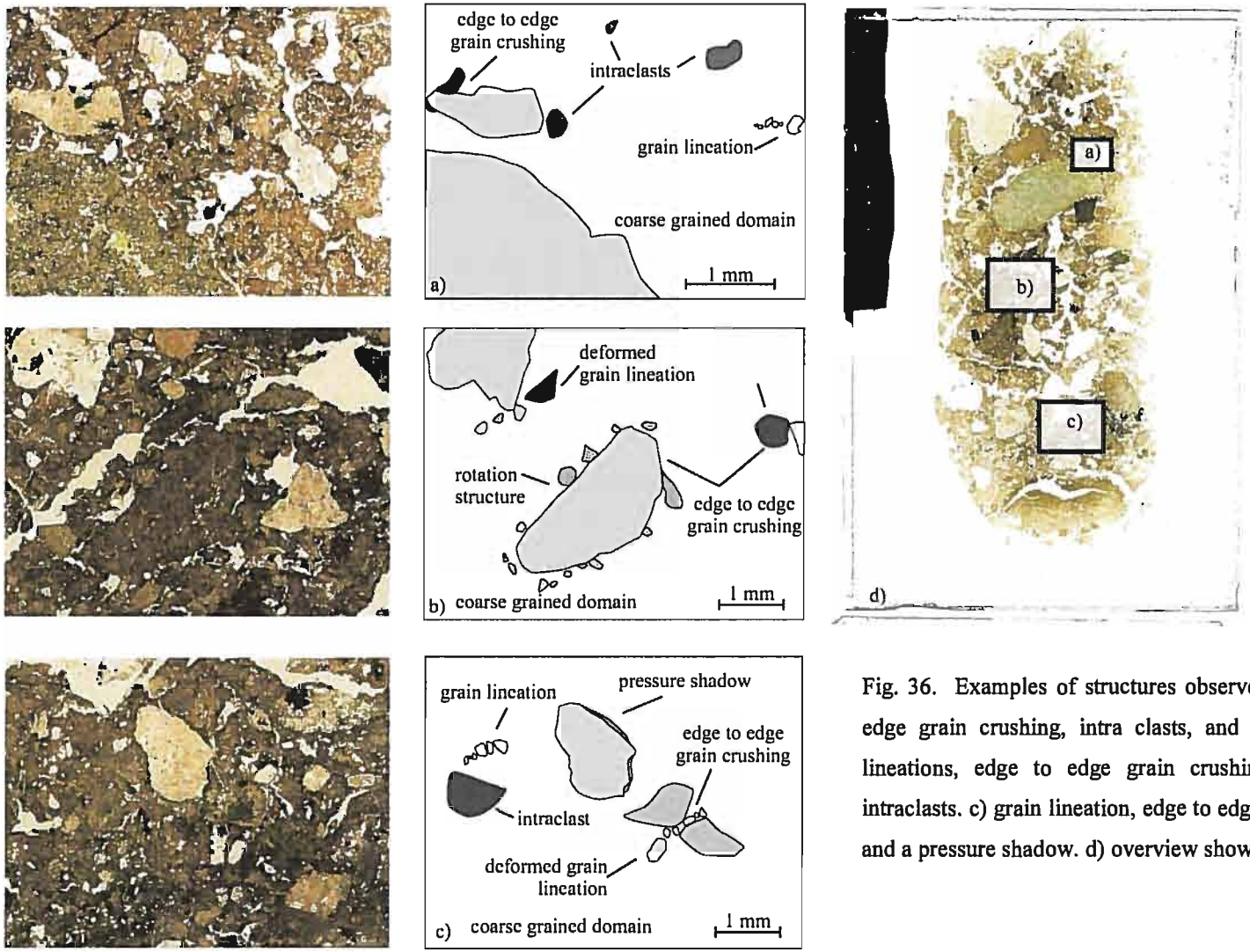

Fig. 36. Examples of structures observed in sample 11. a) edge to edge grain crushing, intra clasts, and a grain lineation. b) grain lineations, edge to edge grain crushing. rotation structure, and intraclasts. c) grain lineation, edge to edge grain crushing, intraclasts, and a pressure shadow. d) overview showing location of examples

embedding into intraclasts (Fig. 35a-b, and 36a-c). Lineations are observed occasionally and are considered to be a minor microstructure (Fig. 35b). A few pressure shadows are observed (Fig. 36c).

4.5.2 Detailed description of Sample 12

Texture: The sample is coarse (coarse silt) grained with a fine (clay) grained domain. The fine grain domain has distinct boundaries on the left side and diffuse boundaries on the right, all were determined using Nikon imaging software. The fine grain domain is separated by voids, or processing artifacts, but is considered a single domain. This fine-grained domain is located at the bottom right of the sample, and is semicircular in shape. There are voids in the sample, which are most likely processing artifacts, and not microstructures. The sample contains 13 skeleton grains over 5 mm in addition to multiple skeletons grains from the large size fraction; comparatively significantly more than sample 13 but less than sample 11. Skeleton grains range from rounded to angular, with subangular the most common shape. There is a variety of lithologies in both the large and small skeleton grain size fractions, including intraclasts of another diamicton (Fig. 37 and 38).

Structure: The structures observed in the thin section are ductile and brittle deformational structures; no porewater induced structures were identified. All structures are found in both the fine and coarse-grained domains. Figures 37 and 38 contain examples of the structures identified in the thin section that will be described in detail as follows. Rotation structures are the most common microstructure in the sample, with grain lineations a very close second. Rotation structures are observed with and without core stones (Fig 37). Figure 38b contains an example of an unusual rotation structure. The rotation structure contains several intraclasts, one of which appears to have three larger skeleton grains embedded in it (edge to edge grain crushing) including the core stone. This larger mass of skeleton grains, and intraclasts have several other skeleton grains and intraclasts rotating with it. This is the only rotation structure composed solely of skeleton grains from the larger size

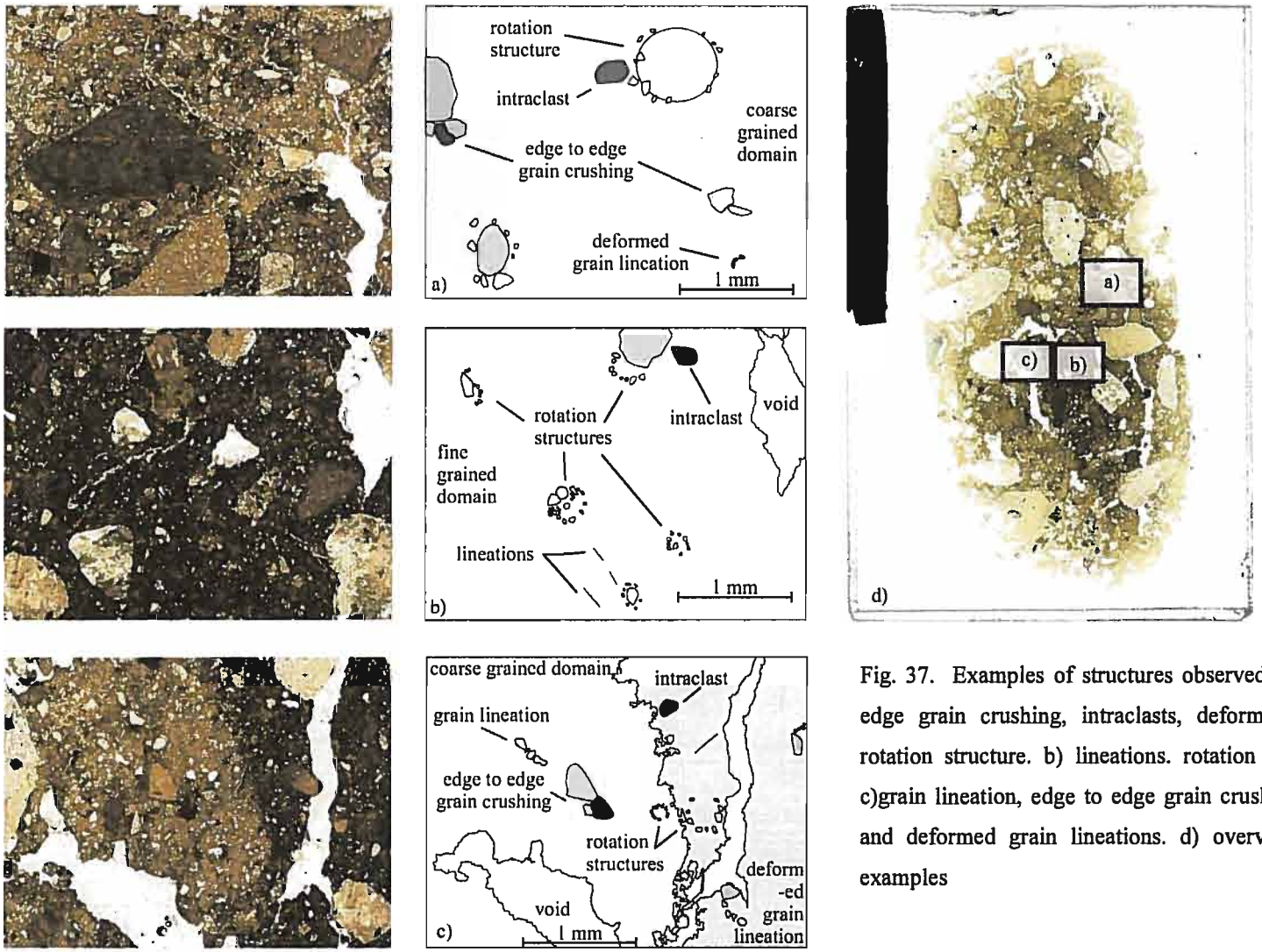

Fig. 37. Examples of structures observed in sample 12. a) edge to edge grain crushing, intraclasts, deformed grain lineation, and rotation structure. b) lineations. rotation structure, and intraclasts. c)grain lineation, edge to edge grain crushing, lineation, intraclasts, and deformed grain lineations. d) overview showing location of examples

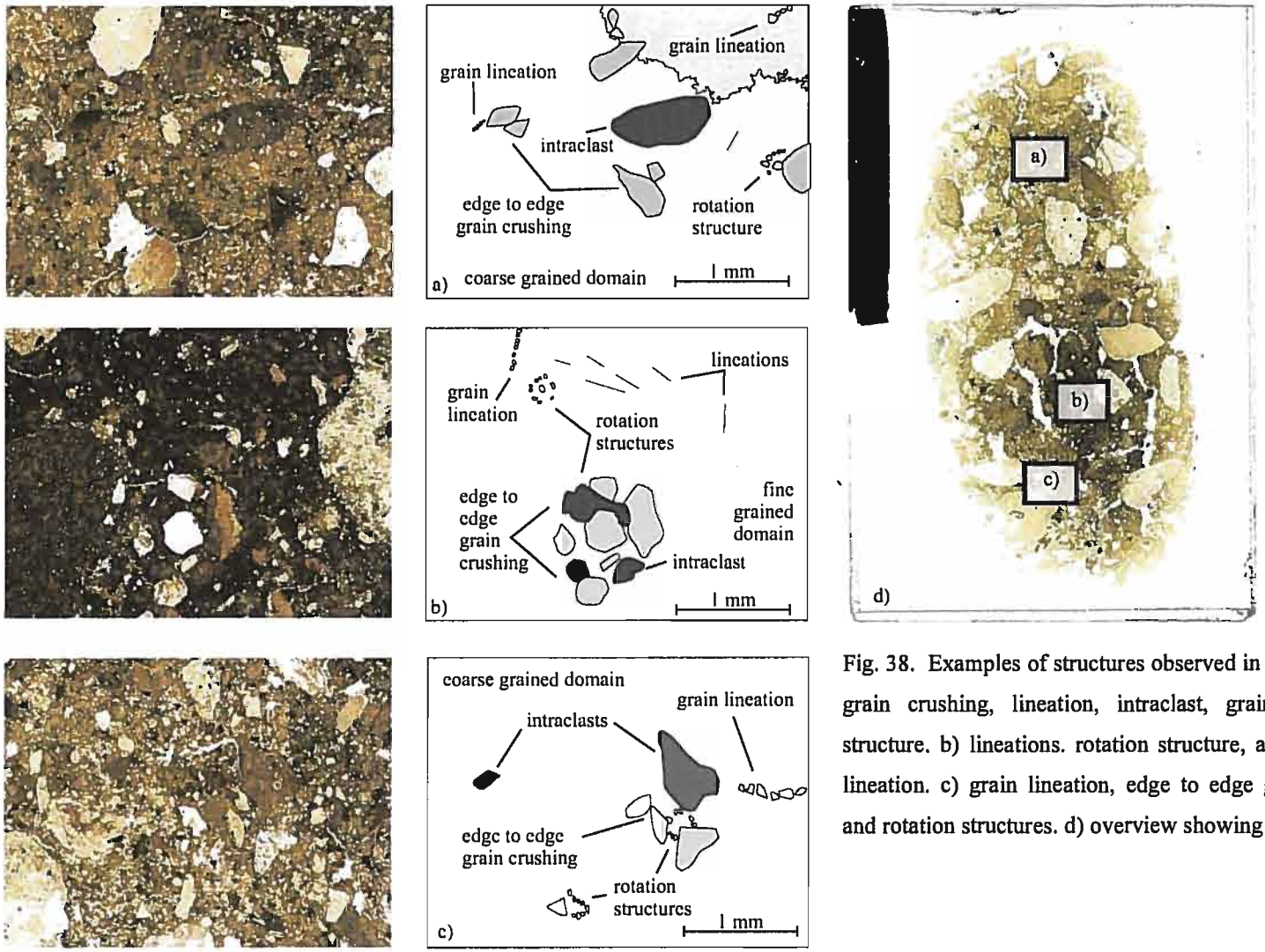

Fig. 38. Examples of structures observed in sample 12. a) edge to edge grain crushing, lineation, intraclast, grain lineation, and rotation structure. b) lineations. rotation structure, and intraclasts, and a grain lineation. c) grain lineation, edge to edge grain crushing, intraclasts, and rotation structures. d) overview showing location of examples

fraction. Grain lineations are observed to be short distance, multi-directional, and some have undergone subsequent deformation (Fig. 37c). There are a few short distance and multi-directional lineations. This structure is more common in the fine-grained domain than in the coarse-grained domain (Fig. 38a-b). Edge to edge grain crushing is observed between two or more skeleton grains or skeleton grains and intraclasts (Fig. 37 and 38).

4.5.3 Detailed description of Sample 13

Texture: This sample is coarse (coarse silt) grained with several fine (clay) grained domains of variable shapes and sizes. The boundaries of the fine grain domains are irregular and diffuse, and are defined using Nikon imaging software. The fine grain domains can be grouped into two clusters. The largest fine grain domains, the three in the bottom of the sample, is considered to be a whole fine-grained domain that has been separated by voids. The other cluster is comprised of the smaller fine grain domains, located in the top left of the sample. The smaller cluster in the top of the sample is consists of individual fine grain domains but will be referred to as a cluster, where the large fine grain domain cluster will be referred to as a single domain. There are several voids in this sample in the form of cracks, and voids produced from over grinding during thin section production, all of which are processing artifacts; one of the cracks completely transects the sample, and the over grinding has removed a significant portion of the coarse-grained domain in the central and upper right of the sample. There is only one skeleton grain over 5 mm in the sample located in the bottom left of the sample. There are only a few skeleton grains in the large size fraction, with the small size fraction dominating the skeleton grain percentages. The shape of the skeleton grains range from rounded to angular, with subangular the most common. The sample contains multiple skeleton grain lithologies; the most variation occurring in the large skeleton grain size fraction. There are a few intraclasts of another diamicton in the sample (Fig. 39c, and 40a and c).

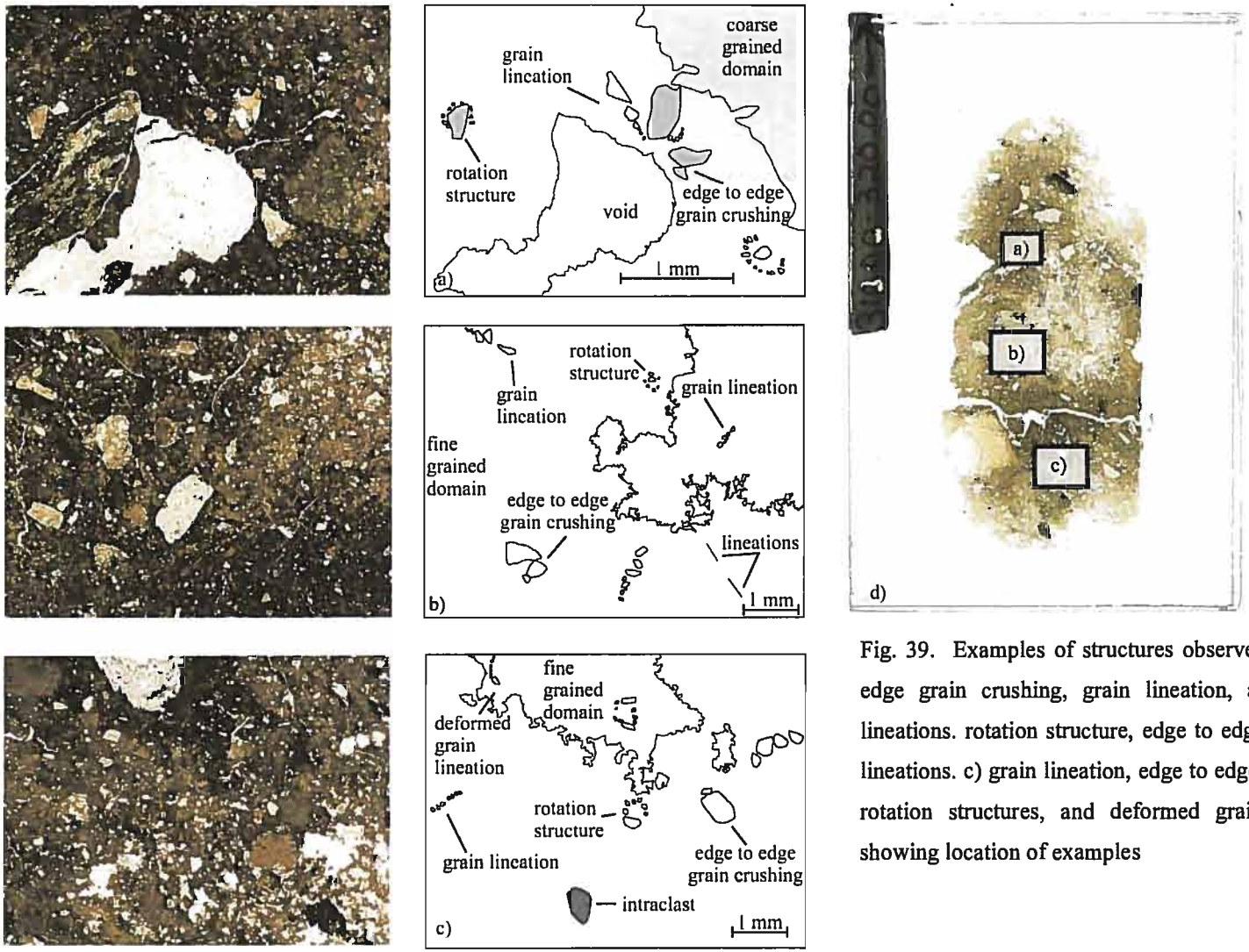

Fig. 39. Examples of structures observed in sample 13. a) edge to edge grain crushing, grain lineation, and rotation structures. b) lineations. rotation structure, edge to edge grain crushing, and grain lineations. c) grain lineation, edge to edge grain crushing, intraclasts, rotation structures, and deformed grain lineations. d) overview showing location of examples

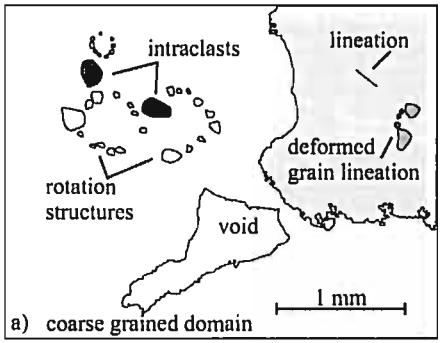

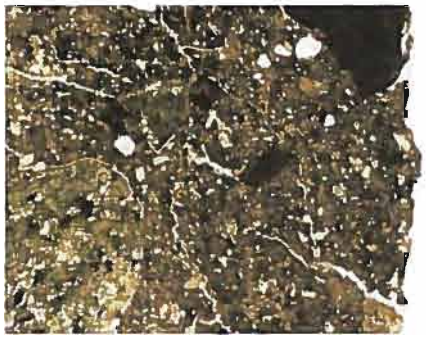

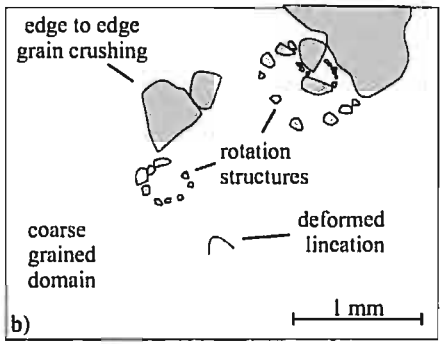

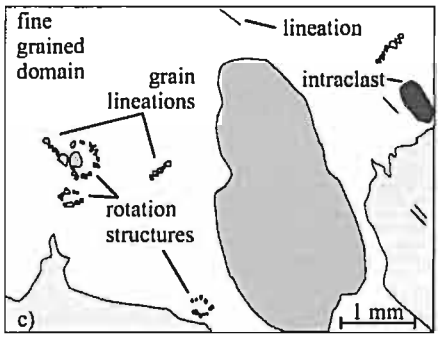

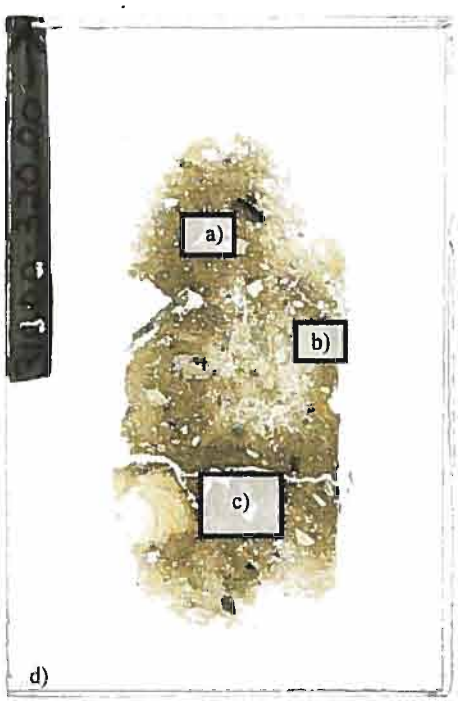

Fig. 40. Examples of structures observed in sample 13. a) lineation, intraclasts, deformed grain lineation, and rotation structures. b) deformed lineation, rotation structures, and edge to edge grain crushing. c) grain lineation, intraclasts, lineations, and rotation structures. d) overview showing location of examples

Structure: The structures identified in this sample are all ductile deformational and brittle deformational structures. No porewater induced structures were identified. The structures are observed in both the fine and coarse-grained domains. Figures 39 and 40 contain examples of the structures identified, and are discussed in detail as follows. It is important to note, again, that a significant amount of the coarse grain domain was lost during sample production, this affecting the amount of, and possibly the type of, microstructures observed. This is taken into consideration when the prevalence of a particular microstructure is interpreted. Grain lineations are the most common microstructure identified. The grain lineations are short distance and multi-directional (Fig. 39 and 40c). Only a few are observed to have been deformed by a subsequent deformation event (Fig. 39c and 40a). Rotation structures are observed with and without a core stone (Fig. 39). Figure 40a and 40b contain examples of a series of rotation structures; Figure 40a contains an example of rotation structures in close proximity to each other, where Figure 40b contains an example of one rotation structure contained inside another. Edge to edge grain crushing is observed (Fig. 39, and 40b). Lineations are the least common structure with the most observed in fine grain domains (Fig. 39b, and 40). These are short distance and multi-directional, with some having undergone subsequent deformation (Fig. 40b). This is one of the structures that could have been affected by the processing artifacts in the coarse-grained domain.

4.6 Core 32

Core 32 sampled the outer shelf of Marguerite Trough, and was collected by Fretwell (2005). The piston core recovered a core length of 363 cm in a water depth of 547 m. A diamicton unit was sampled from 155 cm to the EOC at 384 cm; no lower boundary to this unit was retrieved. The description of the sampled unit is very basic; from 5 cm to EOC is a gravelly sandy mud that is interpreted as a subglacially formed deformation diamicton facies. Three samples were collected from this unit for analysis at the interval of 50-60 cm (sample 14), 250-260 cm (sample 15), and 307-317 cm (sample 16).

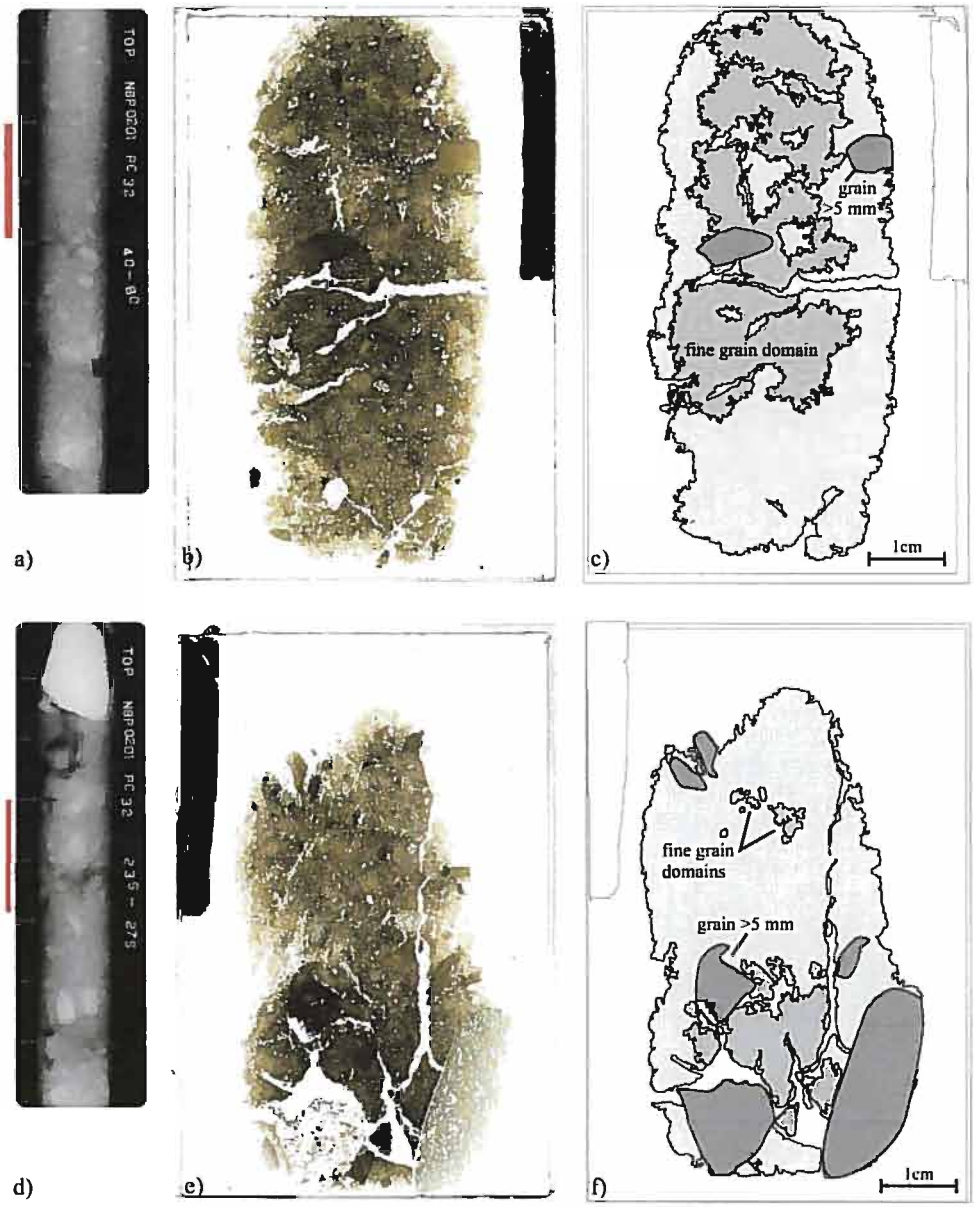

Fig. 41. Overview of samples 14 and 15 from Core 32. a) x-radiograph of section 40-80 cm of core 32, containing sample 14 at interval 50-60 cm highlighted by red bar. b) thin section of sample 14. c) overview of sample 14 displaying locations of fine grain domains and skeleton grains over 5 mm. d) x-radiograph of section 235-275 cm of core 32, containing sample 15 at interval of 25-260 cm highlighted by red bar. e) thin section of sample 15. f) overview of sample 15 displaying location of fine grains domains and skeleton grain over 5 mm (AMGRF, 2002).

X-radiographs of core 32 were obtained as means to compare Fretwell's (2005) unit description to the overview description of the thin section samples from this core. Comparing the textures of the samples has identified some differences. Sample 14 is

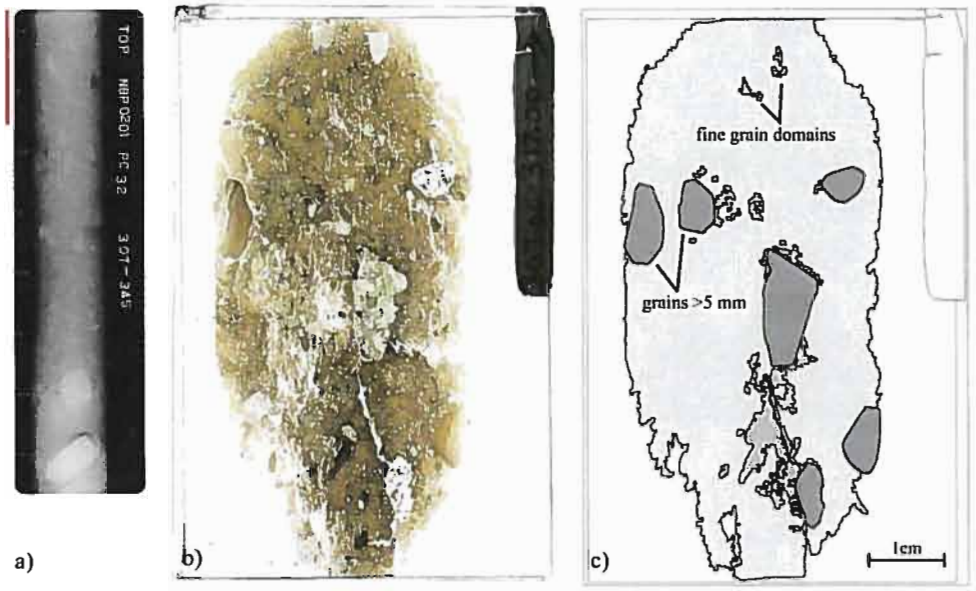

Fig. 42. Overview of sample 16 from Core 32. a) x-radiograph of section 307-345 cm of core 32, containing sample 16 at interval 307-317 cm highlighted by red bar. b) thin section of sample 16. c) overview of sample 16 displaying locations of fine grain domains and skeleton grains over 5 mm (AMGRF, 2002).

fine-grained with coarse-grained domains (for comparative purposes, the fine grain domains were highlighted leaving the sample background as coarse-grained as with the other samples (Fig. 41c)), where sample 15 is coarse-grained with fine-grained domains (Fig. 41f). The textures of the coarse-grained, and fine-grained domains in these two samples are the same. Comparing these textures to sample 16 is where differences are found. Sample 16 is coarse-grained with fine-grained domains, but the texture of the coarse-grained domain in sample 16 is denser than those found in samples 14 and 15. Similarly, the fine grain domains in sample 16 differ in texture from those found in samples 14 and 15; the fine grain domains in samples 14 and 15 being finer, and denser than those found in sample 16.

4.6.1 Detailed description of Sample 14

Texture: The sample is fine (clay) grained with coarse (medium silt) grained domains.

The bottom of the sample is encompassed by a coarse-grained domain with small coarse grain domain scattered throughout the top portion of the sample (Fig. 41b and c). Boundaries between the two domains are identified using Nikon imaging software as they were irregular and diffuse. The sample contains several voids, or processing artifacts, formed during thin section production. There are two skeleton grains over 5 mm in the sample, both are located in the top half of the sample. The sample is dominated by skeleton grains in the fine skeleton grain size fraction; the large skeleton grain size fraction being minimal. Skeleton grain shapes range from rounded to angular with subangular being the most common. A variety of lithologies are present in the sample with the most variety found in the large skeleton grain size fraction. Only a few intraclasts of another diamicton are present in the sample (Fig. 43a, c and 44a).

Structure: The structures observed in the thin section are ductile and brittle deformational structures; no porewater induced structures were observed. All structures are identified in both the fine and coarse-grained domains. Figures 43 and 44 contain examples of the structures identified in the thin section that are described in detail below. Grain lineations are the most common structure observed in the sample. They are short distance, multi-directional, and in some cases have undergone subsequent deformation (Fig. 43 and 44). Rotation structures and lineations are identified nearly equally. Rotation structures are observed with and without core stones (Fig. 43), and some are formed by plasma (Fig. 44c). The lineations are short distance and multi-directional (Fig. 44a). Edge to edge grain crushing is observed but considered a minor microstructure (Fig. 43a and c).

4.6.2 Detailed description of Sample 15

Texture: Sample 15 is coarse (medium silt) grained with fine (clay) grain domains. The boundaries of fine-grained domains are identified using Nikon imaging software as they are irregular and diffuse. There is a concentration of fine-grained domains at the bottom of the sample and a few small fine-grained domains near the top of the

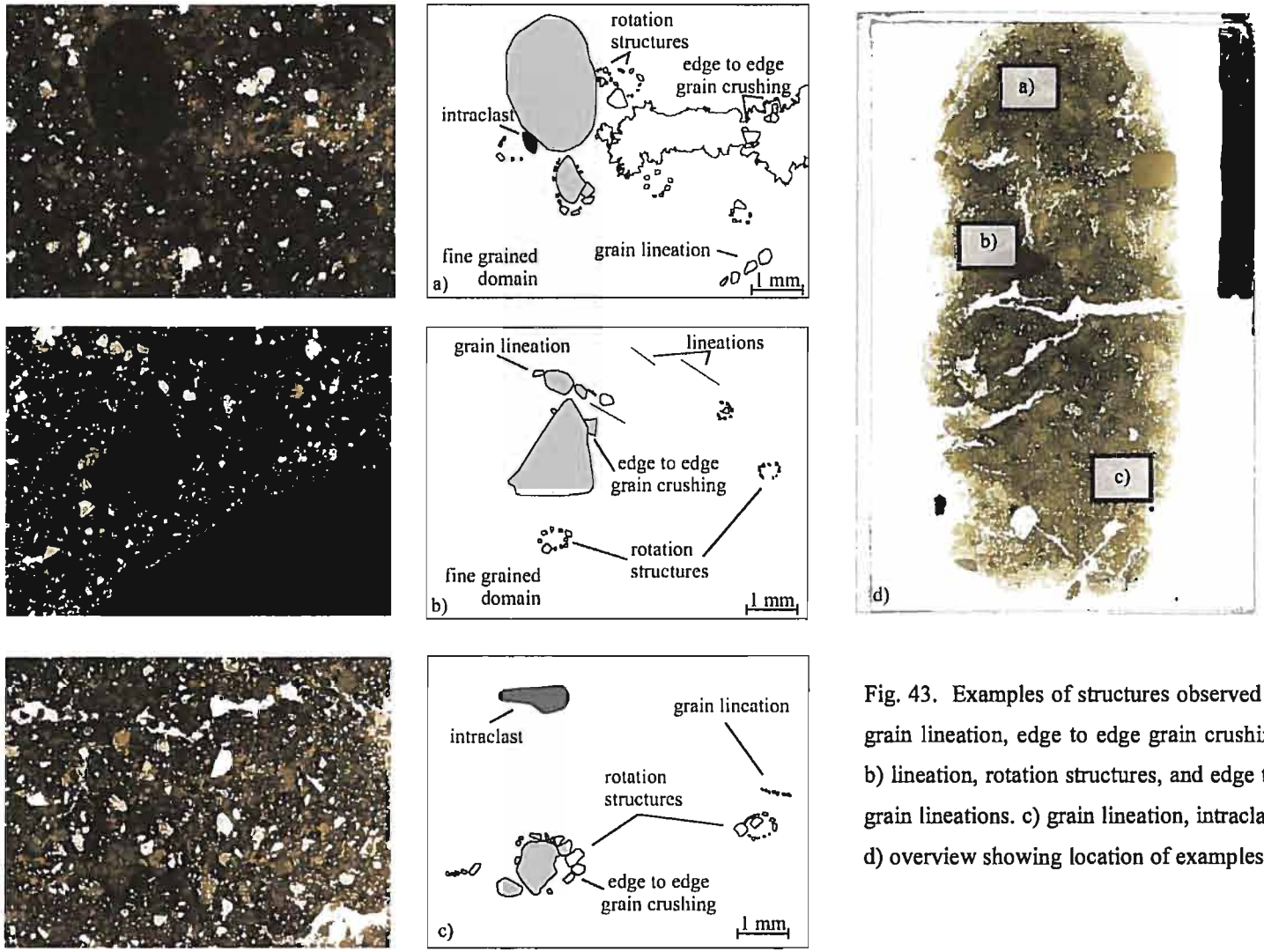

Fig. 43. Examples of structures observed in sample 14. a) intraclast, grain lineation, edge to edge grain crushing, and rotation structures. b) lineation, rotation structures, and edge to edge grain crushing, and grain lineations. c) grain lineation, intraclasts, and rotation structures. d) overview showing location of examples

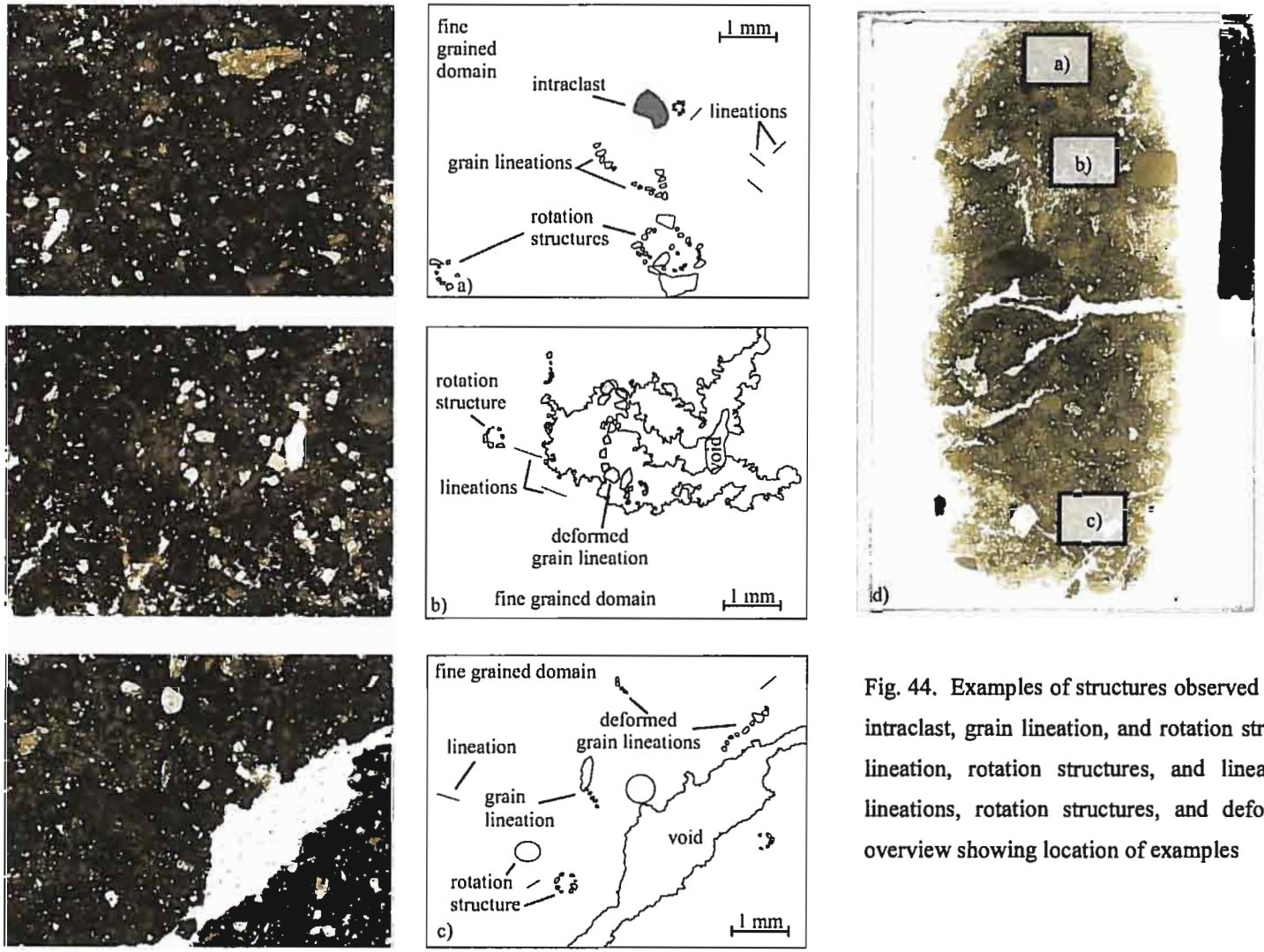

Fig. 44. Examples of structures observed in sample 14. a) lineations, intraclast, grain lineation, and rotation structures. b) deformed grain lineation, rotation structures, and lineations. c) grain lineation, lineations, rotation structures, and deformed grain lineations. d) overview showing location of examples

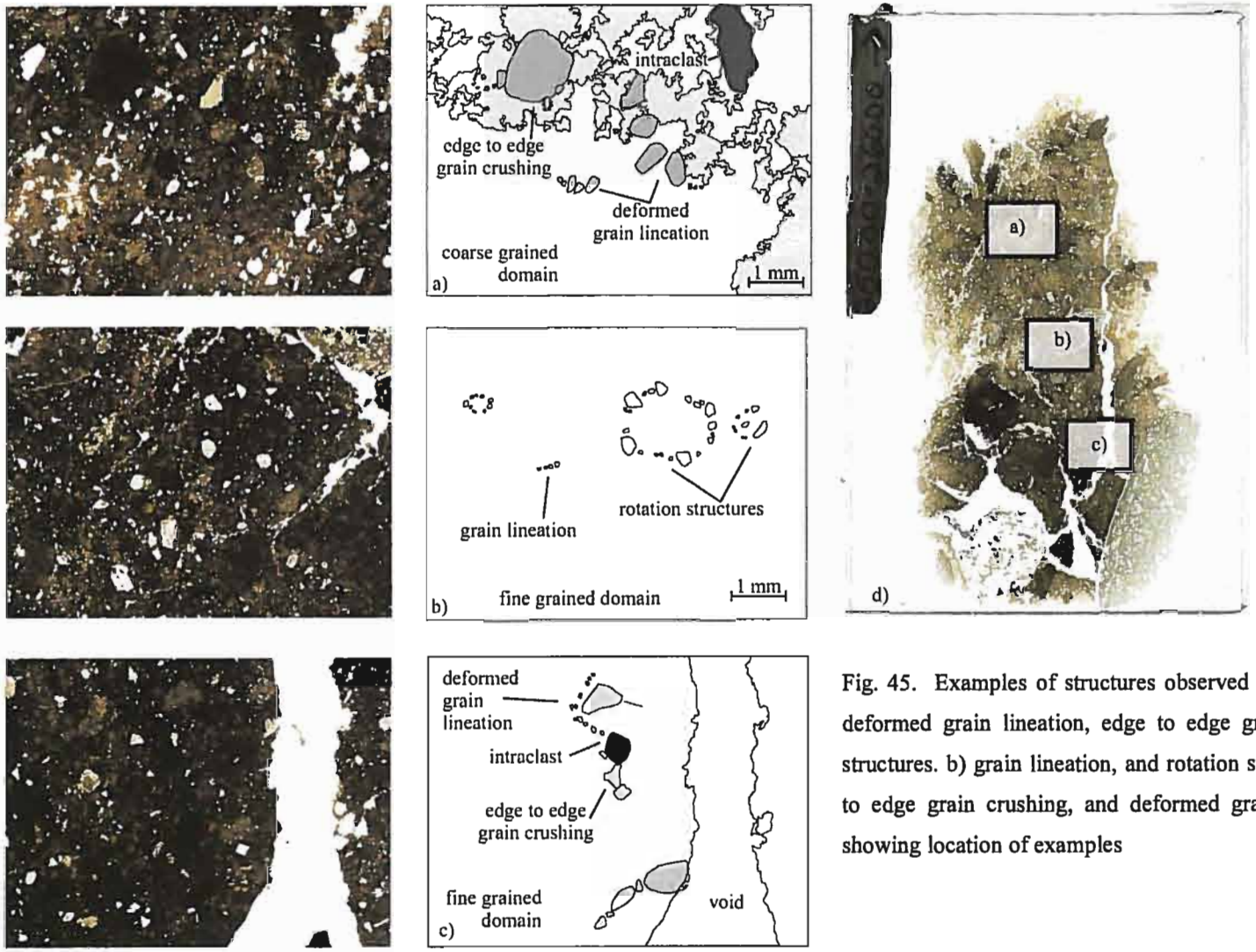

Fig. 45. Examples of structures observed in sample 15. a) intraclast, deformed grain lineation, edge to edge grain crushing, and rotation structures. b) grain lineation, and rotation structures. c) lineation, edge to edge grain crushing, and deformed grain lineations. d) overview showing location of examples

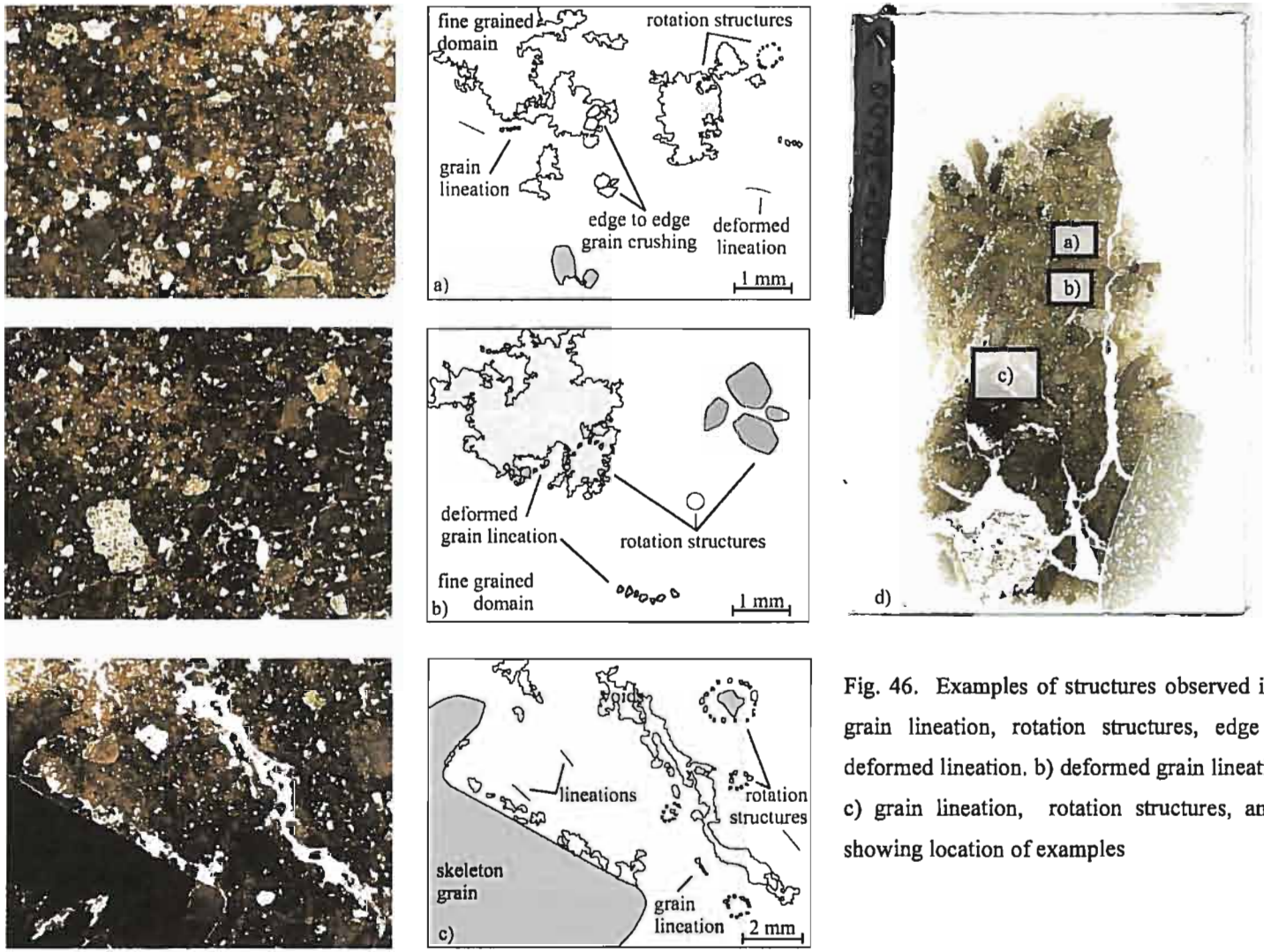

Fig. 46. Examples of structures observed in sample 15. a) lineations, grain lineation, rotation structures, edge to edge grain crushing, deformed lineation. b) deformed grain lineation, and rotation structures. c) grain lineation, rotation structures, and lineations. d) overview showing location of examples

sample. There are several voids (processing artifacts) forming cracks that are concentrated between and around the large skeleton grains. The largest skeleton grains are concentrated in the bottom of the sample, surrounding the large fine-grained domains in that area, with a total of four skeleton grains over 5 mm in that area. There are two additional skeleton grains over 5 mm at the top left edge of the sample. Skeleton grain shape ranges from rounded to angular with subangular being the most common. A variety of lithologies are present in the sample, with the least variation occurring in the small skeleton grain size fraction. Only a few intraclasts of another diamicton present in the sample (Fig. 45a, and c).

Structure: The structures observed in the thin section are ductile deformational and brittle deformational structures; no porewater induced structures were identified. All structures are identified in both the fine and coarse-grained domains. Figures 45 and 46 contain examples of structures identified in the sample and are discussed in detail as follows. Grain lineations are the most common microstructure observed. They are short distance and multi-directional, with some having undergone subsequent deformation (Fig. 45 and 46). Rotation structures are the second most common structure identified; both with and without core stones (Fig. 45b). Lineations and edge to edge grain crushing occurred infrequently (Fig. 45a and c, and 46a and c). Lineations are short distance, multi-directional, and some had undergone subsequent deformation (Fig. 40a).

4.6.3 Detailed description of Sample 16

Texture: Sample 16 is coarse (medium silt) grained with a few small fine (clay) grained domains. The boundaries of the fine grain domains are irregular and diffuse into the surrounding coarse-grained domain; they are identified using Nikon imaging software. The fine grain domains are sporadic but, tend to be located in the centre of the sample. This sample, unfortunately, has numerous voids in the form of cracks and those formed from over grinding during the thin section production, all of which are processing artifacts. The central left portion of the sample has been partially removed,

impacting the amount of, and possibly the type of microstructures observed. This is taken into consideration when the prevalence of a particular microstructure is interpreted. Six skeleton grains over 5 mm are randomly distributed throughout the sample, but sample is dominated by skeleton grains from the small grain size fraction. Skeleton grain shape ranges from rounded to angular, with subangular being the most common shape observed. The most variability in skeleton grain lithology is seen in the large skeleton grain size fraction. A few intraclasts of another diamicton are found in the sample (Fig. 47b, c, and 48c).

Structure: The structures observed in the thin section are ductile deformational and brittle deformational structures; no porewater induced structures were observed. Not all structures are observed in both the fine and coarse grain domains; given the size of the fine grain domains this is not unexpected. Grain lineations are the most common microstructure in both the fine and coarse-grained domains. The grain lineations are short distance and multi-directional (Fig. 47 and 48). Deformed grain lineations are also found in both the fine and coarse grain domains (Fig. 48c, and 47a respectively). Lineations are the second most common microstructure observed in both domain types. The lineations are also short distance and multi-directional. Only a few lineations are subsequently deformed, suggesting multi-event deformation (Fig. 48a). Rotation structures, with and without core stones (Fig. 48a and c), are observed in both domains. Edge to edge grain crushing is more frequent in the coarse-grained domain than in the fine-grained domain (Fig. 47a, c and 48a, b). Pressure shadows are only observed in the coarse-grained domain (Fig. 48b), but are considered a minor microstructure as only two were observed.

4.7 Core 33

Core 33 sampled the mid-shelf of Marguerite Trough, and was collected by Fretwell (2005). The piston core recovered a core length of 78 cm in a water depth of 590 m. A unit of interest was sampled from 39 cm to the EOC at 78 cm; no lower boundary to this unit was retrieved. The description of the sampled unit is very basic; from 39

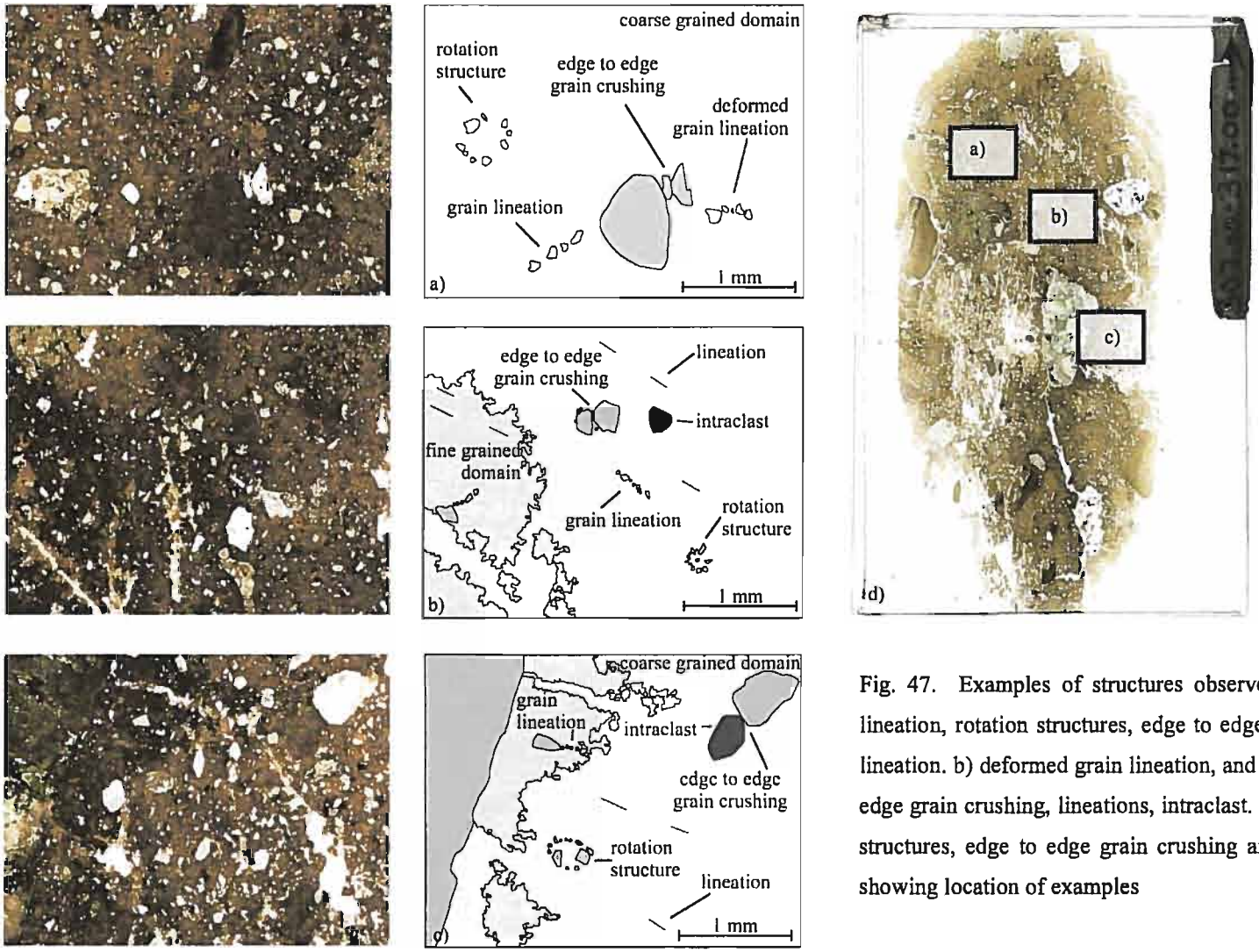

Fig. 47. Examples of structures observed in sample 16. a) grain lineation, rotation structures, edge to edge grain crushing, deformed lineation. b) deformed grain lineation, and rotation structures, edge to edge grain crushing, lineations, intraclast. c) grain lineation, rotation structures, edge to edge grain crushing and lineations. d) overview showing location of examples

Fig. 48. Examples of structures observed in sample 16. a) lineations, grain lineation, rotation structures, edge to edge grain crushing, deformed lineation. b) grain lineation, pressure shadow, edge to edge grain crushing, and lineation. c) grain lineation, rotation structures, intraclasts and deformed grain lineations. d) overview showing location of examples

cm to EOC is a dark grey, subangular sand-rich mud unit with rare subangular pebbles that is interpreted as a proximal grounding zone facies. Two samples were collected from this unit for analysis as the interval of 45-55 cm (sample 17), and 65-75 cm (sample 18).

X-radiographs of core 33 were obtained as means to compare Fretwell's (2005) unit description to the overview description of the thin section samples from this core. Fretwell (2005) identified a single unit but, comparing both the samples and the x-radiograph revealed some differences. The x-radiograph shows a variable texture which is reflected in the differing textures of the two samples. Sample 17 has a crude horizontality in the configuration of the domains found in the sample, with a sequence of coarse, very fine, and very coarse domains. Sample 18, however, is coarse-grained (the same texture as the coarse-grained domain found in sample 17) with fine grain domains (texturally different from the very fine-grained domains found in sample 17). There is no clear boundary in the x-radiograph between these two samples but there is a visible transition from one texture to another.

4.7.1 Detailed description of Sample 17

Texture: Sample 17 overall is coarse (coarse to fine silt) grained with a fine (fine to very fine clay) grained domain. There is top-to-bottom variability in the coarse-grained texture of the sample. At the top of the sample there is a coarse (medium silt) grained domain (labeled as such for comparative purposes as it is the same texture as the coarse (medium silt) grained domain in sample 18) whose boundary slowly diffuses into a fine (fine clay) grained domain to very fine (very fine clay) grained domain on the right of the sample. Unfortunately a large void (processing artifact) cuts through the sample at this location removing, or obscuring some of the boundary interactions, and the extent of the fine-grained domain and its shape. Two examples of the texture of the coarse (medium silt) grained and very fine (very fine clay) grained domain as well as their boundaries are shown in Figure 50a-b. What remains of the fine (clay) grained domain appears to be crudely horizontal and could extend

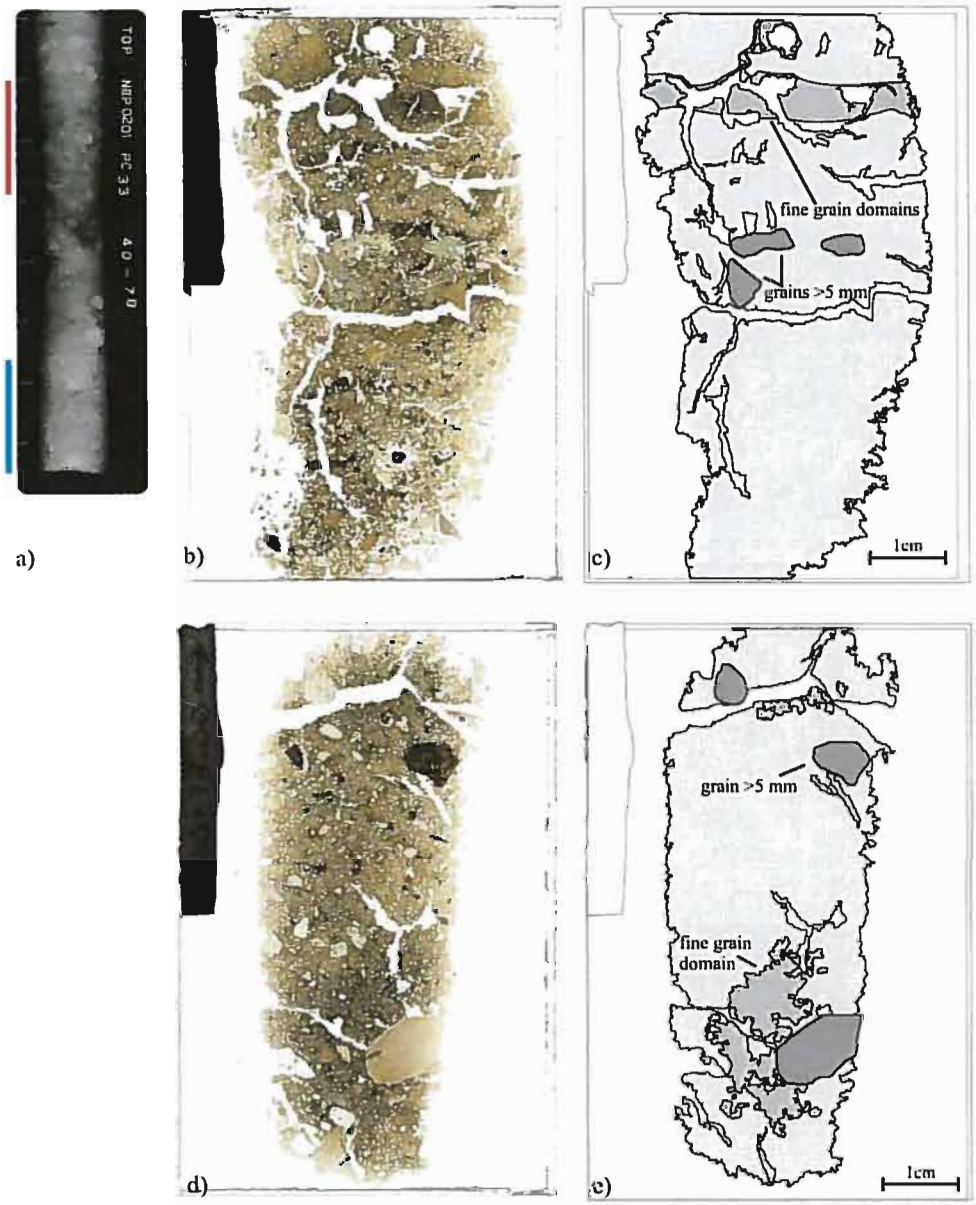

Fig. 49. Overview of samples 17 and 18 from Core 33. a) x-radiograph of section 40-78 cm of core 33, containing sample 17 at interval 45-55 cm highlighted by red bar, and sample 18 at interval of 65-78 cm highlighted by blue bar. b) thin section of sample 17. c) overview of sample 17 displaying locations of fine grain domains and skeleton grains over 5 mm. d) thin section of sample 18. e) overview of sample 18 displaying location of fine grain domains and skeleton grains over 5 mm (AMGRF, 2002).

across the entire sample. Some of the voids in the coarse (medium silt) grained domain have fine (clay) grained domain around them but it is unclear if this is the same domain or a separate one. These upper domains will henceforth be grouped

together, based on textural and structural similarities (see below). Given that the upper boundary between the coarse and fine-grained domain is diffusive where the lower boundary is, in the places visible, distinctive and crudely horizontal, the lower semi-horizontal boundary will be considered a unit boundary. This upper unit will be referred to as unit 1 and rest of the sample will be referred to as unit 2. Below unit 1 is a very coarse (coarse silt) grained domain, unit 2 (Fig. 50b, and for texture comparison see Fig. 50a (medium silt) and Fig 50c, 51a-c (coarse silt)). This lower very coarse-grained domain has a texture that is not as cohesive or as dense as the coarse-grained domain in unit 1; it varies in texture (fine to coarse silt) but is dominated by skeleton grains from the larger size fraction, including three skeleton grains over 5 mm, which are absent in unit 1. Nikon imaging software is used to define the boundaries of the domains or units. There is the only one fine-grained domain in the sample in unit 1; in the sample overview (Fig. 49b-c) there appears to be other horizontal fine grain domains but they are intraclasts of a fine-grained sediment. Voids are prevalent in this sample in the form of cracks, which could be due to the texture of the very coarse-grained domain making it more susceptible to crack formation during thin section production. None of these cracks are rimmed with sediment, which would suggest they were porewater related, so they are more likely processing artifacts and not microstructures. There are multiple lithologies of skeleton grains in this sample; the greatest variety occurring in the very coarse-grained domain, and the least variety in the very fine and coarse-grained domains. Skeleton grain shape ranges from rounded to angular, with subangular the most common. An aside, Fretwell (2005) did state in her description of the unit containing this sample that subangular pebbles are rare; her reference is to clast shape, where the description here refers to skeleton grain shape. There are multiple intraclasts of a different diamicton present in this sample, mostly in the second unit but a few were observed in the first as well (Fig. 50b-c, and 51a-c).

Structure: The structures observed in the thin section are ductile deformation and brittle deformational structures, with no porewater induced structures observed. Not all the structures observed are found in all units. The structures in unit 1 are as

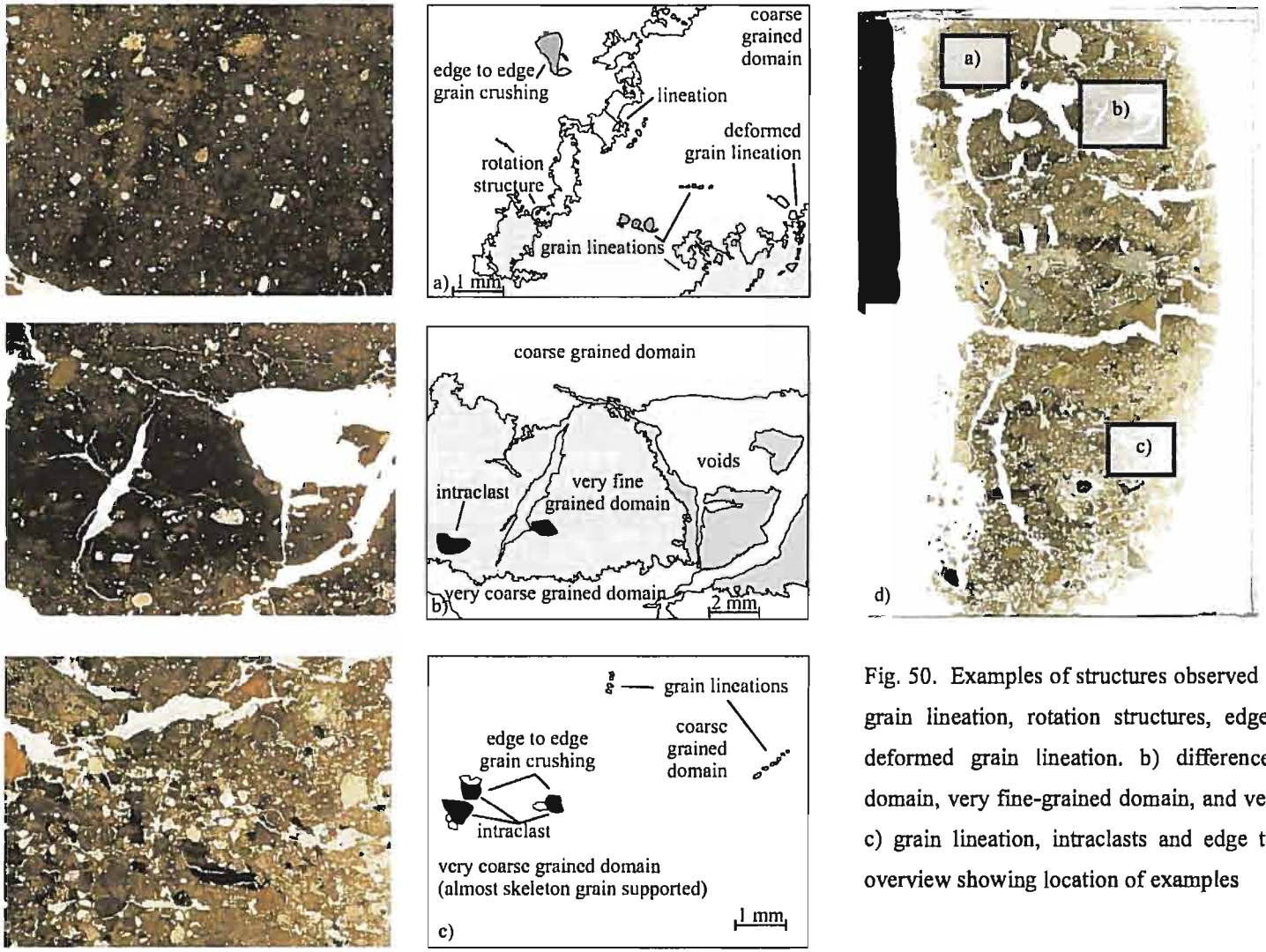

Fig. 50. Examples of structures observed in sample 17. a) lineations, grain lineation, rotation structures, edge to edge grain crushing, deformed grain lineation. b) difference between coarse-grained domain, very fine-grained domain, and very coarse-grained domain.. c) grain lineation, intraclasts and edge to edge grain crushing. d) overview showing location of examples

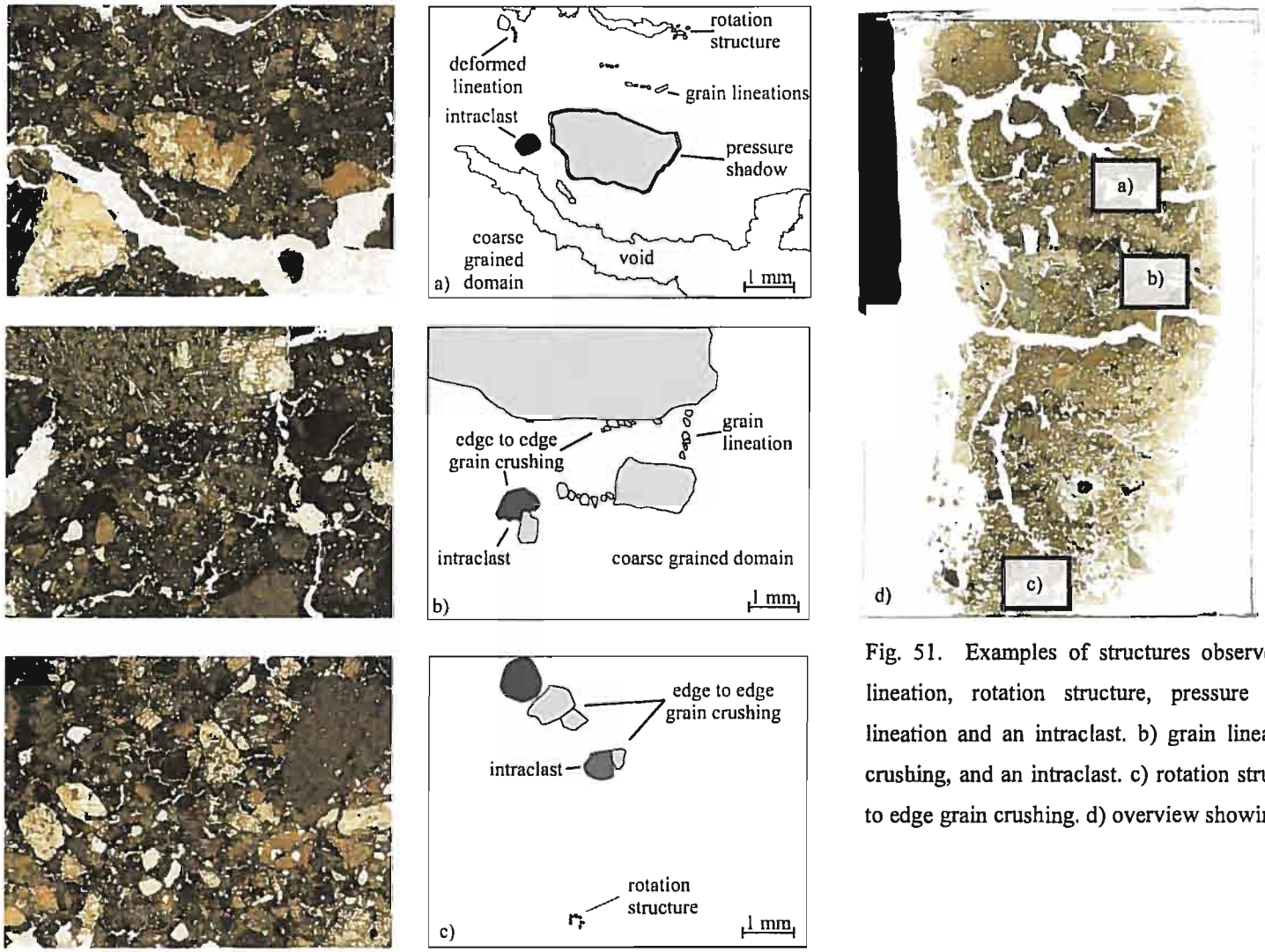

Fig. 51. Examples of structures observed in sample 17. a) grain lineation, rotation structure, pressure shadow, deformed grain lineation and an intraclast. b) grain lineations, edge to edge grain crushing, and an intraclast. c) rotation structure, intraclasts and edge to edge grain crushing. d) overview showing location of examples

follows. The fine-grained domain in unit 1 contained the fewest, and the least variety of microstructures; this is most likely due to the size the unit, and the scarcity of skeleton grains. The coarse-grained domain in unit 1 contained the most microstructures and all the types identified except for pressure shadows; grain lineations are the most common, rotation structures are identified, and lineations are the least common. Grain lineations are short distance, multi-directional, and some had undergone subsequent deformation (Fig. 50a,c and 51a-b). Rotation structures are the second most common microstructure observed in the coarse-grained domain. Edge to edge grain crushing is rare (Fig. 50a). These structures are found in close association with each other. The structures in unit 2 are as follows. Grain lineations are scarce, with only a few observed; mostly composed of the small skeleton grain size fraction (Fig.51a and c). The second most common microstructure observed in the very coarse-grained domain is edge to edge grain crushing (Fig. 50c, 51b-c). Lineations are absent and one pressure shadow is identified (Fig. 51a). There are only a few microstructures identified in total, and of those there isn't any clear association between them. Figure 51b contains a couple of grain lineations but this was the only cluster of structures identified.

4.7.2 Detailed description of Sample 18

Texture: Sample 18 is coarse (medium silt) grained with multiple fine (clay) grained domains. The boundaries of the fine grain domains are irregular and diffuse into the surrounding coarse-grained domain, and are identified using Nikon imaging software. There is a large cluster of fine-grained domains at the bottom of the sample in close proximity to the largest skeleton grain in the sample, and a second smaller cluster at the top of the sample bordering a prominent void in that area. There are several voids in the sample, in the form of cracks; these are processing artifacts created during thin sample production. There are three skeleton grains over 5 mm in the sample, randomly distributed throughout the sample. The shape of the skeleton grains range from rounded to angular, with subangular being the most common shape observed. There are multiple skeleton grain lithologies in this sample, with the greatest variety

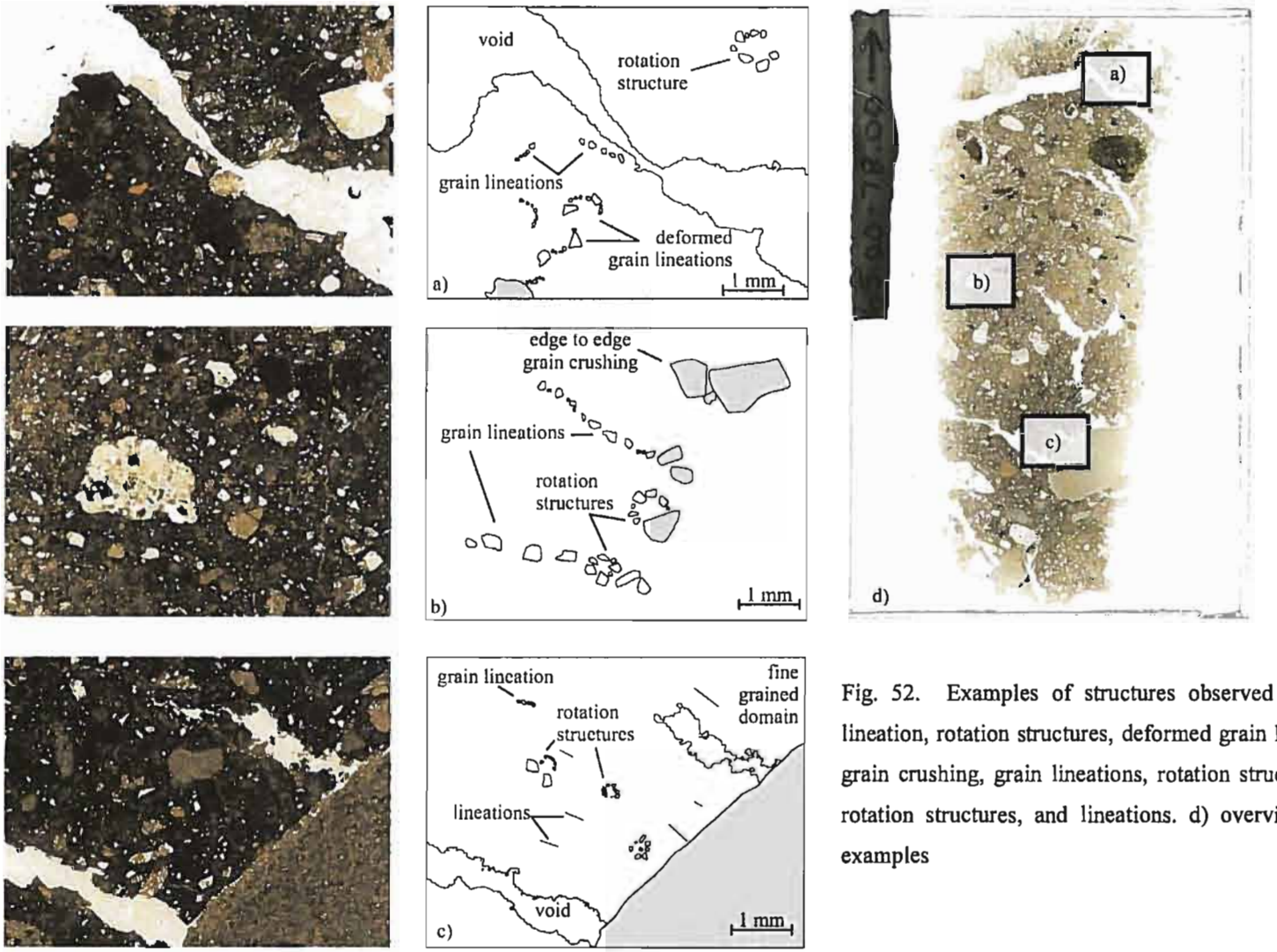

Fig. 52. Examples of structures observed in sample 18. a) grain lineation, rotation structures, deformed grain lineation. b) edge to edge grain crushing, grain lineations, rotation structures. c) grain lineation, rotation structures, and lineations. d) overview showing location of examples

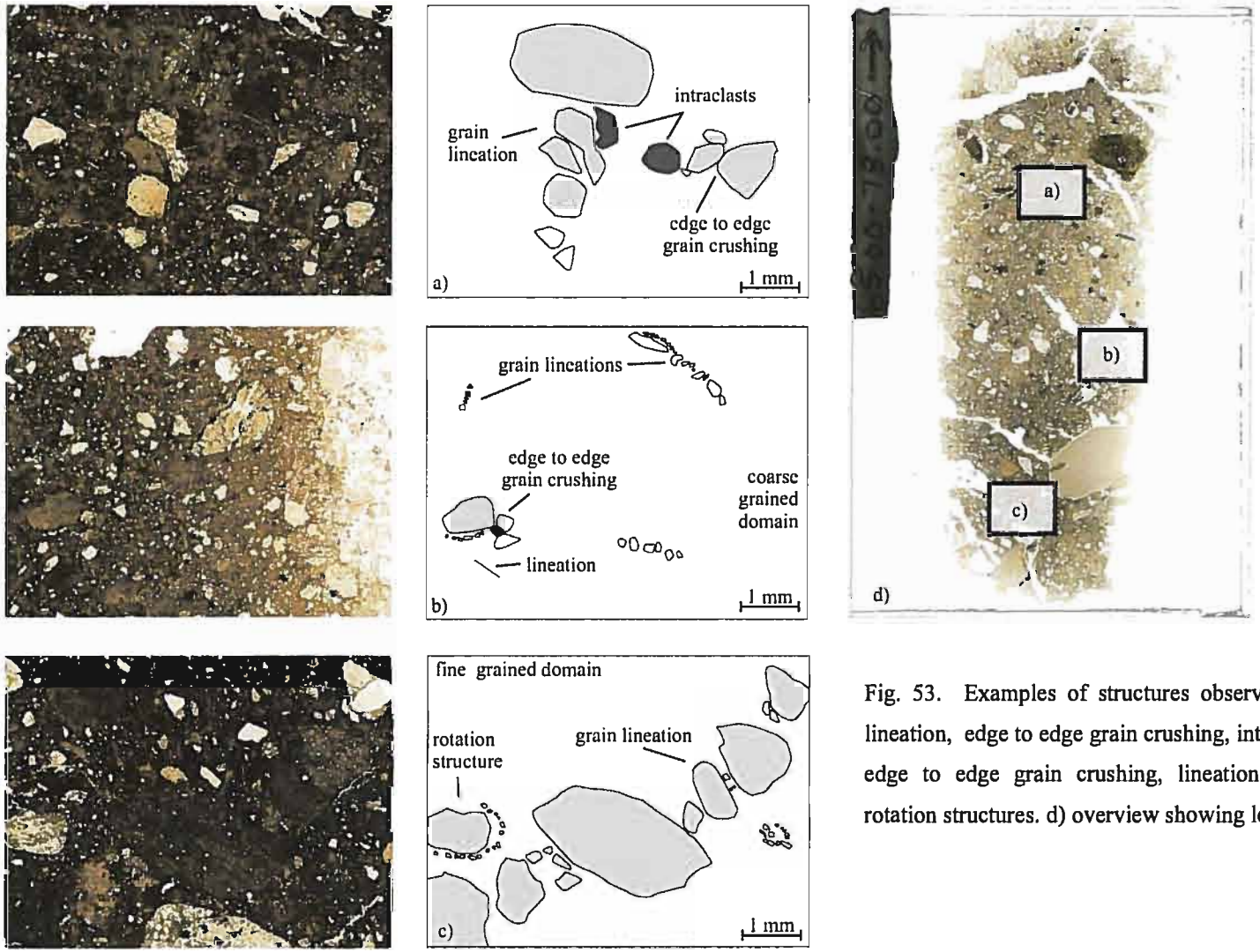

Fig. 53. Examples of structures observed in sample 18. a) grain lineation, edge to edge grain crushing, intraclasts. b) grain lineations, edge to edge grain crushing, lineations. c) grain lineation, and rotation structures. d) overview showing location of examples

occurring in the large skeleton grain size fraction. Intraclasts of another diamicton are present in this sample (Fig. 53a-b).

Structure: The structures observed in the thin section are ductile and brittle deformational structure; no porewater induced structures were observed. All structures observed are identified in both domain types. Figures 52 and 53 contain examples of the microstructures identified that will be discussed in detail as follows. The most common microstructure is grain lineations. The grain lineations are both short and long distance, multi-directional, and some had been subsequently deformed. This structure is observed as being composed of large skeleton grains (Fig. 53a, and c). The second most common microstructure are lineations; these are observed to be short distance and multi-directional. Rotation structures are common and observed with and without core stones (Fig. 52, and 53c). Edge to edge grain crushing is identified (Fig. 52b, 53a-b), although it is a minor microstructure.

Chapter 5 - Interpretation

5.0 Introduction

The micromorphological descriptions of the grounding line deposits in this study show a complex deformational history. Structures indicative of planar and rotational deformation have been found in close association with each other in all but one sample (17). This outlier sample (17), along with another (sample 18), are from a unit previously interpreted as a proximal grounding line facies by Fretwell (2005) in core 33; all other sampled facies have been previously interpreted as subglacial (Fretwell, 2005; Heroy, 2006). It is for this reason that samples 17 and 18 will be discussed separately from to the other samples, as a means of correlating the microscopic interpretations to a possible alternate facies. Then their context to the other samples, and the broader grounding line environment will be discussed. For comparative purposes a qualitative summary table of microstructures is presented (Table 2) with a scale of microstructure development ranging from poorly developed or rare to well developed or abundant.

5.1 Samples 1-16

The microstructures observed in thin section indicate that the sediments were deposited in a warm-based subglacial environment, having undergone multiple deformation events in a variable-stress environment. While no water escape structures were observed, the diffuse boundaries between differing plasma textures in the samples can be attributed to the presence of porewater, as well as the influence of ductile deformation. Ductile deformational structures, such as rotational and necking structures, were observed in thin section. Rotational structures were observed in all samples, ranging from poorly to well developed and abundant (Table 2), with and without core stones. Rotational structures, when observed in glacially derived sediments, are the result of velocity gradients caused by shearing in a low effective pressure environment (van der Meer, 1993, 1997; Phillips & Auton, 2000;

Table 2
Summary of micromorphological descriptions (following Carr (1999) and Reinardy *et al.* (2011)).

Sample	Till type Qualitative	Till type Quantitative	Texture			Voids	Structures					
			Skeleton		Plasma							
			Grain sorting	Intraclasts	Cohesive		Rotation	Pressure Shadow	Crushed/ Fractured grains	Grain lineations	Lineations	Multi event
1	so	so	L	●	H	L	●●	●	●	●●	●●	●
2	ST	Tr	M	●	L	L	●●		●	●●●	●●●	●
3	ST	Tr	L	●●	L	L	●●	●	●	●●●	●●●	●
4	ST	Tr	L	●●	L	L	●●●	●	●	●●	●●●	●
5		so	L	●●●	H	L	●●		●●	●●	●	●
6		so	L	●	H	L	●●	●	●	●●●	●●●	●
7		so	L	●	H	L	●●		●●	●●●	●●●	●
8	so	so	M	●	L	L	●●		●	●●●	●●●	●
9	so	so	L	●	M	L	●●	●	●	●●●	●●	●
10	ST	so	L	●	L	L	●●		●	●●●	●●	●
11	so	so	L	●●	M	L	●	●	●●	●	●	●
12	so	so	L	●●	M	L	●●		●●	●●	●	●
13	ST	ST	L	●	M	L	●●		●	●●	●	●
14		so	L	●	H	L	●●		●	●●●	●●	●
15		so	L	●	M	L	●●		●	●●	●	●
16		Tr	L	●	H	L	●	●	●	●●	●●	●
17		Tr	L	●	M	L	●	●	●	●	●	●
18		Tr	L	●	M	L	●●		●	●●	●●	●

Texture and Structures: ●, rare/poorly developed (L); ●●, common/moderately developed (M); ●●●, abundant/well developed (H).
Till type (qualitative): Samples described as stiff (ST) or soft (so) defined by Heroy (2006)
Till type (quantitative): Using shear strength measurements to determine till type - Soft (so) <12 kPa, Transitional (Tr) 12 kPa - 45 kPa, Stiff (ST) >45 kPa
Voids: L= lab induced voids

Hart & Rose, 2001; van der Meer *et al.*, 2003; Menzies *et al.*, 2006; Piotrowski *et al.*, 2006; Phillips, 2006; Denis *et al.*, 2010), caused by pore water pressure equaling glacial induced pressure. As rotational structures are observed in other environments, their presence is taken as an indication of the presence of porewater within the sample during deformation, not as a diagnostic structure attributed to a specific depositional environment (Hooyer & Iverson, 2000; Thomason & Iverson 2006; Hess, 2009). These rotational deformational structures are observed in close relation to planar deformational structures, such as lineations and grain lineations, which are formed due to shear planes (van der Meer, 1997; van der Meer *et al.*, 2003; Hiemstra & Rijsdijk, 2003). All lineations and grain lineations are short, and their length is attributed to non-pervasive deformation. These structures are also closely associated with *in situ* crushed grains, or edge to edge grain crushing. Edge to edge grain crushing has been related to high stress environments indicative of the subglacial environment (Carr, 1999; Hiemstra & Rijsdijk, 2003; Carr *et al.*, 2006; Larson *et al.*, 2007). It is this grain crushing induced by glacial action that produces the skeleton grain shapes observed in these samples. This cataclastic deformation is the result of rapid and brief deformation (Larson *et al.*, 2007; Denis *et al.*, 2010). Given the presence of structures formed in both low and high stress environments in the sediments occurring in close association, then the depositional environment is concluded to have dynamic stress fields with ductile and brittle deformation occurring concurrently. With some of the structures, such as the grain lineation in Figure 8c, having undergone subsequent deformation, then it is probable that these sediments were formed through multiple deformation events. The presence of soft sediment intraclasts of a different diamict is evidence of the reworking of pre-existing sediments (van der Meer, 1993; Carr, 2000).

While this confirms both Fretwell's (2005) and Heroy's (2006) interpretation of a subglacial origin for these sediments, there are conflicts with their other assertions. First is the identification of a single unit which the micromorphological analysis doesn't support. Instead several units can be identified that have undergone the same or similar processes during transportation to, and deposition at, the grounding line.

Most notably are cores 4, 24, 57, and 55. The boundaries of these units are not visible in thin section, as they were not sampled, nor do there appear to be any sharp unit boundaries visible in the x-radiographs. Sample 11, from core 55, contains a lower fine-grained domain with a visually distinct boundary that is undulating and appears to have skeleton grains embedded into it, suggesting a deformational contact between the two domains. This is possibly a unit boundary, but cannot be said with any confidence; given that only a small amount of this domain/unit is visible for analysis, and a lower boundary to this unit was not sampled, nor is one visible on the x-radiograph. Therefore it is likely that most, if not all, unit boundaries are gradational and represent extensive sediment reworking.

The second assertion involves is the interpretation of emplacement via lodgement or deformation based solely on the descriptors of stiff or soft, respectively. A clear example of this was Heroy's (2006) description of sample 2 as stiff, and sample 8 as soft when micromorphological analysis identified these samples as having nearly identical texture and structures (Table 2). Heroy's (2006) use of this singular descriptor as sole basis for determining emplacement, especially when such other standard techniques as a detailed macroscopic description are neglected, is rejected. Heroy (2006) is not the only author in the Antarctic region to base his interpretation on this criterion (c.f. Wellner *et al.*. 2001; Shipp *et al.*, 2002). However, with the increasing use of micromorphology in the Antarctic, sediments previously attributed to lodgement are being reclassified as deformation (Baroni & Fasano, 2006). Recent work by Reinardy *et al.* (2011) has determined that soft, transitional and stiff diamicton/till do not relate to a change in the process of emplacement but a shift from normal to streaming ice. They clearly identify shear strength boundaries of soft, transitional, and stiff diamicton that relate to the change in proportion of subglacial microstructures. Heroy's (2006) classification of soft or stiff diamicton differs from those of Reinardy *et al.* (2011). These differences are summarized in Table 2. Heroy's (2006) classifications are termed qualitative as they subjectively distinguish between these two types, and there are no evidence to support his classification. Reinardy *et al.*'s (2011) are termed quantitative as they are based on several objective criteria. As

is expected, the greatest differences between the two classifications are Heroy's (2006) identification of stiff diamicton, with only a single sample, 13, identified as stiff by both authors (Table 2). According to Reinardy *et al.* (2011) there is no difference in the type of microstructures found in the soft, transitional, and stiff diamictons but there is a difference in the proportions of these structures. It was determined that the soft till is a reworked homogenized version of the underlying stiff till, all having undergone deformation, which accounts for the presence of the same set of microstructures. Proportionally soft till contains fewer microstructures than the other two types, with an increase in the presence of intraclasts. Stiff till, in contrast contains the most microstructures, with grain crushing occurring most frequently in this type (Reinardy *et al.*, 2011). It is thought that initial emplacement of diamicton was by deformation, and deformation-induced ductile structures were formed. After this initial deposition, dewatering and compaction occurred, as diamicton emplacement continued via deformation, caused by the overriding ice and/or an increase in sediment thickness. As the necessary water for ductile deformation to occur was removed, deformation became brittle, forming such structures as crushed grains. This now "stiff" sediment layer was overlain by a time-transgressive deforming sediment layer that moved upwards creating the transitional layer between stiff and soft diamicton. This incorporated (intraclasts) and homogenized (destruction of previous microstructures and accounting for the decrease in the proportion of structures) the lower stiff sediment layer (Reinardy *et al.*, 2011). As our study only contains a single "stiff" sample, as defined by Reinardy *et al.* (2011), and not a complete "set" of samples from the soft, transitional, and stiff diamicton in a single core, it cannot appropriately confirm these findings, nor was it in the scope to do so. However, as the separate units identified in this study have diffuse boundaries, the idea that lower sediment layers are homogenized into the upper sediment layers (or units) is supported, as is identifying deformational origins for all diamicton types.

Given that these sediments (samples 1 -16) are attributed to be deformational in origin, they contain multiple units with diffusive boundaries, and intraclasts of another diamict, it is proposed that the sediments are the product of extensive

sediment reworking in a subglacial environment. However, it is not known at what stage these sediments were reworked or what contribution soft or stiff diamicton had to overall sediment deformation. Further work is needed to resolve these issues. More extensive sampling in the grounding line environment, as well as detailed descriptions of variations in diamicton, is needed to capture a more complete picture of emplacement.

5.2 Samples 17-18 (core 33)

Sample 18 is considered deformational in origin and contains microstructures indicating that the sediment was deposited in a warm-based subglacial environment, having undergone multiple deformation events in a variable stress environment, as with the previous samples. However, this is not the case for sample 17, which overlies sample 18. Sample 17 contains two units. The uppermost unit (1) contains both ductile and brittle deformational structures in close association. There are minimal microstructures upon which to base an interpretation on, due to the large voids in this unit, but this unit is thought to be subglacial in origin. The second lower unit (2) contains a few random ductile and brittle deformational structures. These structures are not associated, and are not thought to have formed concurrently. The texture of the plasma in this unit is not cohesive, and the unit is nearly skeleton grain supported. This unit is interpreted to be proximal grounding line in origin based on Carr's (2000) criteria for differentiating subglacial and proximal sediments. We consider the sediments in the core to have been deposited during glacial recessional standstill. The lowermost portion of the core (sample 18) was deposited subglacially, and as the grounding line retreated, proximal grounding line sediments were deposited (lower portion of sample 17). In the x-radiograph, a gradual transition can be seen between these two samples. The upper unit in sample 17 represents a possible localized, probably temporary, re-advance of the grounding line given the small unit thickness. Fretwell (2005) identified the entire facies (containing both samples) as proximal grounding line; this interpretation is based on a very brief macroscopic description and it might be only considered valid for a portion of this core.

Chapter 6 – Discussion and Conclusion

From the micromorphological descriptions of all the samples within this study, it is determined that the grounding line sediments were deposited in a deformational subglacial environment, with a warm base, having undergone multiple deformation events in a variable stress environment.

As previously stated, there are two types of grounding line deposits sampled in this study; morainal ridges in Bransfield basin, and grounding line wedges in the Vega Trough, Anvers Trough, Biscoe Trough, and Marguerite Trough. What the analysis in this thesis has shown is that all of these features have been formed by deformation of subglacial sediments. The only core that was not identified as having multiple units was the core obtained in Bransfield basin sampling the morainal ridges. Given this analysis, the ridge sampled in Bransfield basin was likely formed by the squeezing of subglacial sediments out beyond the grounding line as the samples contain microstructures indicative of the subglacial environment and not via fluvial processes or gravity flows. Since there are microstructures that have undergone subsequent deformation after formation, it is possible that this morainal ridge could have undergone deformation by glacial push. In all the other cores multiple units were identified and all those cores are sampling grounding line wedges from different regions. It is thought that the differing textures within the cores, or the different units, are remnants of the old deforming layers that were transported to the grounding line, and subsequently re-eroded and deformed as the grounding line advanced. This re-erosion of these layers during advance could be the source of the intraclasts that are observed within these samples, and re-deformation of these sediments during advance amalgamates the individual layers into a singular deforming layer – which accounts for the lack of unit boundaries and the subglacial multi-event deformational structures.

The use of micromorphology in the investigation of grounding line sediments from around the Antarctic Peninsula has demonstrated that these deposits have complex

deformational histories and subglacial origins. It was determined that grounding zone wedge contain multiple units, or diamicton layers, with homogenized boundaries. The multiple diamicton units/layers are due to the accretionary formation of a grounding line wedge. All the sediments were deposited via deformation, and continual reincorporation, homogenization of lower diamicton layers by upper diamicton layers produced what macroscopically appeared to be a single massive diamicton unit. This could suggest a change in ice-flow dynamics that produced multiple diamicton units/layers, with multiple deformation events homogenizing unit/layer boundaries. The morainal ridge that was sampled, alternatively, is composed of a single unit, or diamicton layer, that was subglacial in origin and believed to have been pushed out to form a ridge that was subsequently deformed via glacial push. The determination of emplacement in a warm based environment, in combination with the spatial coverage of this study across the Antarctic Peninsula, supports Kilfeather *et al.*'s (2011) suggestion that glacial retreat was caused by encroachment of Circumpolar Warm Deep water onto the continental shelf. Work needs to be continued in this environment to confirm these findings, capture a more complete picture of emplacement, and to link to the new work done by Reinardy *et al.* (2011) regarding soft and stiff diamicton.

References:

Alley, R.B., Anandakrishnan, S., Dupont, T.K., Parizek, B.R., Pollard, D., 2007. Effect of sedimentation on Ice-Sheet Grounding-Line stability. Science 315, 1838-1841

AMGRF – Antarctic Marine Geology Research Facility, 2002. Digital X-Radiograph Photos. Retrieved September 27, 2009 from http://www.arf.fsu.edu/digital_data/x_radiographs/palmer_02-01.php

Anandakrishnan, S., Catania, G.A., Alley, R.B., Horgan, H.J., 2007. Discovery of Till deposition at the Grounding-Line of Whillans Ice Stream. Science 315, 1835-1838

Anderson, J.B., 1999. Antarctic Marine Geology. Cambridge University Press, London. pp 90, 92, 103, 177, 220, 207, 233-234, 243, 247-248

Anderson, J.B., Kennedy, D.S., Smith, M.J., Domack, E.W., 1991. Sedimentary facies associated with Antarctica's floating ice masses. In: Anderson, J.B., Ashley, G.M., (Eds.), Paleoclimatic interpretation of glacial marine deposits. Geological Society of America Special Paper, 256, 1-25

Anderson, J.B., Shipp, S.S., Bartek, L.R., Reid, D.E., 1992. Evidence for a grounded ice sheet on the Ross Sea continental shelf during the late Pleistocene and preliminary paleodrainage reconstruction. In: Elliot, D.H. (Eds.), Contributions to Antarctic Research Series III, Vol. 57. American Geophysical Union, Washington, DC., pp. 93-42

Anderson, J.B., Wellner, J.S., Lowe, A.L., Mosola, A.B., Shipp, S.S., 2001. Footprint of the Expanded West Antarctic Ice Sheet: Ice Stream History and Behavior, GSA Today 11 (10), 4-9

Anderson, J.B., Shipp, S.S., Lowe, A.L., Wellner, J.S., Mosola, A.B., 2002. The Antarctic Ice Sheet retreat during the Last Glacial Maximum and its subsequent retreat history: a review. Quaternary Science Reviews 21, 49-70

Banfield, L.A., Anderson, J.B., 1995. Seismic facies investigation of late Quaternay glacial history of Bransfield Basin, Antarctica, American Geophysical Union. Antarctic Research Series 68, 123-140.

Bard, E., Hamelin, B., Fairbanks, R.G., 1990. U-Th ages obtained by mass spectrometry in corals from Barbados: sea level during the past 130,000 years. Nature 346, 456-458

Barker, P.F., Diekmann, B., Escutia, C., 2007. Onset of Cenozoic Antarctic glaciation. Deep Sea Research II: Topical Studies in Oceanography 54 (21-22), 2293-2307

Baroni, C., Fasano, F., 2006. Micromorphological evidence of warm-based glacier deposition from the Ricker Hills Tillite (Victoria Land, Antarctica). Quaternary Science Reviews 25, 976-992

Barrett, P.J., 1991. Antarctic and global change: a geological perspective. In: Harris, C., and Stonehouse, B., (Eds.) Antarctica and Global Climate Change. Belhaven Press, London, pp. 35-50

Bart, P.J., Anderson, J.B., 1995. Seismic record of glacial events affecting the Pacific margin of the northwestern Antarctic Peninsula. In: Cooper, A.K., Barker, P.F., and Brancolini, G., (Eds.), Geology and Seismic Stratigraphy of the Antarctic margin. Antarctic Research Series, vol. 68. American Geophysical Union, Washington, D.C., pp. 75-95

Bentley, M.J., Anderson, J.B., 1998. Glacial and marine geological evidence for the ice sheet configuration in the Weddell Sea – Antarctic Peninsula region during the last glacial maximum. Antarctic Science 10, 309-325

Boulton, G. S., 1979. Processes of glacier erosion on different substrata. Journal of Glaciology 23, 15–37.

Boulton, G.S., 1986. A paradigm shift in glaciology? Nature 322, 18

Boulton, G.S., Hindmarsh, R.C.A., 1987. Sediment deformation beneath glaciers: rheology and glacial consequences. Journal of Geophyiscal Research, 92, 9059-9082

Brewer, R., 1976. Fabric and Mineral Analysis of Soils. Krieger, Huntington: New York. 482pp.

Canals, M., Estrada, F., Urgeles, R., GEBRAP 96/97 Team, 1998. Very high-resolution seismic definition of glacial and postglacial sediment bodies in the continental shelves of the northern Trinity Peninsula region, Antarctica. Annals of Glaciology 27, 260-264

Canals, M., Urgeles, R., Calafat, A.M., 2000. Deep sea-floor evidence of past ice streams off the Antarctic Peninsula. Geology 28, 32-34

Canals, M., Casamor, J. L., Urgeles, R., Calafat, A. M., Domack, E., Baraza, J., Farran, M. & De Batist, M. 2002: Seafloor evidence of a subglacial sedimentary system off the northern Antarctic Peninsula. Geology 30, 603–606.

Carr, S., 1999. The Micromorphology of the Last Glacial Maximum sediments in the Southern North Sea. Catena 35, 123-145

Carr, S., 2000. Micromorphological evidence supporting Late Weichselian glaciation of the Northern North Sea. Boreas 29, 315–328.

Carr, S., 2001. Micromorphological criteria for discriminating subglacial and glacialmarine sediments: evidence from a contemporary tidewater glacier, Spitsbergen. Quaternary International 86, 71-79

Carr, S., 2004. Microscale features and structures. In: Evans, D., Benn, D. (Eds.), 2004. A practical guide to the study of Glacial Sediments. Arnold: London. pp 115-144

Carr, S., Homes, R., van der Meer, J.J.M., Rose, J., 2006. The Last Glacial Maximum in the North Sea Basin: micromorphological evidence of extensive glaciation. Journal of Quaternary Science 21 (2), 131-153

Conway, H., Hall, B.L., Denton, G.H., Gades, A.M., Waddington, E.D., 1999. Past and Future Grounding-Line retreat of the West Antarctic Ice Sheet. Science 286 (5438), 280-283

Cowan, E.A., Seramur, K.C., Cai, J., Powell, R.D., 1999. Cyclic sedimentation produced by fluctuations in meltwater discharge, tides and marine productivity in an Alaskan Fjord. Sedimentology 46, 1109-1126

Dahlgren, K.I.T., Vorren, T.O., Laberg, J.S., 2002. The role of grounding-line sediment supply in ice-sheet advances and growth on continental shelves: an example from the mid-Norwegian sector of the Fennoscandian ice sheet during the Saalian and Weichselian, Quaternary International 95-96, 25-33

Denis, M., Guiraud, M., Kontae, M., Buoncristiani, I.F., 2010. Subglacial deformation and water-pressure cycles as a key for understanding ice stream

dynamics: evidence from the Late Ordovician succession of the Djado Basin (Niger). International Journal of Earth Sciences 99 (6), 1399-1425

Denton, G.H., Hughes, T.J., 2002. Reconstructing the Antarctic Ice Sheet and the Last Glacial Maximum. Quaternary Science Reviews 21, 193-202

Denton, G.H., Prentice, M.I., Burckle, L.H., 1991. Cenozoic history of the Antarctic Ice Sheet. In: Tingey, R.J. (Eds.), The Geology of Antarctica. Claredon Press, Oxford, pp. 365-433

Domack, E.W., Jacobson, E.A., Shipp, S., Anderson, J.B., 1999. Sedimentologic and stratigraphic signature of the late Pleistocene/Holocene fluctuations of the West Antarctic Ice Sheet in the Ross Sea: a new perspective Part 2. Geological Society of America Bulletin 111, 1486-1516

Domack, E.W., Leventer, A., Gilbert, R., Brachfeld, S., Ishman, S., Camerlenghi, A., Gavahan, K.., Carlson, D., Barkoukis, A., 2001a. Cruise reveals history of Holocene Larsen Ice Shelf. EOS 82, 13-17

Domack, E.W., Leventer, A., Dunbar, R., Taylor, F., Brachfeld, S., Sjunneskog, C., and the ODP Leg 178 Scientific part, 2001b. Chronology of the Palmer Deep site, Antarctic Peninsula: a Holocene paleoenvironmental reference for the circum-Antarctic. The Holocene 11, 1-9

Dowdeswell, J.A., Ó Cofaigh, C., Pudsey, C.J., 2004. Thickness and extent of the subglacial till layer beneath an Antarctic paleo-ice stream. Geology 32, 13-16

Dreimanis, A., 1989. Tills, their genetic terminology and classification. In: Goldthwait, R.P., Matsch, C.L. (Eds.), Genetic classification of Glacigenic Deposits. Balkema, Rotterdam, pp. 17-84

Evans, D.J.A., Pudsey, C.J., Ó Cofaigh, C., Morris, P., Domack, E.W., 2005. Late Quaternary glacial history, flow dynamics and sedimentation along the eastern margin of the Antarctic Peninsula Ice Sheet. Quaternary Science Reviews 24 (5-6), 741-774

Evans, D.J.A., Phillips, E.R., Hiemstra, J.F., Auton, C.A., 2006. Subglacial till: Formation, sedimentary characteristics and classification. Earth-Science Reviews 78, 115-176

Flower, B.P., Kennett, J.P., 1994. The middle Miocene climatic transition: East Antarctic Ice sheet development, deep ocean circulation and global carbon cycling. Palaeogeogaphy, Palaeoclimatolology, Palaeoecology 67, 3-17

Fretwell, L.O., 2005. Glacial history in Marguerite Bay, Antarctic Peninsula, since the Last Glacial Maximum. Ph.D. Dissertation. Rice University. Pp. 189-209

Gagliardini, O., Durand, G., Zwinger, T., Hindmarsh, R.C.A., Le Meur, E., 2010. Coupling of ice-shelf melting and buttressing is a key process in ice-sheets dynamics. Geophysical Research Letters 37, L14501

Goldberg, D., Holland, D., Schoof, C., 2009. Grounding line movement and ice shelf buttressing in marine ice sheets. Journal of Geophysical Research-Earth Surface 114, (F04026)

Harden, S.L., DeMAster, D.J., Nittrourer, C.A., 1992. Developing sediment geochronologies for high-latitude continental shelf deposits: a radiochemical approach. Marine Geology 103, 69-97

Hart, J., Rose, J., 2001. Approaches to the study of glaicer bed deformation. Quaternary International 86, 45-48

Heroy, D.C., 2006. The Antarctic Peninsula Ice sheet since the Last Glacial Maximum. Ph. D. Dissertation. Rice University pp 12, 33, 103, 170-172, 174, 192, 198, 200, 202

Heroy, D.C., Anderson, J.B., 2005. Ice-sheet extent of the Antarctic Peninsula region during the Last Glacial Maximum (LGM)—Insights from glacial geomorphology Geological Society of America Bulletin, November/December 2005, 117 (11-12), 1497-1512

Heroy, D.C., Anderson, J.B., 2007. Radiocarbon constraints on Antarctic Peninsula Ice Sheet retreat following the Last Glacial Maximum (LGM). Quaternary Science Reviews 26 (25-28), 3286-3297

Hess, D.P., 2009. Using geospatial analyses to understand Laurentide Ice Sheet dynamics in New York State from landform morphometry and till fabrics. Ph.D. Dissertation. SUNY Buffalo.

Hiemstra JF. 1999. Microscopic evidence of grounded ice in the sediments of the CIROS-1 core, McMurdo Sound, Antarctica. Terra Antarctica 6, 365–376.

Hiemstra, J.F., 2001. Microscopic analyses of Quaternary glacigenic sediments of Marguerite Bay, Antarctic Peninsula. Arctic, Antarctic and Alpine Research 33, 258-265

Hiemstra, J.F., Rijsdijk, K.F., 2003. Observing artificially induced strain: implications for subglacial deformation. Journal of Quaternary Science 18, 373–383.

Hjort, C., Ingólfsson Ó., Moller, P., 1997. Holocene glacial history and sea-level changes on James Ross Island, Antarctic Peninsula. Journal of Quaternay Research 12, 259-273

Hollin, J.T., 1962. On the glacial history of Antarctica. Journal of Glaciology, 4, 173-195

Hooyer, T.S., Iverson, N.R., 2000. Clast-fabric development in a shearing granular material: implications for subglacial till and fault gouge. Geological Society of America Bulletin 112, 683–692.

Huybrechts, P., 2002. Sea-level changes at the LGM from ice-dynamic reconstructions of the Greenland and Antarctic ice sheets during the glacial cycles. Quaternary Science Reviews 21, 203-231

Ingólfsson Ó., 2004. Quaternary glacial and climate history of Antarctica. Developments in Quaternary Science 2 (3), pp. 3-43.

Kanfoush, S.L., Hodell, D.A., Charles, C.D., Guilderson, T.P., Mortyn, P.G., Ninnemann, U.S., 2000. Millennial-scale instability of the Antarctic Ice Sheet during the Last Glaciation. Science, New Series, 288 (5472), 1815-1818

Kemp, R.A., 1985. Soil Micromorphology and the Quaternary. Q.R.A. Tech. Guide No. 2, 80pp.

Kennedy, D.S., Anderson, J.B., 1989. Quaternary glacial history of Marguerite Bay, Antarctic Peninsula. Quaternary Research 31, 255-276

Khatwa, A. and Tulaczyk, S. 2001. Microstructural interpretations of modern and Pleistocene subglacially deformed sediments: the relative role of parent material and subglacial processes. Journal of Quaternary Science 16,507–517

Kilfeather, A.A., O Cofaigh, C., Lloyd, J.M., Dowdeswell, J.A., Xu, S., Moreton, S.G., 2011. Ice-stream retreat and ice-shelf history in Marguerite Trough, Antarctic

Peninsula: Sedimentological and foraminiferal signatures, GSA Bulletin 123 (5-6), 997-1015

Kubiëna, W.L., 1938. Micropedology. Collegiate Press, Ames, Iowa, 242pp

Lajeunesse, P., Allard, M., 2002. Sedimentology of an ice-contact glaciomarine fan complex Nastapoka Hills, eastern Hudson Bay, northern Quebec. Sedimentary Geology 152, 201-220

Larsen, N.K., Piotrowski, J.A., Menzies, J., 2007. Microstructual evidence of low-strain time-transgressive subglacial deformation. Journal of Quaternary Science 22, 593-608

Larter, R.D., Barker, P.F., 1989. Seismic stratigraphy of the Antarctic Peninsula Pacific margin: a record of Pliocene-Pleistocene ice volume and paleoclimate. Geology 17, 731-734

Larter, R.D., Vanneste, L.E., 1995. Relict subglacial deltas on the Antarctic Peninsula outer shelf. Geology 23, 33-36

Licht, K.J., Dunbar, N.W., Andrews, J.T., Jennings, A.E., 1999. Distinguishing subglacial till and glacial marine diamictons in the western Ross Sea, Antarctica: Implications for a last glacial maximum grounding line. Geological Society of America Bulletin 111(1), 91-103

Menzies, J., 2000. Micromorphological analyses of microfabrics and microstructures indicative of deformation processes in glacial sediments. In: Maltman, A.J., Hubbard, B., Hambrey, M.J. (Eds.), Deformation of Glacial Materials. Geological Society, London, Special Publications, 176, 245-257

Menzies, J., 2001. Short course manual on micromorphology of glacigenic sediments. Geological Society of America

Menzies, J., 2004. Antarctic Samples – Earth Sciences, Rice University. Department of Earth Sciences, Brock University

Menzies, J., van der Meer, J.J.M., Rose, J., 2006. Till – as a glacial "tectomict", its internal architecture, and the development of "typing" method for till differentiation. Geomorphology 75, 172-200

Menzies, J., van der Meer, J.J.M., Domack, E., Wellner, J.S., 2010. Micromorphology: as a tool in the detection, analysis and interpretation of (glacial) sediments and man-made materials. Proceedings of the Geologists' Association 121, 281-292

Mosola, A.B., Anderson, J.B., 2006. Expansion and rapid retreat of the West Antarctic Ice Sheet in eastern Ross Sea: possible consequence of over-extension ice streams? Quaternary Science Reviews 25, 2177-2196

Nakada, M., Kimura, R., Okuno, J., Moriwaki, K., Miura, H., Maemoku, H., 2000. Late Pleistocene and Holocene melting history of the Antarctic Ice Sheet derived from sea-level Variations. Marine Geology 167, 85-104

O'Brien, P.E., Santis, L.DE., Harris, P.T., Domack, E., Quilty, P.G., 1999. Ice shelf grounding zone features of western Prydz Bay, Antarctica: sedimientary processes from seismic and sidescan images. Antarctic Science 11 (1), 78-91

Ó Cofaigh, C., Pudsey, C.J. Dowdeswell, J.A., 2002. Evolution of subglacial bedforms along a paleo-ice stream, Antarctic Peninsula continental shelf. Geophysical Research Letters 29, 1-4

Ó Cofaigh, C., Dowdeswell, J.A., Allen, C.S., Heimstra, J.F., Pudsey, C.J., Evans, J., Evans, D.J.A., 2005. Flow dynamics and till genesis associated with a marine-based Anarctic palaeo-ice stream. Quaternary Science Reviews 24, 709-740

Ó Cofaigh, C., Larter, R.D., Dowdeswell, J.A., Hillenbrand, C.D., Pudsey, C.J., Evans, J., Morris, P., 2005. Flow of the West Antarctic Ice Sheet on the continental margin of the Bellingshausen Sea at the Last Glacial Maximum. Journal of Geophysical Research 110 (B11103), 1-13

Ó Cofaigh, C., Evans, J., Dowdeswell, J. A. & Larter, R. D. 2007: Till characteristics, genesis and transport beneath Antarctic paleo-ice streams. Journal of Geophysical Research 112, doi:10.1029/2006JF000606.

Payne, A. J., Vieli, A., Shepherd, A.P., Wingham, D.J., Rignot, E., 2004. Recent dramatic thinning of largest West Antarctic ice stream triggered by oceans. Geophysical Research Letters 31.

Phillips, E., 2006. Micromorphology of a debris flow deposit: evidence of basal shearing, hydrofracturing, liquefaction and rotational deformation during emplacement. Quaternary Science Reviews 25 (7-8), 720-738.

Phillips, E.R., Auton, C.A., 2000. Micromorphological analyses ofmicrofabrics and microstructures indicative of deformation processes in glacial sediments. In: Maltman, A.J., Hubbard, B.,Hambrey, M.J. (Eds.), Deformation of Glacial Materials. Geological Society, London, Special Publications, Vol. 176,pp. 279–292.

Piotrowski, J.A., Larsen, N.K., Menzies, J., Wysota, W., 2006. Formation of subglacial till under transient bed conditions: deposition, deformation, and basal decoupling under a Weichselian ice sheet lobe, central Poland. Sedimentology 53, 83-106.

Pope, P.G., Anderson, J.B., 1992. Late Quaternary glacial history of the northern Antarctic Peninsula's western continental shelf. In: Elliot, D.H. (Eds.), Evidence from the Marine Record, Contributions to Antarctic Research III, Antarctic Research Series, Vol. 57. American Geophysical Union, Washington, DC, pp. 63-91

Powell, R.D., 1988. Processes and Facies of Temperate and Subpolar Glaciers with Tidewater Fromts, Short Course Notes, Geological Society of America, Denver, Colorado, pp 114

Powell, R.D., Alley, R.B., 1997. Grounding-line systems: Processes, Glaciological inferences and the Stratigraphic record, Geology and Seismic Stratigraphy of the Antarctic Margin, Part 2 Antarctic Research Series 71, 169-187

Powell, R.D., Domack, E., 2002. Modern glaciomarine environments. In: Menzies (Ed), Modern and Past Glacial Environments. Butterworth Heinemann, Oxford. Pp 361-389

Pudsey, C.J., Evans, J., 2001. First survey of Antarctic sub-ice shelf sediments reveals mid-Holocene ice shelf retreat. Geology 29, 787-790

Pudsey, C.J., Barker, P.J., Larter, R.D., 1994. Ice sheet retreat from the Antarctic Peninsula shelf. Continental Shelf Research 14, 1647-1675

Reinardy, B. T. I., Hiemstra, J. F., Murray, T., Hillenbrand, C.-D. & Larter, R. D., 2011. Till genesis at the bed of an Antarctic Peninsula palaeo-ice stream as indicated by micromorphological analysis. Boreas 40, 498–517.

Schoof, C., 2007. Ice sheet grounding line dynamics: Steady states, stability, and hysteresis. Journal of Geophysical Research-Earth Surface 112 (F3), F03S28, 1-19

Seramur, K.C., Powell, R.D., Carlson, P.R., 1997. Evaluation of conditions along the grounding line of temperate marine glaciers: an example from Muir Inlet, Glacier Bay Alaska. Marine Geology 140, 307-327

Shipp, S., Anderson, J.B., 1994. High-resolution seismic survey of the Ross Sea continental shelf: implications for ice-sheet behavior. Antarctic Journal U.S. 29, 137-138

Shipp, S., Anderson, J.B., 1997. Grounding zone wedges on the Antarctic continental shelf, Ross Sea. In Davies, T.A., Josenhans, H., Polyak, L., Solheim, A., Stoker, M.S., Stravers, J.A., (Eds.): Glaciated Continenteal Margins, An Atlas of Acoustic Images. Chapman and Hall, London, 104-105

Shipp, S., Anderson, J.B., Domack, E.W., 1999. Seismic signature of the Late Pleistocene fluctuation of the West Antarctic Ice Sheet system in Ross Sea: a new perspective, Part I. Geological Society of America Bulletin 111, 1486–1516.

Shipp, S.S., Wellner, J.S., Anderson, J.B., 2002. Retreat signature of a polar ice stream: sub-glacial geomorphic features and sediments from the Ross Sea, Antarctica. In: Dowdeswell, J.A.,O′ Cofaigh, C. (Eds.), Glacier-influenced Sedimentation on High-Latitude Continental Margins, vol. 203. Geological Society, Special Publication, London, pp. 277–304.

Sloan, B.J., Lawver, L.A., Anderson, J.B., 1995. Seismic stratigraphy of the Plamer Basin. In: Cooper, A.K., Barker, P.F., Brancolini, G. (Eds.), Geology and Seismic Stratigraphy of the Antarctic Margin, Antarctic Research Series, Vol. 68. American Geophysical Union, Washington, DC, pp. 235-260

Taylor, J.M., 2005. The Micromorphology of Paleoseismic Soft Sediment Deformation Structures in Glacial Deposits from Three Sample Sites in Scotland. MSc. Dissertation. Brock University

Taylor, J., Dowdeswell, J.A., Kenyon, N.H., Ó Cofaig, C., 2002. Late Quaternary architecture of trough-mouth fans: debris flows and suspended sediments on the Norwegian margin. Geological Society, London, Special Publications 203, 55-71

Thomas, R.H., Bentley, C.R., 1978. A model for Holocene retreat of the West Antarctic Ice Sheet. Quaternary Research 10, 150-170

Thomason, J.F., Iverson, N.R., 2006. Microfabric and microshear evolution in deformed till. Quaternary Science Reviews 25, 1027-1038

Trusel, L.D., Powell, R.D., Cumpston, R.M., Bringham-Grette, J., 2010. Modern glacimarine processes and potential future behaviour of Kronebreen and Kongsvegen polythermal tidewater glaciers, Kongsfjorden, Svalbard. Geological Society, London, Special Publications 344, 89-102

USAP - United States Antarctic Program, 2008. Antarctic peninsula map. Retrieved April 31, 2008 from http://antarcticsun.usap.gov/science/images/Ant-pen_map.png

van der Meer, J.J.M., 1993. Microscopic evidence of subglacial deformation. Quaternary Science Reviews 12, 553–587.

van der Meer, J.J.M., 1996. Micromorphology. In: Menzies, J. (Ed.), Past Glacial Environments — Sediments, Forms and Techniques, Vol. II. Butterworth-Heineman, Oxford: 335– 356.

van der Meer, J.J.M., 1997. Subglacial processes revealed by the microscope: particle and aggregate mobility in till. Quaternary Science Reviews 16, 827-831

van der Meer, J.J.M., Menzies, J., Rose, J., 2003. Subglacial till the deforming glacier bed. Quaternary Science Reviews 22, 1659-1685

Vanneste, L.E., Larter, R.D., 1995. Deep-tow boomer survey on the Antarctic Peninsula Pacific margin: an investigation of the morphology and acoustic characteristics of late Quaternary sedimentary deposits on the outer continental shelf and upper slope. In Cooper, A.K., Barker, B.F., Brancolini, B. (Eds.): Geology and Seismic Stratigraphy of the Antarctic Margin. Antarctic Research Series, vol., 68. American Geophysical Union, Washington, D.C., pp. 97-121

Wellner, J.S., Lowe, A.L., Shipp, S.S., Anderson, J.B., 2001. Distribution of glacial geomorphic features on the Antarctic continental shelf and correlation with substrate: implications for ice behavior. Journal of Glaciology 47, 397–411